AN ABSTRACT OF THE THESIS OF

Jae-Woo Kim for the degree of Doctor of Philosophy in Wood Science presented on May 20, 2002.

Title: Gas Injection Consolidation of Miniature Natural Fiber Beams

Abstract approved: Redacted for privacy

Philip E. Humphrey

The internal structure of natural fiber composites can be manipulated by controlling the spatial distribution of fiber orientation and internal chemical and thermodynamic conditions during their consolidation. Objects highly tailored to specific service demands may thereby be produced. Techniques to form miniature structural beams from oriented hemp and random wood fiber networks with phenol formaldehyde (PF) adhesive have been explored. Beams have been consolidated in a specially developed rectangular gas injection pressing system using ammonia as a softening agent and an ester as a low-temperature adhesive catalyst.

A range of natural fiber and adhesive types for use in producing the small composite beams are reviewed and hemp and wood fibers selected. Anatomical, tensile strength, and bonding characteristics of hemp fibers are explored. Adhesion kinetics of PF adhesive with both individual hemp strands and fiber networks in the presence of methyl formate at 50°C was also studied. Methyl formate was found to hasten the rate of strength development and final network strength by 51% and 22% respectively. The presence of waxy epidermal surfaces on hemp fibers has been found to limit strength of PF adhesive-to-fiber bonds to approximately 1.0MPa, while opposing surfaces bond well (4.5MPa).

The effect of testing temperature on the strength of partially cured PF resin-to-wood bonds was investigated to explore the possibility of reducing hot pressing time in conventional hot pressing processes of wood-based composite manufacturing and also to take advantage of temperature control that may be affected in sealed pressing methods. The shear strength of partially cured PF-to-wood bonds was found to be significantly increased by reducing temperature. This temperature effect was greatest at the beginning of bond formation and progressively decreased to zero with increasing isothermal cure.

Chemicals have been selected to sequentially stimulate fiber softening (anhydrous ammonia) and adhesion (methyl formate) in the sealed pressing system under near-ambient temperature conditions. It was found that density gradients can be created within beams by injecting ammonia from one platen. Stress analysis of a density graded beam showed that such a beam performs more efficiently than homogeneous beams of the same weight.

Gas Injection Consolidation of Miniature Natural Fiber Beams

by

Jae-Woo Kim

A THESIS

Submitted to

Oregon State University

in partial fulfillment of

the requirements for the

degree of

Doctor of Philosophy

Presented May 20, 2002

Commencement June 2003

Doctor of Philosophy thesis of Jae-Woo Kim presented on May 20, 2002

APPROVED:

Redacted for privacy

Major Professor, representing Wood Science

Redacted for privacy

Head of Department of Wood Science and Engineering

Redacted for privacy

Dean of Graduate School

I understand that my thesis will become part of the permanent collection of Oregon State University libraries. My signature below authorizes release of my thesis to any reader upon request.

Redacted for privacy

Jae-Woo Kim, Author

ACKNOWLEDGMENTS

First of all, I would like to express my sincere appreciation to Dr. Philip E. Humphrey, my advisor, for his guidance, support and encouragement. This work would never been accomplished without his invaluable advice and suggestions.

I also appreciate my committee members, Dr. Terry Brown, Dr. Barbara Gartner, Dr. Bill Warnes, and Dr. David Marshall for their encouragement and help. I'd like to appreciate Dr. Thomas McLain, for his generous financial support especially for the difficult times. I also want to thank Dr. Richard Holbo and Mr. Milo Clauson for their kind help throughout this research work. I wish to thank all my friends and colleagues for sharing their expertise in my project. My thanks also extend to all well-wishers who always accompany and encourage me.

My very special and cordial thanks go to my wife Keon-Hee and my daughter, Diane, for their love, encouragement and patience.

Lastly, I'd like to thank gracious God, my Lord, who gave me this great opportunity and also empower me to accomplish this work.

TABLE OF CONTENTS

TABLE OF CONTENTS (Continued)

TABLE OF CONTENTS (Continued)

TABLE OF CONTENTS (Continued)

LIST OF FIGURES

LIST OF FIGURES (Continued)

LIST OF FIGURES (Continued)

LIST OF FIGURES (Continued)

LIST OF FIGURES (Continued)

LIST OF FIGURES (Continued)

LIST OF TABLES

LIST OF APPENDIX FIGURES

LIST OF APPENDIX FIGURES (Continued)

To my parents

GAS INJECTION CONSOLIDATION OF MINIATURE NATURAL FIBER BEAMS

1. INTRODUCTION

Long tubular shaped natural plant fibers with rigid walls consist of very sophisticated arrangements of ligno-cellulosic sub-elements. Plant fibers of many types have high specific strength and stiffness which compare favorably with non-ferrous alloys and many synthetic engineering-fibers. They are also accessible for chemical modification during processing by virtue of the accessibility of the cell wall material to small polar molecules. Further, natural fibers display hygro-thermo-viscoelastic properties which means that they may be softened and re-formed by the judicious application of heat and water (or other polar molecules). In spite of their inspiring physical properties, most natural fibers are rather poorly utilized in conventional composite materials. They have been utilized in various applications such as cord, paper, and reinforcement in mud huts for thousands of years. Industrial utilization of these fibers can be seen in the manufacturing of wood-based panel products.

Conventional engineered products made out of natural fibers may be categorized into panels such as plywood, oriented strand board (OSB), particleboard, and medium density fiberboard (MDF); engineering products such as laminated veneer lumber (LVL), parallel strand lumber (Parallem®), molded objects such as door skins, and other products such as geotextiles, filters, and sorbents. By definition, these types of product are composed of natural fibers and adhesives or matrices that can bond them together. Types of natural fiber raw materials range from veneers, various sizes and shapes of particles, and fibers. In industrial manufacturing, thermosetting adhesives are mainly used to rapidly bond

fibers together. These engineered products do not, however, fully utilize the attributes of natural fibers. The design rationale of conventional products is rather primitive.

There is much potential to use natural fibers in some alternative ways in high performance engineered components. Such components can be achieved by optimizing outer shape and internal microstructure. Most conventional structural materials such as pressed steel and aluminum alloy are homogeneous and isotropic and thus the outer shape is the most important variable in design. Fiber composites in general, on the other hand, can be synthesized such that their internal microstructure (usually orientation of fibers) can be manipulated to achieve desired properties.

Examples where shape and internal structure are manipulated are to be found in some wood-based composites. Glue-laminated beams, which are made by grading of lumber and subsequent judicious placement, are one example of controlling internal structure. Another example is density profiles to be found in hot-pressed panel products. The transformed section of a panel may be likened to the shape of an "I-beam" and thus effect load-bearing properties of the product in service. This process-induced internal structure will be taken further in the present work. The extension of the mechanisms used to affect density profiles in panel products will be explored for the development of miniature natural fiber-based beams tailored to efficiently support loads in bending.

It is useful at this stage to summarize how the above-mentioned density profiles are established in conventionally hot-pressed panel products. Physical mechanisms are complex and interactive. The mechanisms can be broadly categorized as heat and moisture transfer, densification and stress relaxation, and adhesion. During the hot pressing of wood-based panel products, unsteady-state heat and moisture transfer and subsequent phase change toward the center of the mat leads to non-uniform softening in the consolidation direction which is mainly due to the thermo-hygro-viscoelatic properties of wood fiber. The consequence of

these ever-changing mechanisms is the generation of the above-mentioned cross-sectional density gradient. The flexural properties of the panel products are greatly effected by this density profile as mentioned earlier.

A long-term goal of the research of which the present thesis is a part is to develop means of producing composite objects whose internal structure and external shape are optimized for specific engineering applications. The outcome will, it is anticipated, be a wide range of products which may partially replace steel, aluminum alloy, and some polymers in various types of engineering application. Some important aspects of the strategy for the creation of the composite components are listed below.

1. Fiber separation and selection;

   Natural fibers may be derived from various sources including wood and agricultural crops. Man-made fibers may be combined with natural fibers if necessary. Fast but accurate fiber separation and sorting techniques will be needed when working with fiber sources which have populations of fiber types within them.

2. Fiber modification before re-constitution:

Natural fibers may be modified with various chemical and mechanical treatments which may impart desirable properties. This may encompass adhesive addition, addition of ferromagnetic elements for the subsequent orientation of fibers in a magnetic field, and other chemical modification for enhancement of dimensional stability and mechanical properties.

3. Consolidation of fiber pre-forms

Since the consolidation process of wood-based composites greatly influences their internal structure, it is necessary to look at the mechanisms operative during the consolidation process. These mechanisms include, but are not

limited to, heat and moisture transfer, rheology, and adhesion. Chemical modification may also be included. Computer simulation models of these mechanisms, which are already being developed, will greatly help the development of methods to consolidate new composites. A sealed pressing system which is capable of injecting and removing reactive gases and provide desired thermodynamic environments for *in-situ* modification will be required. Having developed the technology for the creation of such objects, structure and properties of the products for specific end-uses need to be considered.

The present work is, therefore, devoted to manipulating the structure and consequent properties of natural fiber composites during the consolidation process.

2. LITERATURE REVIEW

2.1. INTRODUCTION

Many important properties of fiber-based composite materials are dictated by the spatial distribution of fiber type and fiber orientation within them. Also of importance are the properties of the matrices or adhesives used to make bonds between fiber elements, and localized conditions to which the pre-formed fiber networks are exposed during the consolidation process. Understanding the properties of various types of fibers and matrices (more appropriately termed adhesives due to their low volume-fraction in most natural fiber-based composites), as well as how they are assembled, will therefore be important for the creation of efficient new composite materials. A number of fiber and matrix possibilities will be surveyed in the following discussion and a broader range are included in Appendix A. This is both in order to explore the potential of using such raw materials in new ways as new methods of synthesis are developed, but also in order to converge on the particular fibers for use in the present study.

A dauntingly wide variety of natural and synthetic fibers may be regarded as potential candidates for inclusion in engineering composites. Clearly, wood fibers are dominant in present-day structural composite products, but many non-wood plants have the potential to play important roles in the future. Some plant fibers are already being used on an industrial scale. Natural plant fibers have some specific attributes that make them particularly interesting compared to human-made fibers such as those from glass and carbon (Bunsell, 1988; Jang, 1994). The walls of most natural fibers are accessible to, and reactive with, chemicals-particularly small and polar ones- (Hon, 1996). This accessibility and reactivity makes the fibers amenable to modification *in situ* during processing (which is largely not the case for glass, carbon and aramids). Furthermore, the natural fiber cell walls exhibit

hygro- thermo-viscoelastic characteristics under applied stress (Ren, 1991). This means that they may be temporarily softened in readiness for compaction and bonding. Still, synthetic fibers may have potential to be used along with natural plant fibers in hybrid composite products.

Properties of matrices or adhesives are clearly also important because they play the important role of transferring stress. Especially in wood-based composites manufacturing, bond strength development during hot pressing is critical to production speed, the attainment of final micro-structure, spatial sequencing of internal mechanisms, as well as to the final properties of the composites. Mechanisms of adhesion and how they may be assessed will therefore also be considered (section 2.5) in this review. The discussion will, however, begin with a consideration of possible strategies for composite development (section 2.2).

2.2. STRATEGIES FOR SYNTHESIZING ADVANCED NATURAL FIBER-BASED COMPOSITES

Bolton (2000) proposed a view to efficiently utilize a diversity of plant fiber resources. He reviewed present uses of biomass, except the ones used for food or fuel. Then he identified the forces which will drive future changes in natural fiber resource utilization. The growing global population and consequent increased demand for fiber resources, production of agricultural residues which require methods of utilization, and dwindling reserves of wood for fuel were identified as the most important driving forces for change. Bolton suggested that the potential for expanding the resource base lies in the greater use of agricultural fibers. Given that the nonwood fiber resources are likely to be increasingly utilized in the future, Bolton pointed out several issues in nonwood plant fiber processing technologies that must be addressed if their potential is to be realized. These include, for example, the presence of substantial quantities of pith cells, silica and hot water-

soluble chemical constituents in many of the fibers and the frequent presence of waxy layers at the surface of some types of stem. Bolton suggested that such issues must be solved in order to make overall processing operations more viable. He also pointed out that there might be some competition between wood and nonwood fibers in terms of properties and costs but that plant fibers may replace synthetic and nonrenewable materials in many applications such as insulation, packaging, and semi-structural composites.

Kessler and Kohler (1996) and Nebel (1995) proposed more specific strategies for utilization of natural plant fibers such as flax and hemp. Kessler and Kohler (1996) presented processing strategies for natural plant fibers for a variety of uses and found that steam explosion treatment of bundles of hemp and flax can be useful to produce fibers with chemical and physical properties suitable for a range of applications. They also pointed out possible applications of flax with respect to value and composition. Coarse fibers may, for example, be used as nonwovens and geotextiles without binder, and products such as plant pots and fruit drawers with binder. Fibers with medium fineness may be used as bands, belts, and strings without binder, and nonwovens, packaging material and automotive interior parts with binder. Fine fibers may be used as rovings and fine yarns without binder and filters and fiber-reinforced composites with binder. However, Kessler and Kohler mentioned that hemp and flax are only economically viable when political and economic circumstances are appropriate. Nebel (1995) reviewed traditional hemp processes and divided them into three areas: long fiber processing, tow processing, and cottonization. However, in order to maximize the potential for new products, Nebel also proposed the steam explosion process. He found that such techniques, which use high-pressure steam and very small amounts of additives, might be economically and ecologically viable for the production of high quality hemp fibers.

Humphrey (1994) proposed a strategy to synthesize high performance engineering composite components from natural fibers. He suggested a design

rationale which combines shape optimal design (SOD) and internal property distribution control (IPDC). Since most components used in engineering applications are designed by manipulating their outer shape as the principal variable, shape optimal design using numerical methods of analysis are commonly employed in design. Internal property distribution control implies manipulation of the spatial distribution of properties within an object of defined shape. The concept of combining shape optimal design and internal property distribution control was established by looking at the internal microstructure of natural objects such as animal bones and insect shells in which elaborate and complex mixing of diverse cell types and orientations lie (Neville, 1993). The complex outer shape and internal structure of these objects is a product of natural selection. Combination of these two concepts (SOD and IPDC) yields natural systems which are more efficient and viable than any human-made objects. Humphrey identified two examples where shape and property control are attained in the current wood utilization field, namely glue-laminated beams and density profiles in hot pressed panel products.

With the above concepts in mind, Chowdhury (1999) explored the concept of gas-injection pressing. His preliminary results suggest that the concept has the potential to be used to create innovative natural fiber composites. The groundwork for the development of new natural fiber based engineering components does, however, depend upon our understanding of the mechanisms operative within conventional wood-based panel products during the hot pressing process. In such processes, thermodynamic and rheological mechanisms interact to affect the attainment of final structure and properties. These mechanisms are therefore briefly reviewed below.

2.3. MECHANISMS OPERATIVE WITHIN WOOD-BASED COMPOSITES DURING CONVENTIONAL HOT PRESSING PROCESSES

Most natural fiber-based composites are manufactured by hot pressing processes, depending on the shape and size of final product as well as the adhesive being used. Large volumes of natural fiber-based composites, especially panel products such as oriented strand board (OSB), particleboard (PB), and medium density fiberboard (MDF) are produced by the hot pressing process.

Hot pressing is often the most important stage in the industrial manufacturing of natural fiber-based composites. The hot press is the most expensive part of the entire process to acquire and to operate. The hot pressing process is closely related to the maximum production capacity of most mills and also greatly effects various physical and mechanical properties of final products. A fundamental understanding of such processes is essential for optimizing production speed, cost, and energy consumption, as well as in manipulating in-use properties. Analyses of the mechanisms will lead to the development of new and advanced technology and products such as those in the present research.

Many physical changes occur within natural fiber-based composites during conventional hot pressing, and these changes interact with each other as pressing proceeds. These can be summarized as heat and mass transfer, densification and consequent stress relaxation, and adhesion between the wood elements (Humphrey, 1994; Humphrey *et al.* 2001). The literature concerning these mechanisms will be briefly reviewed in the following sections.

2.3.1. Heat and mass transfer

During pressing, high temperature and compaction pressure are applied to loosely formed mats of adhesive-treated natural fiber elements. Heat is transferred

first from the heated platens to the mat surfaces and then toward the interior. As a consequence of heating, water sorbed in the cell wall material also changes its phase into vapor and the resultant water vapor penetrates toward the central plane of the mat by convection. This phase change, consequent migration of vapor and subsequent diffusion and re-adsorption leads to the redistribution of adsorbed water. Therefore, non-uniform temperature and moisture re-distribution occurs within the composites as pressing proceeds (Strickler, 1959; Kamke and Wolcott, 1991; Thömen, 2000). The temperature change at different locations can be monitored by positioning thermocouples within the loose mat before pressing (Strickler, 1959; Zavala and Humphrey, 1996; Song and Ellis, 1997). Internal gas pressure change can be also monitored by inserting small-diameter steel tubes into the mat which are attached to pressure transducers and monitored digitally (Strickler, 1959; Humphrey, 1982; Kamke and Casey, 1988a,b; Song and Ellis, 1997; Steffen *et al.*, 1999).

As mentioned earlier, heat transfer mechanisms can be summarized as conduction, convection, and the diffusion of water vapor and air. Heat conduction may be the major heat transfer mode at the hot platen-mat boundary. As the vapor front proceeds toward the center of the mat, it is important to transfer heat through the outer layer to the vapor front (or zone of evaporation). The moisture level at the outer layers rapidly decreases and thus a minimal amount of vapor is generated in this region (Humphrey and Bolton, 1989a). Knowledge of the coefficient of thermal conductivity of mat materials is therefore important if the system is to be modeled and optimized.

In order to measure thermal conductivity of wood fiber networks, Shao (1989) developed an unsteady-state technique as a function of density and moisture content. Her results were used by Haselein (1998) to derive an equation which gives thermal conductivity as a function of density and moisture content. Humphrey and Bolton (1989a) measured thermal conductivity in directions both perpendicular and parallel to the panel plane as a function of consolidation and

estimated that the thermal conductivity parallel to the panel surface direction is typically about 50% higher than that perpendicular to it.

Since mats are porous media with voids and pores between and within the natural fiber elements, vapor and air can reside and flow through the mat. It also has been recognized that during the hot pressing process, convection of water vapor is crucial in the transfer of heat and moisture. Almost all of the gas flow occurs through the void spaces between the natural fiber elements rather than through the pores within their walls (Lehmann, 1972). Therefore, the shape and size distribution of pores are closely related to the gas flow. Permeability is a material property that describes flow rate through a unit cube of a porous solid with unit pressure differential between two faces. It depends on the shape and size distribution of the pores which, in turn, is dictated by the size, shape, and orientation of fiber elements. If some or all fiber elements are aligned in any preferred direction, then permeability will clearly be affected (Bolton and Humphrey, 1994). Such is the case in oriented hemp fiber structures to be investigated in the present study.

The permeability of natural fiber mats can be experimentally determined and some work has been done in the past to measure it (Bolton and Humphrey, 1994; Haselein, 1998). Those methods involved measurement of the amount of gas flow through variously compacted miniature mat samples where total pressure differentials were applied. Permeability values can be identified as two types; those applicable to flow through a panel thickness (transverse flow) K_T, and those applicable to flow parallel to the board surface (longitudinal flow), K_L. The value of K_T largely influences the rate of flow of heat and moisture from the hot platen towards the core of the mat, which is crucial for the curing of resin and softening of natural fiber cell walls, while that of K_L determines the rate of flow from the center of the board toward the edges and thus heat and moisture loss from the board and reduction of internal vapor pressure (Bolton and Humphrey, 1994). It has been known that the K_T of composite boards is usually much higher than K_L and far

higher than the K_T of wood from which the board is made. This suggests that board permeability is mainly determined by the size, shape and distribution of pores rather than that of the natural fiber elements themselves (Bolton and Humphrey, 1994.). Bolton and Humphrey (1994) pointed out that K_T is important when vapor phase chemical modification agents and/or curing agents are used during pressing of natural fiber-based composites. Such is the case in the present investigation.

Christiansen *et al.* (1987) measured permeability values for the different layers in particleboard. They successively sanded samples which had density profiles through their thickness and compared the permeability values that were measured before and after sanding. By doing this, they calculated the permeability values of each layer. However, the variation of permeability across the sample thickness appeared larger than the variation of density, which suggested that the result might not be accurate enough to calculate precise permeability values. Bolton and Humphrey (1994) pointed out such experimental methods and analysis may not be able to derive true permeability values because of the assumption of the uniform sub-layer density, which is not the case (variation in density is continuous) and the experimental method; it is tedious and subject to error.

Bowen (1970) explored permeability K_T values of particleboard over a density range from 510 to 740Kg/m^3 and observed a slightly curvi-linear decrease of $\log_{10}K_T$ with increase in density. The real decrease of K_T value over this range was about 60 fold. Lehmann (1972) collected data from insulation board, particleboards, and hardboards with density ranges from 230 to 980kg/m^3 and observed a more linear relationship between density and K_T. The decrease of K_T values over that range was about 600 fold.

The above data were obtained from hot pressed boards with density profiles through the thickness. The surfaces of the boards are clearly much denser than the center, which leads to the difference in the permeability of surface and core layers. Thus, average permeability values reported by Bowen (1970) and Lehman (1972) may not be useful to analytically model flow through parts of boards.

Haselein (1998) proposed a technique to determine both in-plane and cross-sectional permeability of wood fiber mat material simultaneously as a function of compaction. He formed small circular mat specimens and compressed them stepwise to different thicknesses. At each thickness, air was passed through the perforated pressing platens. The airflow was measured for each step and the data were used to compute in-plane and cross-sectional permeability values for different densities.

2.3.2. Rheological characteristics

When a natural fiber mat is consolidated in a hot press, both instantaneous and time-dependant deformation occur. According to Ren (1991) and Thömen (2000), the term 'rheology' means behavior of material (such as the natural fiber mat) which include not only instantaneous deformation but also time-dependant behavior.

Burger's model has been used to express various types of visco-elastic behavior of materials. This model also has been applied to wood composites by some researchers (Bodig and Jane, 1982). Ren (1991) developed a more advanced 5-element model (Burger-Humphrey model) by incorporating a series plastic and micro-fracture (PMF) element in order to explain both visco-elastic behavior of the mat and also irreversible changes of cell wall and mat structure which instantaneously occur upon pressing (Figure 2.1). Such behavior may be represented by a spring that only operates in one direction because PMF only occurs when compressive stresses exceed the yield strength of the microstructures and is not recoverable upon load removal.

Ren (1991) developed a technique to determine the coefficient of each of the elements of the Burger-Humphrey model (Figure 2.1). He applied carefully selected loading cycles in a specially designed sealed and computer controlled

hydraulic pressing system and evaluated the strain response to defined loading cycles under a diversity of temperature and moisture conditions. It was found that the PMF element has the largest effect on overall deformation of the mat during pressing, especially at the initial stages of pressing.

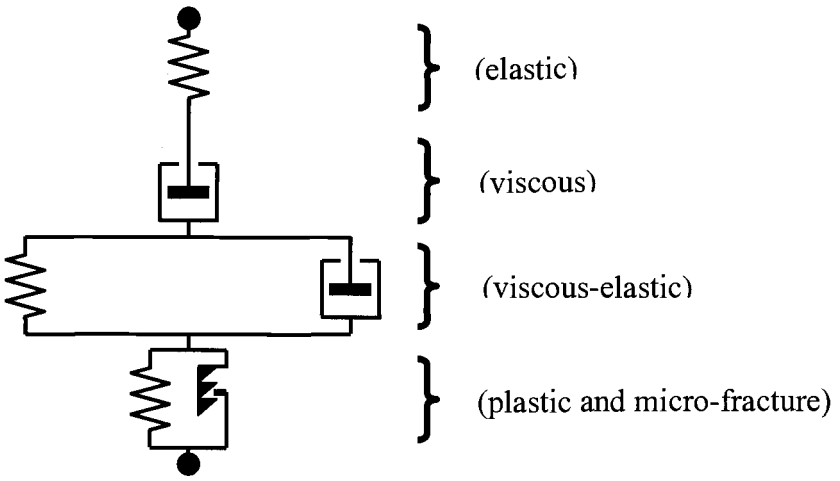

Figure 2.1. Five-element Burger-Humphrey model presenting non-linear temperature and moisture content-dependant elastic, viscous, viscoelastic, and micro-fracture (Refined after Thömen, 2000).

The rheological characteristics of the loose natural fiber mat depend on density, moisture content, and temperature. Since natural fiber networks are hygro-thermo-viscoelastic, they densify differently in different locations of an industrially pressed mat depending on the time, temperature, and moisture conditions as well as applied compression stress from the platen. The above rheological material models (and associated experimental equipment) therefore takes account of moisture and temperature effects on each model element. Future forms of such models (and

associated experimental arrangements) will also account for the effect of chemical modification of rheological properties (such as ammonia used in the present study).

2.3.3. Adhesion

During the hot pressing process, applied thermosetting resin in the furnish mat cures with time and thus develops bonds between wood elements. The bond strength development rate between fibers is greatly effected by temperature, and this changes with time and spatial position during pressing (Humphrey and Bolton, 1979; Humphrey and Bolton, 1989b). Evidently, inter-fiber bonding characteristics differ throughout mats during hot pressing processes. Bond strength development between fibers is crucial in resisting residual stress when the press opens. These stresses are derived from the residual elasticity of the deformed fibers and within-void gas pressure. Therefore, bond strength development is one of the most important aspects in optimizing hot pressing processes. A literature review on the curing behavior of selected adhesive types may therefore be found in section 2.5.

2.3.4. Modeling of mechanisms operative during hot pressing

A number of research initiatives have been devoted to quantitatively addressing physical and chemical mechanisms operative during the hot pressing process of natural fiber-based composites. There has been two different approaches to modeling the hot pressing process; the ones that use fundamental principles to describe the relevant physical or chemical processes, and others that apply statistical methods to link material and process variables to output parameters such as mechanical properties of the final product. Although the latter has provided valuable data on relationships between process variables and output parameters,

they do not provide fundamental understanding of the mechanisms necessary for them to be used as tools for innovation.

Humphrey (1982) seems to be the first researcher who modeled heat and mass transfer in composites during pressing based on fundamental physical principles. The models incorporated heat conduction, phase change and vapor convection. His models predicted temperature, vapor pressure and moisture content changes during hot pressing of circular samples and agreed well with measured data (Bolton *et al.*, 1989). Haselein (1998) refined Humphrey's model, in which instantaneous press closing was assumed, to account for press closure and added a rheological component to explain mat differential compression and stress relaxation.

Thömen (2000) further improved Humphrey's and Haselein's model and made it fully three-dimensional. A typical predicted data set is presented in Figure 2.2. These data are for thermomechanically generated wood-fiber mat compressed at 160°C to a bulk density of 600kg/m^3. Such pressing simulation models for conventional hot pressing process will evidently aid in optimizing gas injection pressing process presented in this research. Computer modeling of gas injection pressing processes will provide more efficient ways to achieve highly controlled properties within natural fiber composite objects.

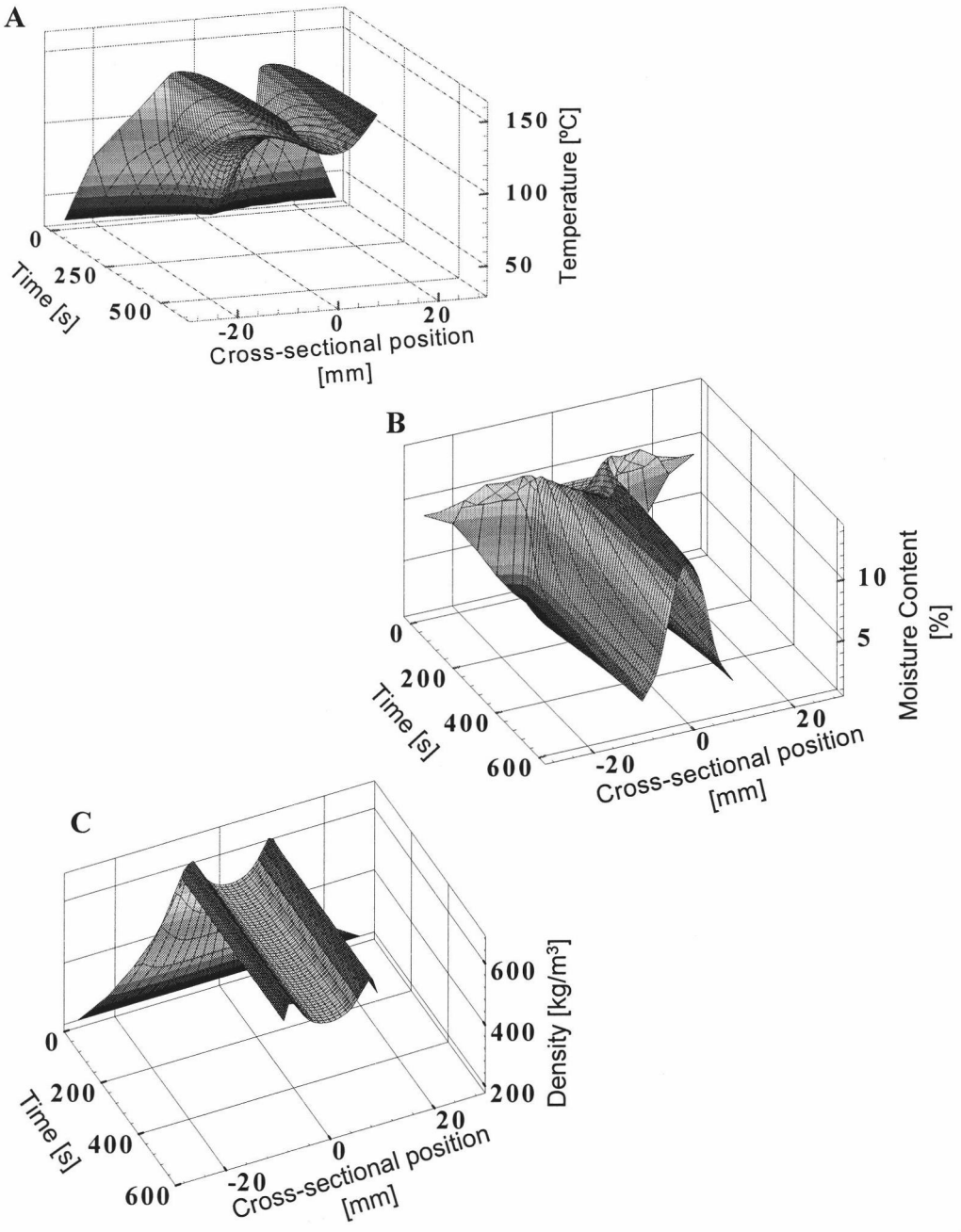

Figure 2.2. Three-dimensionally predicted temperature (A), moisture content (B), and density profile (C) over time and cross-sectional position during hot pressing. [Softwood thermomechanical fiber mat of 9% MC /60seconds press closing time/160°C platen temperature/600kg/m^3 final density/20mm final thickness] (From Thömen and Humphrey, 1998).

2.4. FIBERS AND ADHESIVES THAT COULD BE USED FOR COMPOSITE MATERIALS

Fibrous composite materials consist of reinforcing fibers that are usually selected to have high tensile strength and modulus, and a matrix that acts as a load - transferring medium. The matrix may also protect fibers from environmental damage due to the ingress of biological organisms or chemicals, although affecting coverage that usefully reduces such susceptibility is very difficult to achieve (Mallick, 1993). The physical, chemical, and mechanical properties of fibers, together with their size, shape, volume fraction, and orientation in a composite greatly influence its final properties.

All plants are principally composted of basic structural and physiological units called cells. The cells are diverse and complex in type and vary considerably in shape and function. A dictionary definition of natural fiber is:

> "An elongated tapering cell that has at maturity a small lumen and no protoplasm content, that is found in many plant organs and is especially well developed in the xylem and phloem of the vascular system, and that imparts elasticity, flexability, and tensile strength to the plant".
>
> (Webster's New International Dictionary)

Such natural fibers in plants are characterized by the presence of a rigid or semi-rigid wall. Lignificaion largely imparts rigidity to the cells of woody plants. The outer shape of most plant fibers that are currently utilized industrially for structural composites are long and tube-like in shape with enveloped blunt ends (Panshin, 1981). The aspect ratio (length/width) of such fibers is typically high (usually 50 to 100). Some representative average fiber length and width values are shown in Table 2.1.

Table 2.1. Length and width of selected natural fibers (Ilvessalo-Pfäffli, 1994; Rowell, 1996)

Fiber type	Fiber length (mm)	Fiber width (mm)
Cereal straw	0.4-3.4	0.005-0.03
Flax:		
Fiber bundles	250-1200	0.04-0.6
Single fibers	9-70	0.019
Hemp:		
Fiber bundles	1000-4000	0.5-5
Single fibers	5-55	0.01-0.05
Jute:		
Fiber bundles	1500-3600	
Single fibers	2-5	0.01-0.025
Hardwood	0.7-1.6	0.01-0.04
Softwood	2.7-4.6	0.015-0.06

Fibers that could be used for composites can be broadly categorized into two groups; natural plant fibers and synthetic fibers. A range of natural fiber types will be briefly surveyed here with emphasis on those with potential for use in future composite materials. A review of a range of synthetic fiber types is also to be found in Appendix A since they are less directly relevant to the present study.

2.4.1. Wood fibers

Wood is the most abundant and important fiber resource for composite manufacturing. However, over 50% of wood is used as fuel. The rest of wood is utilized as sawn lumber, virgin pulp, wood-based panels and other products (Bolton, 2000). In order to break down wood into fiber, various types of processing methods are used such as mechanical, thermo-mechanical, and chemical pulping.

Chemical and physical properties of wood fiber are greatly influenced by the processing methods employed.

Wood fibers and fiber bundles are utilized as raw materials for many types of wood composite such as medium density fiberboard (MDF) and hardboard as well as papers and paper boards. In softwoods, most (up to 98%) of fibers are composed of tracheids; these are long and narrow tube-like fibers. In hardwoods, fibers are more diverse and evolutionarily advanced; vessel elements, which are relatively wide and short with open ends, fibers (anatomically termed) that resemble softwood tracheids but are relatively short and narrow. As mentioned earlier, the wood fibers used for composite manufacturing are mainly softwood tracheids and hardwood fibers. The length and width of wood fibers varies within a species as well as between them (Table 2.1). The cell wall thickness of these fibers typically ranges from 2.0 to 7.0 μm.

Since wood fibers have hygro-thermo-viscoelastic properties, their physical and mechanical properties are very much dependent on moisture content, temperature, and duration of load. Also, because of their anisotropic properties due to the microfibril structure and orientation in the cell wall, the strength and stiffness of wood fibers are much higher in the longitudinal direction than transverse direction. The tensile strength of wood fiber in the axial direction varies within and between species and depends heavily on the processing methods as well as testing methods used. Usually tensile strength of wood fiber ranges from 200 to 1300MPa (Haygreen and Bowyer, 1982; Tsuomis, 1991).

2.4.2. Nonwood fibers

The demand for natural fiber-based products has increased in recent years. This is due to in part increasing population and the decreasing production of wood fiber sources from over exploitation and environmental protection policies. As a

result, alternative raw materials for manufacturing various composite products have been explored (Dalen *et al.*, 1996; McKeever *et al.*, 1995; Sauter, 1996). The structure and properties of a selection of nonwood fibers will be summarized here with a view to identifying those that are appropriate for the present research.

2.4.2.1. Stalk fiber

Stalk fibers include those from straw, sugar cane, grass, and a range of types of reed. After harvesting the crops, the stalk residue material left in the field can be used as a fiber source for a number of applications. Straw fibers are hollow tubes surrounded by a waxy epidermis, cellulose tube, and pithy ring. The stems of straw are built up of parenchymatous ground tissue and the vascular bundles imbedded in it. Vascular bundles are distributed in two distinct ways; at the periphery of the stem as in cereal straw, or scattered in the ground parenchyma throughout the stem cross-section (Ilvessalo-Pfäffli, 1994). Figure 2.3 is a schematic diagram of the structure of straws.

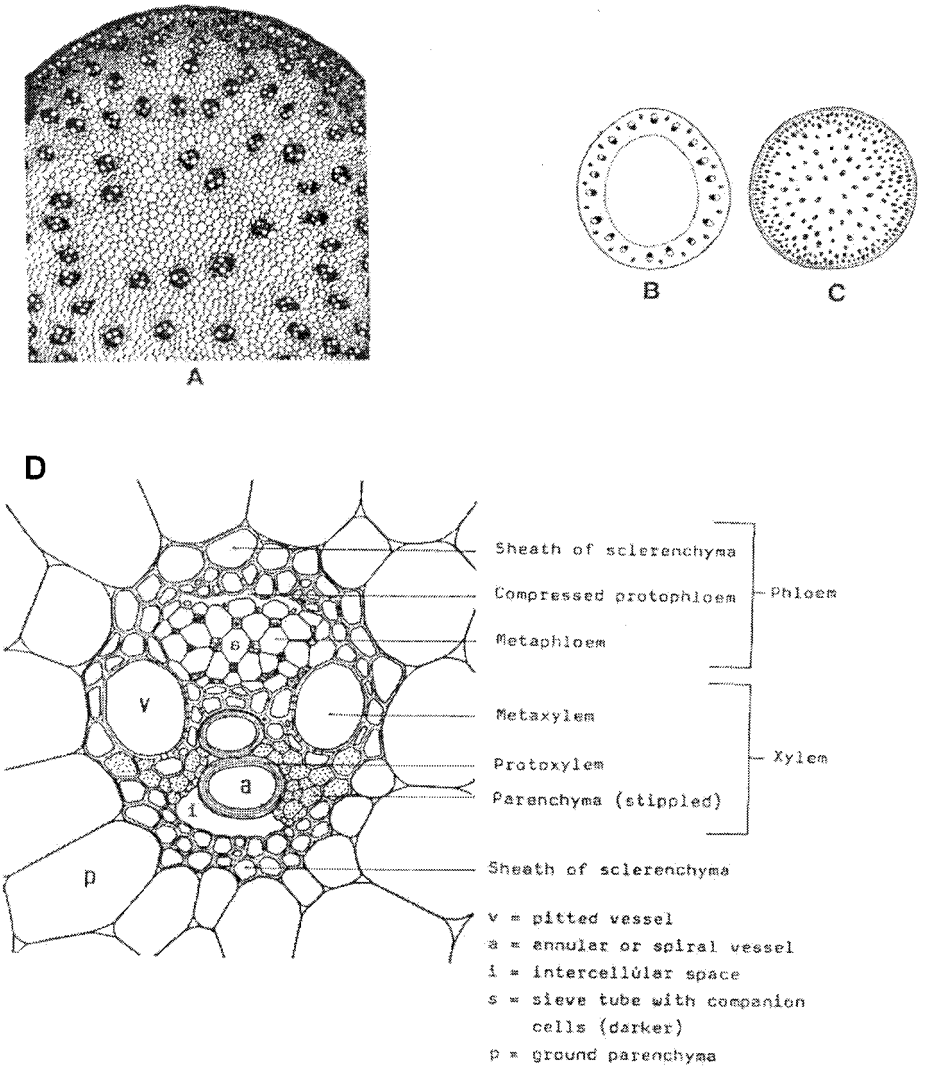

Figure 2.3. Structure of straw cross-section A: Cross section view; B: vascular bundles in two rings; C: vascular bundles are scattered throughout the cross-section; D: Structure of vascular bundle (Ilvessalo-Pfäffli, 1994).

The function of vascular bundles in the plant is to transport water and food and to impart rigidity. Fibers from straws of wheat, rice, barley, rye and corn stalks are of small diameter (typically 1.5mm) but have a high aspect ratio (up to 110).

Fibers from rice straws typically have higher aspect ratios of around 170. Straw fibers generally contain higher percentages of cellulose than do wood fibers, while their lignin component is typically less than that of wood fiber (Russell, 1996).

Sugar cane is cultivated in many parts of the world and bagasse is the residual material obtained during sugar production. In general, it has been used as fuel for sugar plants and some of the remainder is used as a fiber source for panel production. The bagasse consists of pith, rind, and epidermis material. The rind constitutes approximately 50% of the dry weight of the material and contains most of the usable fiber. These fibers are somewhat similar to hardwood fibers, averaging 1.7 mm in length and 0.02 mm in diameter, leading to an aspect ratio of 85 (Kozlowski *et al.*, 1994; Rowell *et al.*, 1996).

Reed stalks are typically 1.5-5m long with fiber lengths ranging from 0.6 to 2mm. The properties of the reed straw are similar to those of sugar cane. However, an often quoted limitation of reed is that it has a high ash content (about 2.5-2.7 %) which may cause quick blunting of cutting tools (Rowell *et al.*, 1996).

Grass fibers have been considered mainly as a fiber source for paper manufacturing. However, because of their limited (seasonal) availability and processing difficulties, few of these fibers have been widely used. Compared to softwood fibers, grass fibers tend to have a greater diversity of cell type among species, which vary greatly in shape and size. Typical grass fibers are narrow, have blunt ends with a large aspect ratio (Kozlowski *et al.*, 1994).

2.4.2.2. Bast fiber

Bast fibers exist in the inner bark or phloem of many dicotyledonous plants to provide structural rigidity to the stem. They are characterized by long, strong fiber bundles, which comprise the outer part of the stalk. Flax, hemp, kenaf, and jute are the main bast fiber bearing plants. These plant fibers have long been noted

for their exceptional strength in cordage and paper. The bast portion typically comprises 10 to 40 percent of the mass of the stem, depending on species (Kozlowski *et al.*, 1994). In general, bast plants have the following advantages:

- High tensile strength
- Relatively low density (280 to 620 Kg/m^3) which leads to especially high specific strength
- Generally high fiber productivity rates which rival, and even surpass, those of most commercial tree species
- Potential for even greater productivity of bast portion and mechanical properties through genetic breeding and engineering

The overall limitations of bast plants are:

- Rotations of at least alternate years are generally required (with associated seasonal harvesting limitations)
- Relatively high moisture sorption in the core portion
- Difficulties in handling long fiber bundles

2.4.2.2.1. *Flax*

Flax is grown in many parts of the world, mainly for the production of linen from the fiber and linseed oil from the seed. Oil seed flax is distinctive from the other bast fibers such as hemp and kenaf. First, the diameter of the stalk of the oil seed flax is much less than that of kenaf or hemp, thus making the flax stalk more slender. Secondly, the flax bast fiber yields per acre are considerably lower than those of other bast fibers. Figure 2.4 shows a schematic cross-section of flax (Kozlowski, 1994; Rowell, 1996).

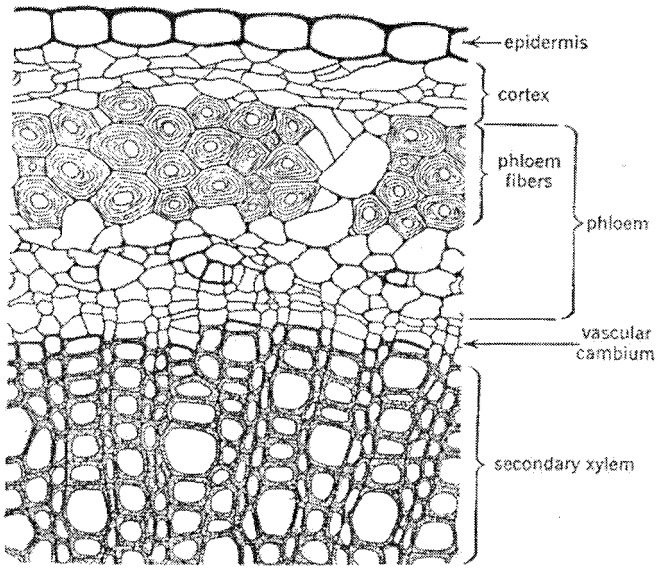

Figure 2.4. Schematic cross-section of a flax stem showing phloem (bast) fibers (Ilvessalo-Pfäffli, 1994)

The advantages of flax fibers follow:

- Relatively low cost for the bast portion
- Commercially available in production level quantities
- Oil seed flax is an established crop thus less risky for farmers to grow

Disadvantages are:

- Low yield per acre
- Limited rotations, generally three years
- Low tensile strength compared to others in the bast fiber group

2.4.2.2.2. *Kenaf*

Kenaf is a member of the Malvaceae family and may grow to 2.4 to 6 m in height. It is generally un-branched in thick strands. Kenaf has some promising characteristics along with certain limitations. Nutrient requirements in the soil are low, with no significant improvement in yield above certain relatively low thresholds. However, the growth becomes quite minimal when temperatures fall below about 20°C.

Kenaf contains a bast fiber portion comprising 26 to 35 percent of its stem. Bast fibers average 2.5mm in length while the length of fibers in the core is about 0.5mm. This composition provides a desirable blend for many pulp and paper applications (Kozlowski *et al.*, 1994; Rowell *et al*, 1996). The advantages and limitations of kenaf are as follows:

- High yield in some warm regions
- High bast portion
- Low productivity in cool regions
- High moisture requirement

2.4.2.2.3. *Hemp*

Hemp is a strong, durable, though harsh bast or phloem fiber. It has a core that somewhat resembles the characteristics of hardwood fibers. Typically, the bast portion comprises about 14 percent of the total mass. Hemp is an annual plant that, at maturity, develops a rigid woody stem ranging from 1.2 to 5.5 m in height and a diameter from 8 to 20 mm. It has the highest tensile strength of all of the bast fibers. However, since the leaf of certain hemp types is a source of narcotics, the growing of this plant is restricted in some countries (Kozlowski et al., 1994). The advantages and limitations follow:

- Requires little moisture to grow
- Resistant to weeds and other competition, thereby not costly in cultivation
- Stronger and tougher than kenaf and flax
- Restrictions in cultivation because of the narcotic leaf (of some strains).
- Low bast fiber yield

2.4.2.3. Leaf fiber

In many monocotyledons, long strand leaf fibers are embedded in parenchymatous tissues to provide mechanical support for the long, broad leaves. In general, leaf fibers are more coarse than bast fibers and are commonly used as cordage, mats, rugs, and carpet backings. An example of these materials is manila hemp (abaca), and sisal. The abaca stalk consists of a central stem enclosed by leaf stalks or sheaths. The fiber is obtained from the outer sheath of the stem by separating the outer layers and then separating them from other parenchymatous cells. The sisal fibers are embedded longitudinally in the leaves which are typically cut into short segments and then defibrated by means of a hammermill (Rowell *et al.*, 1996).

2.4.2.4. Other natural fibers

Other natural fibers include coir, which is a husk fiber of coconut, palm fibers, bamboo, and cotton. Especially bamboos are being used in composites such as laminated veneer lumber, parallel strand lumber, and panel products. Some fibers from these sources have the potential to be used as a fiber source in spite of the limitations such as availability and cost. Fibers from recycled wood and paper

also can be candidates though use in sophisticated composites is unlikely because of their variability and non-specificity.

2.4.3. Synthetic fibers

Synthetic fibers are quite different from natural fibers in a number of regards. These fibers can be manufactured to have desired properties by the selection of raw materials and process. They include fibers derived from glass of diverse micro-structures (Gupta, 1988), carbon (Fitzer and Heine, 1988), polymers (Calundann *et al.*, 1988; Yang, 1988), boron (Wawner Jr., 1988), and ceramic materials (Bunsell *et al.*, 1988). Properties of selected synthetic fibers are summarized in Table 2.2.

Table 2.2. Properties of selected synthetic fibers (Bunsell, 1988)

Fiber Type		Typical Diameter (μm)	Specific Gravity	Tensile Strength (GPa)	Tensile Modulus (GPa)	Strain To Failure (%)
Glass	E-glass	10	2.54	3.45	72.4	4.8
	S-glass	10	2.49	4.3	86.9	5.0
Carbon		5-10	1.8-2.0	1.52-5.65	207-1035	0.32-1.81
Aramid		12	1.39-1.45	3.0-3.62	70-179	1.9-4.4
Spectra®		27-38	0.97	2.59-3.0	117-172	2.7-3.5
Boron		140	2.7	3.1	393	0.79
SiC		14-140	3.08	2.75-3.44	196-400	0.86-1.4
Al_2O_3		2-20	2.73-3.95	1.03-1.09	103-379	0.4

2.4.4. Thermosetting adhesives for natural fiber composite materials

The role of matrices in fibrous composites is predominantly to bind the fibers together and thus to enable stress to be transferred between them (Shaler, 1993). Matrix materials generally play a less important role in the uniaxial load carrying properties of composites than those in shear and compression modes. The length of reinforcing fibers do, however, play a key role in dictating the magnitude of shear stresses at interfaces during uniaxial loading (Chou, 1992). The processability and spatial distribution of discontinuities of many types of composite depends on the mechanical and thermal characteristics of the matrix employed. The chemical composition of matrix and fiber, especially the surface structure and chemistry effects bonding properties.

The distinction between matrix and adhesive should be made clear here. Matrices are predominantly used for human-made fibers and encrust the fibers with minimum voids; matrix contents typically range from 30 to 70% by volume. Adhesives are mainly used for natural fiber-based composites and are not normally used to fill all the voids. Large volumes of voids are inevitable because of the lumens and voids between the fibers. Efficient distribution of adhesives on the fibers is critical because the final properties of the composites largely depend on the adhesion between fibers and the cost of adhesives is high in most natural fiber-based composites. Adhesives or matrices that may be used in composite materials can be broadly categorized as thermosetting and thermoplastic, and other types such as adhesives from natural resources or metal or ceramic matrices. The main adhesive types used in natural fiber-based composites will be summarized in the following sections. Other types of adhesives or matrices less commonly used but of possible future potential are surveyed in Appendix A. Such reviews of adhesives and matrices are to select one that may be appropriate for use in the new composite structures being explored in the present work.

In a thermosetting polymer, the constituent molecules are chemically joined together by cross-links and form a rigid three-dimensional network structure. Once these cross-links are formed by the polymerization reaction, the thermosetting polymer cannot normally be melted or reshaped by applying heat or pressure. It will, however, become evident in the research presented later in the present thesis that certain polymers (including phenol formaldehyde) do exhibit thermally-dependant physical properties (see section 4.3.5 and 5.4). Most wood adhesives, such as urea formaldehyde and phenol formaldehyde, are regarded as thermosetting polymers.

2.4.4.1. Urea formaldehyde resin

Urea formaldehyde (UF) resins are most commonly used in manufacturing wood-based composites such as particleboard (PB) and some types of medium density fiberboard (MDF). The first stage of the reaction is the addition of formaldehyde to urea molecules to form monomethylol urea. Then, the monomethylol urea reacts with itself in a second stage to form a large molecule (Pizzi, 1983). Figure 2.5 shows the reaction of UF adhesives.

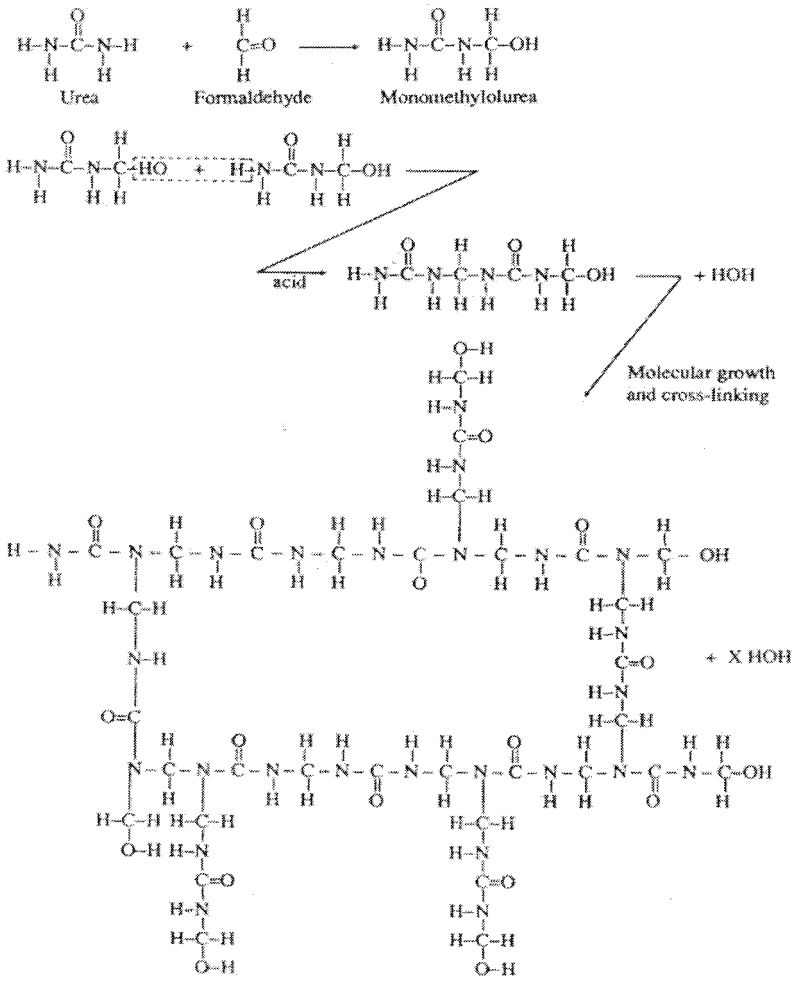

Figure 2.5. Reaction of urea formaldehyde adhesive (Marra, 1992)

By proper selection of catalyst and additive, it is possible to employ UF adhesives in a wide range of applications. Most forms of the cured resin are hard, brittle and creep-resistant. The cost of the resin is lower than most alternatives. The disadvantage of UF resin is its relatively poor resistance to long periods of wetting, and it emits formaldehyde vapor which may be toxic to human health (Marra, 1992).

2.4.4.2. Melamine formaldehyde adhesive

Melamine formaldehyde (MF) adhesives are often used to improve the water resistance of UF adhesive and may also act as a scavenger for excess formaldehyde and thereby reduce formaldehyde emission. Therefore, they are used for wood composites where better water resistance than UF is needed. The first stage of the reaction is the same as that for UF resins such that amine groups in melamine are reacted with formaldehyde to form methylol groups, which can condense to methylene bridges. The cyclic structure of melamine imparts greater stability and the three amine groups assure a three dimensional, cross-linked structure (Figure 2.6).

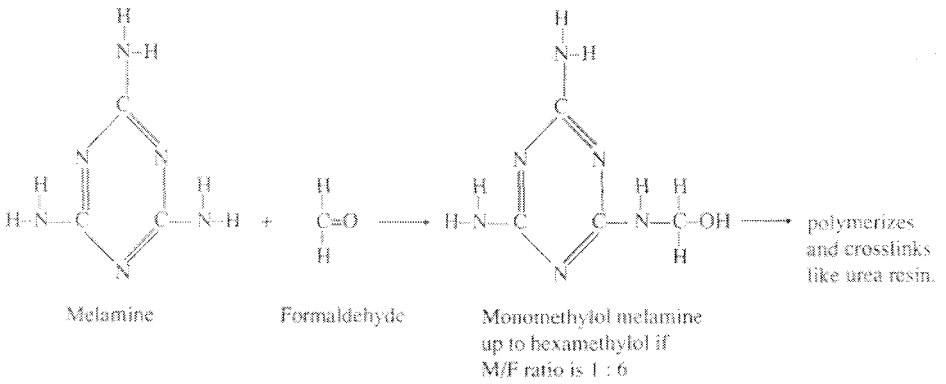

Figure 2.6. Reaction of melamine and formaldedhyde (Marra, 1992)

2.4.4.3. Phenol formaldehyde adhesives

Phenolic resin is widely used in manufacturing wood-based composites which need greater water resistant properties than those offered by UF. Phenolic

resin is the reaction product of phenol with formaldehyde (Figure 2.7). The first stage of the reaction is the addition of formaldehyde to the active ortho- or para-positon of the phenol to form mono-, di- and tri- methylol derivatives. The second stage of the reaction is the condensation of methylol phenol with itself or other phenol. Under proper temperature and pH conditions, three dimensionally cross-linked molecules are formed through methylene bridging (Pizzi, 1983).

Two distinctly different types of resin are made depending primarily on the molar ratio of phenol to formaldehyde. If the ratio is less than 1, the resin will be rich in methylol groups and capable of polymerizing to a cross-linked, insoluble state without adding other catalysts. Such resin is called a "resole" type. It's main characteristic is that it is ready for curing provided that it is exposed to the appropriate environmental conditions (principally temperature). A disadvantage of resole PF is that it continues to cure in storage and therefore has a limited shelf-life. When the ratio of phenol to formaldehyde is greater than 1, the resulting resins will lack methylol groups and its molecules will be linear in nature under acid condition. Such resin is called "novolac". The main characteristic of novolac is that it is unable to polymerize independently; to start curing, some type of hardener should be added at the point of use. Both the resole and novolac resins go through distinct stages from initial to final reaction. The A-stage represents the first reaction products of methylol. The B-stage is the early condensation products of A-stage in which polymerization has begun. However, the polymerization process is confined to relatively low molecular-weight resin. The C-stage leads to the final cured state; this must be attained in order to assure maximum strength and durability. Schematic diagrams of curing mechanisms of resole and novolac are presented in Figure 2.7. Most forms of fully cured phenolic resin are glassy, hard and brittle.

Resole type phenolic resins are the most widely used thermosetting adhesives for manufacturing structural wood-based composites because of their high bond strength, resistance to degradation, and relatively high bond strength in wet condition (Marra, 1992; Pizzi, 1983). However, the drawback of PF resin is

that it requires high temperature and longer time to form a bond than that of UF or MF.

Pizzi and Stephanou (1994b) found that some types of ether such as polycarbonate and methyl formate can accelerate curing of PF resin (see section 2.8.2). The acceleration of PF resin curing by the addition of an ester was confirmed by Chowdhury (1999). In the present research, PF resin will be used because of the feasibility of catalyzing PF by the application of a chemical (such as methyl formate) at near-ambient temperatures.

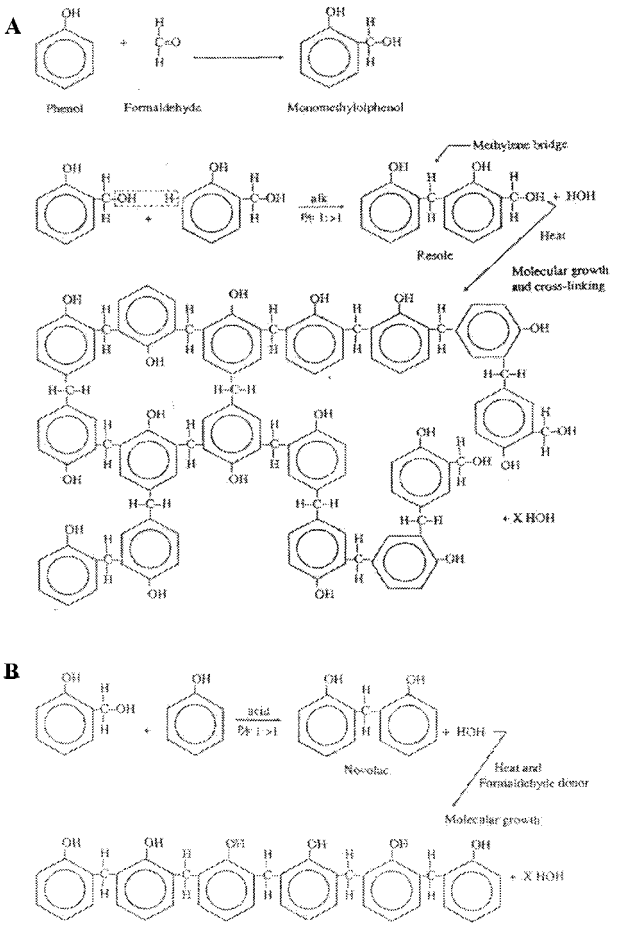

Figure 2.7. Reaction of phenol formaldehyde adhesives A: resol; B: novolac (Marra, 1992)

2.4.4.4. Isocyanate adhesives

Isocyanate resins are dependant on the high reactivity of the isocyanate radical (-N=C=O). Combined with strong polarity, the compounds that carry this radical have not only good adhesion potential, but also the potential for forming covalent bonds with substrates having reactive hydrogen (Marra, 1992). Reaction of a bi-functional isocyanate with a bi-functional alcohol produces linear molecules, while tri- and tetra functional molecules allow cross-linking. So, the properties of these materials can be varied through a wide range from elastomeric to rigid structural parts. The isocyanate that is most commonly used is polymeric methylene-diphenyl-diisocyanate(PMDI). The isocyanate resin provides good bonding properties, high moisture resistance, and high dimensional stability compared to phenolic or amino resin. However, the resin can cause unwanted sticking to press platens or cauls in panel pressing and is toxic in the uncured state (Skinner, 1999). Initial and polymerization reaction of isocyanate resin is shown in Figure 2.8.

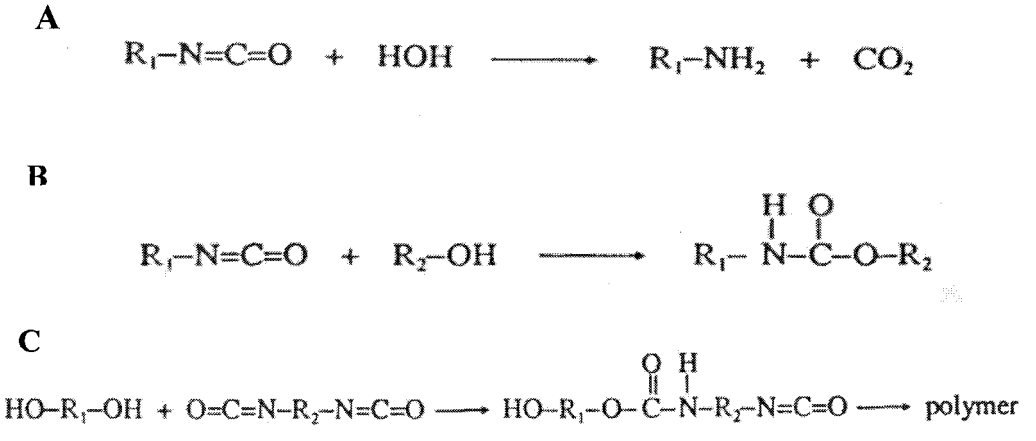

Figure 2.8. Initiation reaction of isocyanate resin with water and alcohol A: initiation with water; B: initiation with alcohol; C: polymerization with dihydric alcohol and di-isocyanate (Marra, 1992)

2.5. CURING BEHAVIOR OF SELECTED THERMOSETTING ADHESIVES

2.5.1. Bond strength development during processing

The rate of polymerization and consequent strength development of thermosetting adhesives are highly, but variously, dependent on temperature. A number of research efforts have been devoted to understanding curing and consequent bond strength development of thermosetting adhesives. Analytical techniques have been used to characterize curing behavior by monitoring either mechanical, physical, or chemical changes during the curing process. These techniques include dynamic mechanical analysis (DMA) (Young *et al.*, 1981; Geimer *et al.*, 1990; Kim *et al.*, 1991; Follensbee *et al.*, 1993; Christiansen *et al.*, 1993), torsional braid analysis (TBA) (Steiner and Warren, 1981), differential scanning calorimetry (DSC) (Chow and Steiner, 1979; Christiansen and Gollob, 1985; Wang *et al.*, 1994), differential thermal analysis (DTA) (White and Rust, 1965; Katovic, 1967; Chow, 1972; Chow *et al.*, 1975), ultraviolet spectroscopy (Chow, 1969), nuclear magnetic resonance (NMR) (Maciel *et al.*, 1984), and Fourier transform infrared spectroscopy (FTIR) (Meyers *et al.*, 1991). Each of these will be summarized below.

2.5.2. Dynamic Mechanical Analysis

Dynamic mechanical analysis (DMA) systems measure in-phase or out-of-phase responses of samples subjected to controlled mechanical oscillation in tensile, compression, shear, or bending modes. The storage modulus (E′), loss modulus (E″), and tan-delta which is given by E″/E′, can be calculated from the

data. The major application of DMA to thermosets has been in the identification of glass transition temperatures (Tg). This is detected by identifying temperatures at which the loss modulus or tan-delta have maxima (Prime, 1997).

Kim (1991) and his co-workers have used DMA to investigate the cure of phenol-formaldehyde resole resin over a wide temperature range. Curing temperatures began at 50°C, and thereafter were increased at a rate of 25°C/min up to various temperatures between 110°C and 225°C. This fast initial heat up was affected to reproduce hot pressing conditions being used in the manufacture of wood composites. However, the temperature variations at specific locations within such composites during pressing differ through the thickness direction. This is because heat energy is transferred into the core both by conduction and vapor convection (as described in section 2.3.1.). Temperatures used in DMA analysis may be increased according to the measured or simulated temperature variation at one specific location during pressing in order to explore exact property changes of the resin at specific locations.

From their DMA study, Kim and his co-workers inferred that the adhesive strength at the core layer of oriented strand board (OSB) when the press is opened resulted from gelation of adhesives, not from vitrification. This is because conventional hot pressing time and temperature for OSB were not sufficiently long to vitrify the adhesive. However, since their main objective was to provide detailed observations of the rigidity increase and loss modulus change during curing of PF adhesives, no concrete evidence was provided to reliably infer physical states of adhesives during hot press opening. It was in part due to this deficiency that physical transformations of adhesives were explored in the present thesis.

Follensbee and his co-workers (1993) used DMA to measure the degree of cure of PF resole resins as a result of exposure to various temperature-humidity-time regimes. They refined the conventional DMA technique in order to measure the curing of aqueous PF resin. This included the selection of a substrate for resin loading, clamping geometry, and sample humidification prior to analysis. It was

found that the storage modulus ultimately attained in a DMA scan was effected by the amounts of pre-cure and moisture in the sample prior to scanning. Follensbee and his co-workers suggested that this behavior was induced by a change in glass transition temperature due to the level of cure and plasticization by water. They also indicated that the area under the isothermal DMA tan-delta curve might represent the relative degree of cure. Such an assertion does not however, have any fundamental analytical justification, though it does provide a qualitative indication of cross-linking and associated physical effects on the adhesive.

For the selection of an optimum substrate for the DMA experiments, Follensbee defined several criteria and a pure borosilicate glass microfiber filter (WhatmanGF/C) was selected. Usually, the substrate for DMA analysis is a glass fiber filter because it does not interact chemically with resin and maintains constant mechanical properties over a wide range of temperature. This type of substrate may provide good information on the curing of thermosetting resins without any interaction with substrates. However, during curing of thermosetting resins in wood-based composites, complicated interactions between wood and resin almost certainly do take place. Although the result from DMA analyses with non-interacting substrates may provide useful data, such as the storage modulus, the loss modulus, and the glass transition temperature, it may not be feasible to directly relate the results to bond-strength development of wood based composites during hot pressing.

2.5.3. Torsional Braid Analysis

Torsional braid analysis (TBA) is a special form of dynamic mechanical technique which measures torsional oscillation of resin-impregnated braid (Prime, 1997). In TBA, a fibrilar braid is impregnated with the liquid resin. The braid is then intermittently torqued through a small angle and allowed to freely oscillate

during a curing or temperature scanning experiment. The response of the resin-impregnated braid provides a relative storage modulus and relative loss modulus which can provide some indication of physical and mechanical changes sustained by the resin (Sperling, 1986).

Gillham and his co-workers have carried out extensive research work on solventless thermosets such as epoxies using TBA (Enns and Gillham, 1983; Wisanrakkit *et al.*, 1990; Simon and Gillham, 1994). They showed that the mechanical response of the resin is highly dependent on the two phenomenological events of gelation and vitrification. Gelation can be defined as a process in which the liquid polymer turns into a rubbery state. From the chemical point of view, gelation may be regarded as the point when the cross-linking extends throughout the polymer. Vitrification is the process by which the polymer passes into a glassy state. During vitrification, the molecular segment of the polymer is immobilized and the rate of chemical cross-linking is depressed. Enns and Gillham (1983) measured gelation and vitrification times at various curing temperatures with TBA and developed time-temperature-transformation (TTT), and continuous heating transformation (CHT) diagrams. Details about curing diagrams, including TTT and CHT, will be discussed later in this chapter (see section 2.5.7.) along with other curing diagrams since they relate directly to the bond cooling experiments conducted in the present thesis.

Steiner and Warren (1981) studied rigidity and damping changes during and after cure for different types of wood-adhesives using TBA. A multifilament glass braid was impregnated with resin and this was analyzed both isothermally and at a programmed heating rate in a nitrogen atmosphere. Steiner and his co-workers found that the relative damping curve of phenol formaldehyde adhesive scanned at constant heating fluctuated at the early part of the scan and later, relative damping decreased. This is consistent with adhesion kinetics studies reported by Humphrey and Bolton (1979) where strength development at early and intermediate stages of cure exhibited complex fluctuations before the establishment of a well-defined and

near-linear isothermal strength development phase. Relative rigidity in Steiner's approaches slowly increased between 80°C and 120°C. Above 120°C, rigidity increased dramatically. Steiner compared TBA with DSC thermograms of the same resin at identical heating rates. DSC thermograms showed two endothermic peaks. The first peak, which had a large endothermic region, appeared at about 100°C and might be attributed to liquid water loss and some polymerization of the resin. The second peak occurred at about 120°C and was possibly due to the condensation reaction of the resin. Steiner concluded that, together with chemical reactivity data and other thermal analysis data, the onset of an increase in rigidity might be used to define minimum pressing time for composites. However, it is questionable to infer minimum pressing time from such chemical reactivity and thermal analysis data without detailed discussion about interactions with wood. Also, it may be more logical to follow a heating profile in TBA testing which is similar to that at specific locations in wood-based composites during hot pressing to simulate the curing of the resin.

2.5.4. Differential Scanning Calorimetry

Differential scanning calorimetry (DSC) measures heat generation and consumption of a material as a function of time and temperature. This technique is useful when exploring curing kinetics such as the extent and rate of chemical conversion, and thermodynamic properties like glass transition temperature and associated vitrification.

Wang and his co-workers (1994) studied PF resin cure at various pre-cure, moisture, and relative humidity conditions using DSC. They impregnated laboratory-synthesized phenolic resin into a pure borosilicate glass microfiber filter and pre-cured it at various times, temperatures and moisture conditions before conducting DSC scans. Wang *et al.* found that the rate of resin cure increases with

increasing pre-cure temperature. In addition, they suggested that moisture within a sample promotes resin cure by increasing molecular mobility and allowing more complete and higher degrees of cure. On the other hand, the moisture may retard resin cure by diluting reactive components of the resin. Wang found that the resin cured faster and achieved a higher degree of cure with increasing relative humidity, which indicates that the absorbed moisture in the sample did indeed enhance molecular mobility and thus increased reactivity of the resin.

2.5.5. Combined analysis

Other researchers have investigated curing of PF and other thermosetting resins by combining two or more analytical techniques. Geimer and his co-workers (1990) explored the curing of PF resins using DMA and DSC. From this, they explored correlations between mechanical and chemical cure behavior. They also proposed a technique to determine resin-flake bond strength development under various environmental conditions and explore resin penetration into wood and other spectroscopic techniques to provide supplementary data to rationalize curing of PF resins.

Myers and his co-workers (1991) carried out extensive research on the curing and bonding of two different PF resole resins. They characterized the two resins in terms of their structure and chemistry during synthesis, aging, and cure using viscometry measurement, GPC, NMR, FTIR, DSC, and DMA. Meyers *et al.* also evaluated the suitability of DSC, DMA, and FTIR techniques for measuring the degree of cure. The chemical and mechanical cure data measured by DMA and DSC were also studied in detail by Christiansen and his co-workers (1993). They applied DMA and DSC to analyze PF resole resins that had been previously cured under dry conditions. This research was extended by incorporating lap-shear bond strength tests and pre-conditioning prior to DMA and DSC analysis, and internal

bond strength testing at various relative humidity conditions. From the study, they concluded that the chemical cure measured by DSC generally develops at slower rates than mechanical cure measured by DMA. They raise the interesting hypothesis that the major limiting factor in press opening in wood composite manufacturing is low strength of the cured resin rather than the extent of resin cure. They indicated that the strength of cured resin is substantially weakened by moisture. They inferred that bond strength may be increased by lowering moisture content at the end of hot pressing, which has some potential for minimization of hot pressing time.

2.5.6. Direct measurement of bond strength development

The above-mentioned analytical techniques mainly focus on the measurement of physical and chemical characteristics during curing of thermosets. These methods may be closely correlated with the rate of bond strength development. However, in the absence of adherends, the rate may not be reliably assessed.

Aside from mostly indirect methods of inferring bond strength development upon curing, direct methods under controlled conditions have been investigated. Humphrey and Bolton (1979) developed a technique to evaluate bonding reactivity of UF adhesives by constructing bond strength versus time curves with various hot pressing temperatures for miniature test bonds cured isothermally. Similar tests were subsequently conducted by Humphrey and Zavala (1989). In their research, identically assembled adhesive bonds were formed under a diversity of near-isothermal conditions (temperature and time) and immediately thereafter tested in tension perpendicular (Humphrey and Bolton, 1979) and in lap-shear mode (Humphrey and Zavala, 1989). Humphrey and Ren (1989) also investigated the combined effects of temperature and moisture content on powdered PF adhesive

bond strength development. They developed a device enabling bonds to be formed under highly controlled temperature and moisture conditions in a hermetically sealed environment; such bonds were tested right after the end of pressing to various levels.

Following from the above experiments, Humphrey (1993) developed an Automated Bonding Evaluation System (ABES) enabling bonds to be formed efficiently under various temperatures, pressing pressures and time conditions and tested immediately after in shear mode (Figure 2.9). The system can be used to explore bond strength development rates of a variety of adhesives and adherend combinations as a function of time and temperature.

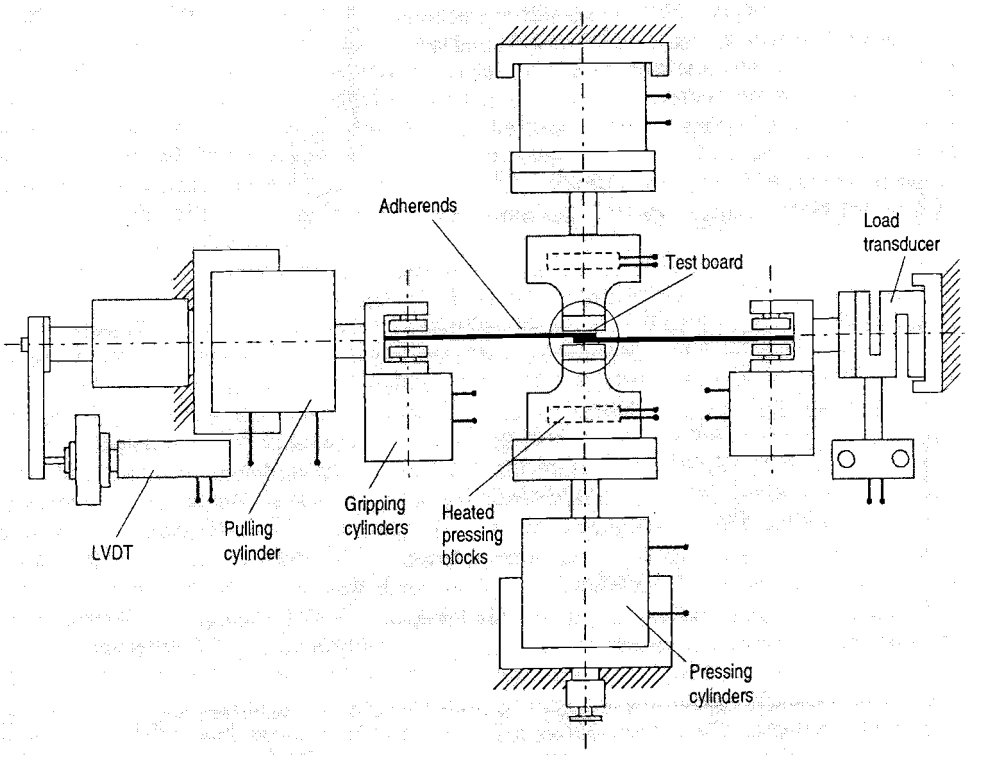

Figure 2.9. Schematic diagram of the ABES concept.

The above-mentioned studies have been conducted while test bonds were at curing temperature rather than being cooled down before testing. This is of importance because upon industrial press opening, loads from "destructive" factors (internal residual micro-stress and pressures of entrapped fluids) are transferred to the bonds in the hot condition. Most of the research work to date has therefore concentrated on the bond strength dictated by curing rather than testing temperatures. Preliminary trials in the present study have, however, revealed that the testing temperature of partially cured phenol-formaldehyde lap shear bonds greatly effects their strength. In that work, the ABES device has been enhanced by incorporating a computer controlled and pneumatically driven cooling head, which provides rapid cooling of the formed bonds immediately after pressing but before pulling.

In readiness for discussing these innovations (see sections 4.3.5 and 5.4), the underlying concepts of the time-temperature-transformation (TTT) diagram proposed by Gillham and his co-workers will be discussed.

2.5.7. Concept of various bond curing diagrams

One notable piece of research on the curing of thermosetting adhesives concerns the conceptualization of isothermal time-temperature-transformation (TTT) cure diagrams (Figure 2.10). In such diagrams, phenomenological changes such as gelation and vitrification of thermosets are plotted with isothermal cure temperature and time (Enns and Gillham, 1983).

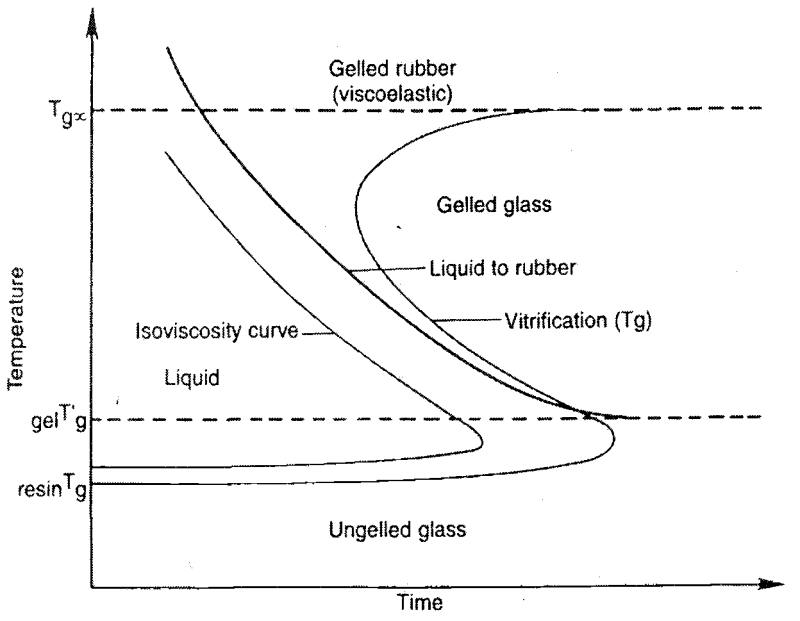

Figure 2.10. Generalized time-temperature-transformation diagram for thermosetting polymers (Enns and Gillham, 1983)

The TTT diagram may be divided into four distinct regions, which demarcate liquid, rubber, ungelled glass, and gelled glass. The s-shaped curves reflect transitions of vitrification and gelation. Further, continuous heating transformation diagrams, which are similar to TTT diagrams, report the times and temperatures required to reach similar phenomenological changes such as gelation and vitrification during continuous heating at a constant heating rate (Wisanrakkit *et al.*, 1990). Although a useful contribution to analyzing curing process of thermosets, TTT and CHT diagrams mostly have been applied to adhesives cured under artificial conditions such as glass braids; results are largely specific to the resin alone.

Pizzi and his co-workers (1999) developed a modified CHT (TTT) diagram which incorporates interaction of formaldehyde-based thermosetting resins

and wood substrates (Lu and Pizzi, 1998; Pizzi *et al.*, 1999). Figure 2.11 shows a modified CHT diagram of formaldehyde based adhesives.

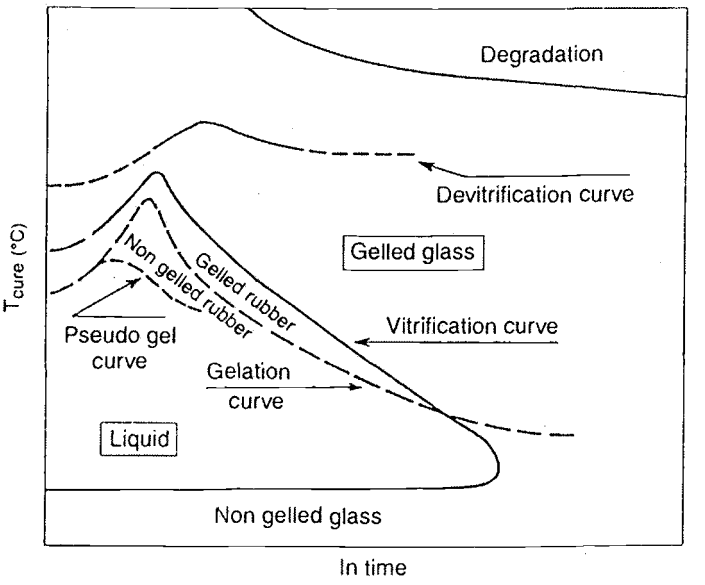

Figure 2.11. Modified, generalized continuous heating-transformation diagram for UF and PF polycondensates cured with interacting lignocellulosics (Lu and Pizzi, 1998)

The research results suggest that resin phase transitions due to resin-wood substrate interactions are complex. This modified CHT diagram can be used to investigate the behavior of formaldehyde based resins such as UF and PF when used with wood.

From the above mentioned research, it is clear that curing time and temperature effect the physical state of the thermosetting resin. The transition between liquid, gelled rubber, and glass is closely related to the degree of cure which is, in turn, positively related to glass transition temperature (T_g). It has been acknowledged that some properties of thermosetting resins may be little affected by

temperature within certain defined limits. In the present research however, the effect of testing temperature on bond strength of PF adhesive will be explored directly (see sections 4.3.5 and 5.4).

2.6. ORIENTATION OF NATURAL FIBERS

One of the important factors to achieve material properties that meet specific end-use requirements in the strategy proposed by Humphrey (1994) is spatial distribution of fiber orientation. The influence of particle orientation on the properties of wood composites was first explored by von Klauditz and his co-workers (1960) who proposed using electrostatic fields to orient wood particles. This led to the development of an electrostatic orientation process for manufacturing oriented particulate wood-based composites (Talbott and Stefanakos, 1972; Talbott, 1974; Suchsland and Woodson, 1987; Kawai *et al.*, 1989; Yoshida *et al.*, 1988; Yoshida *et al.*, 1989; Kawai *et al.*, 1987; Yoshida *et al.*, 1990; Pulido, 1991a; Pulido, 1991c; Pulido, 1991b). Recently a mechanical orientation method for non-wood fibers was also developed (Kenji *et* al., 2000).

Little attention has, however, been directed towards control of orientation in natural fiber-based composites. Medium density fiberboard (MDF) exhibits poor specific strength and stiffness due to the lack of orientation of the fibers in the X-Y plane (Kawai and Sasaki, 1989). A research objective of the initiative of which the present thesis is a part, is to find means of affecting high levels of spatial orientation in fiber-based composite products. With this objective in mind, Zauscher and Humphrey (1997) explored the use of magnetic fields to orient wood fiber bundles pre-treated with very small quantities of a ferromagnetic substance. They suspended ferromagnetically modified wood fiber bundles in silicon oil and found that the magnetic torque, which causes rotation, linearly increased with the amount of magnetic substance applied on the wood fiber bundle. Also, the

correlation between magnetic torque and strength of the applied field below magnetic saturation was quantified.

In the present thesis, manually pre-oriented hemp fibers have been used to form small rectangular composite beams. No attempts were made to orient wood fibers used in this study. However, some preliminary work related to the magnetic orientation of wood fiber bundles were conducted to produce an array of oriented pre-forms but this work will not be reported in this thesis.

2.7. CHEMICAL MODIFICATION

In conventional hot pressing processes, heat from high temperature platens and moisture inside the fiber mat plays an important role in affecting stress relaxation, and creating density gradients, as well as curing of adhesives. However, in the present thesis research, alternative ways to create such density gradients and to accelerate curing of PF bonds at low temperatures were explored. This may greatly reduce energy consumption necessary to synthesize natural fiber composites and provide the potential to control internal structure of molded composite objects. Ammonia has been used as a plasicizing agent and methyl formate as a low-temperature catalyst of applied PF adhesive. The underlying nature of these effects will be summarized below.

2.7.1. Treatment with ammonia

Chemical modification of natural plant fiber had been widely studied to enhance various properties such as dimensional stability and resistance to biodegradation. Chowdhury (1999) as well as Rowell (1983) and Hon (1996) thoroughly reviewed a variety of chemical modification approaches for natural

fibers including wood. Most methods depend upon substituting a portion of the hydroxyl groups in the cell wall, or blocking such groups with other groups. The major types of chemical modification of natural fibers employed to date are broadly termed esterification, etherification, and acetylation.

One of the specific objectives of the present thesis research is to plasticize fibers with chemicals injected during pressing, thus resulting in internal structure and property gradients. Plasticization of wood can be achieved by benzyation, acetylation, and treatment with ammonia. In this research, ammonia was selected to plasticize natural fiber mats.

Stamm (1955) first recognized that ammonia can cause plasticization in wood and reported that liquid ammonia swelled wood more than does water. Schuerch (1963) showed that wood can be effectively plasticized and formed into various shapes. He also found that ammonia-plasticised wood may be more easily rendered permanent than when using steam. Davidson (1968) also reported that wood plasticization can be affected with gaseous anhydrous ammonia at room temperature under ammonia pressures of 0.99MPa. He pointed out that the moisture content (about 10-12%) of the wood enhanced the rate of sorpion of ammonia. Bariska *et al.* (1969) and Davidson and Baumgardt (1970) also reported that plasticization of wood can be obtained by treating it with gaseous ammonia when relative vapor pressure of ammonia was close to saturation. Bariska *et al.* (1969) reported some similarities between the sorption of ammonia vapor and that of water by wood.

The general mechanism of the plasticizing process is such that adsorbed ammonia first breaks some hydrogen bonds within both amorphous and crystalline regions of the carbohydrate and lignin portions of the cell wall. This is in contrast to the effects of water molecules which appear only to penetrate portions of the amorphous regions of carbohydrates; the carbohydrate and lignin then sustains permanent relocation. Removal of ammonia by evaporation appears to form new

hydrogen bonds at new locations and new cross-linked structures are thus produced. This mechanism results in a substantial level of permanent set.

All of the above mentioned work was conducted with solid wood specimens and rates of softening were found to be rather too low for application to many high-volume production technologies. Chowdhury (1999) did, however, apply gaseous ammonia to more accessible networks of wood fibers in order to explore the potential for rapid softening approaches.

Using a small circular sealed gas injection press, he injected gaseous anhydrous ammonia into wood fiber mats and explored the softening that resulted. Under various treatment times, temperatures and ammonia vapor pressures he found that the softening action occurred very rapidly at moderate vapor pressures (above 0.16MPa) and at relatively low temperatures (below 40°C). The results of Chowdhury's work indicated that ammonia vapor pressures above 0.16MPa might be sufficient to produce useful levels of softening of wood fiber mats at acceptable speed. The softening action of ammonia stayed almost constant at temperatures ranging from 20 to 40°C, but, surprisingly, above 40°C, the softening action appeared to decrease. The present work will suggest that this effect may be the result of decreasing saturation level that occurs with increasing temperature (section 5.5).

The above findings indicate that plasticizing of fiber networks and reduction of residual stress may be achieved at low temperature as ammonia gas is injected. It appears that ammonia gas injection has potential to be used to control the internal structures of composite products during consolidation, especially in affecting softening- induced density variations during pressing at low temperature.

When ammonia is used to plasticize adhesive-treated wood elements, care has to be taken to consider the possible effect of the ammonia on the polymerization mechanisms of the adhesive being employed to bond the composite together. Phenol formaldehyde adhesive has also been employed in the present work. This clearly raises the issue of the effect of elevated pH on PF resin cure. The

effect of pH on PF resin cure kinetics and acceleration of PF cure will therefore be summarized below.

2.7.2. Treatment of PF with methyl formate

It had been widely accepted that the curing of PF (resole) resins accelerates at high pH (Pizzi, 1983; Skeist, 1990). Figure 2.12 shows the effect of pH on gel time of PF resin. The solid line in Figure 2.12 up to pH 9 had been experimentally verified, but the dashed line for pH above 9 was extrapolated.

Until recently, no experimental research was performed to verify this trend in the literature regarding the reactivity of PF resins over pH of 9. Pizzi and Stephanou (1994a) did, however, measure the reactivity of resole type PF resins beyond pH 9 and found that the curing behavior of the resin is very different from that previously assumed. They reported that gel time of PF resin greatly increased (cure rate decreased) beyond pH 9 (Figure 2.12).

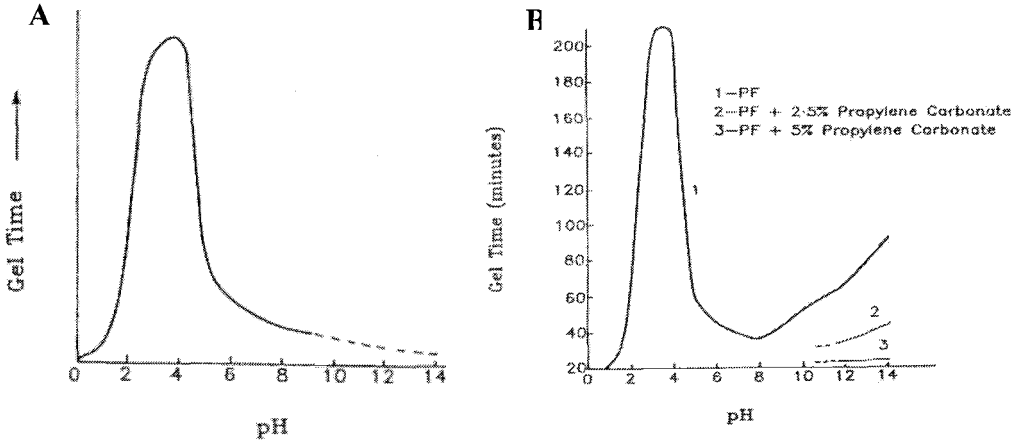

Figure 2.12. Effect of pH on gel time of PF resin. A:The dashed-line indicates extrapolated assumption of PF resin at such pH; B: Solid line beyond pH 9 indicates measured reactivity on the gel time (Pizzi and Stephanou, 1994a)

Pizzi and Stephanou (1994b) also found that curing of resole type PF resin can be accelerated by applying esters such as propylene carbonate and methyl formate. Dependence of curing time of PF resin on types of ester added is shown in Figure 2.13. Propylene carbonate was found to rapidly accelerate curing at low concentration, but at higher concentration the effect diminishes. Methyl formate also shows very good curing acceleration. In a gas injection system, a degree of volatility is required so that the esters can be injected in a gaseous form. Methyl formate, which has a relatively low boiling point (about 33°C) at atmospheric pressure is therefore a good potential candidate for acceleration of PF curing. The acceleration of curing by esters is due to an increase in the number of cross-linking sites in the PF resin. The chemistry of this reaction is explored fully in Pizzi and Stephanou (1994a,b).

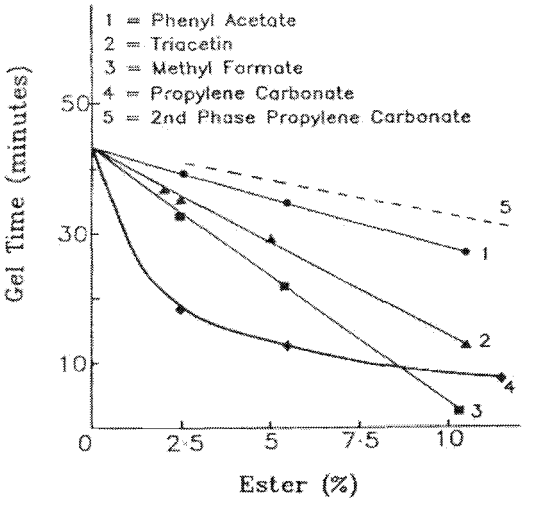

Figure 2.13. Effect of the addition of various esters on gel time of PF resin (Pizzi and Stephanou, 1994b)

2.8. DENSITY GRADIENTS IN CONVENTIONAL NATURAL FIBER-BASED COMPOSITES

It has been widely acknowledged that many of the hot pressing process parameters effect the internal structure, especially density gradient, of conventional panel products such as particleboard and MDF (Strickler, 1959; Heebink *et al.*, 1971; Geimer *et al.*, 1975). It has also been recognized that important physical and mechanical properties, such as in-plane bending, in wood panel products such as MDF or PB are greatly effected by density profile (Suchsland, 1967; Geimer *et al.*, 1975; Woodson, 1976; Wong *et al.*, 2000). The present work involves taking a pro-active approach to manipulating density distributions in structural members. Prior work on density profiles in conventional composites will therefore be surveyed with a view to laying groundwork for the present work.

Strickler (1959) performed a comprehensive study to investigate the effect of press cycle, moisture content, and moisture distribution on physical properties such as layer density, modulus of elasticity, modulus of rupture, and dimensional stability. He was one of the first to find that press cycle, moisture content and moisture distribution had a strong effect on the creation of density variations. Strickler appreciated qualitatively that higher initial furnish moisture content created greater density variations and the variations become even greater with elevated surface moisture content. Such a non-uniform moisture distribution along with high initial compaction pressure resulted in high surface density and low core density. Strickler also mentioned that during hot pressing, the rate of initial heat penetration to the center layer increases as over-all moisture content of the mat increases, as the surface moisture content increases, and as initial platen pressure increases. High surface moisture content within limits improved modulus of rupture (MOR). When high moisture content with high initial pressure was used, modulus of elasticity (MOE) was significantly increased. However, excessively high moisture content degraded bond strength beneath the surface. Also, high moisture

content distribution through the thickness adversely effected the internal bond strength while constant-pressure press cycle developed superior internal bond strength. These empirical observations have been recently verified theoretically by Thömen and Humphrey (2002) using the deterministic simulation models mentioned in section 2.3.

Suchsland (1959) suggested a statistical model for a particleboard mat by deriving relationships between the degree of densification and particle geometry, relative air volume, and component wood density. The particle thickness varied substantially; when the entire mat was compressed to a given uniform thickness; some regions with high total particle thickness were compressed to a larger extent than those with low thickness. Suchsland determined that relative compression area is the important factor in developing bending strength in a flakeboard.

Heebink *et al.* (1971) explored the effect of several pressing variables on panel structure and properties. Those variables included species, particle geometry, board density, board thickness, moisture content and distribution, and pressing time, temperature, and closing speed. Initial moisture content and distribution within the mat were again found to be the most influential factors on density gradient. Press closing speed and press temperature also had affects on the density gradient. The results obtained by Heebink and his co-workers on the effect of moisture distribution on density gradient agree with those of Strickler's (1959).

Geimer *et al.* (1975) investigated the effects of several processing variables and panel thickness on the density distribution. They constructed three-layered particleboard and found that thicker boards had steeper density gradient. They predicted board stiffness using the theory describing structural sandwich construction and compared it to the measured stiffness. The predicted stiffness values ranged from 63 to 110% of the measured data for two-point loading, and 72 to 120 % for single point loading. A multilayer analysis method was also used to more precisely predict board stiffness.

Woodson (1976) evaluated density profiles and fiber orientation in order to investigate their effects on some mechanical properties of medium density fiberboard. He used x-ray techniques to measure the density profiles and predicted MOE for panels. In his research, orientation of fibers was manipulated by electric field. Woodson found that most mechanical properties, such as bending MOR, tensile strength, compressive strength, and MOE, were greater for the MDF with a density gradient. He pointed out that the oriented fiberboards made at lower overall densities had properties equal to those of random boards of higher densities.

Smith (1982) was another that reported the press closing time influences the shape and range of the density profile. He suggested fast press closing time because of the consequent denser face layers which provide higher bending strength. Although he mentioned that the shape of the density profile strongly influenced the board strength, he clearly neglected the effect of the density profile on internal bond strength.

Plath and Schnitzler (1974) found a high correlation between density profile of particleboard and tensile strength perpendicular to the panel surface. Schulte and Früwald (1996a) investigated five different thicknesses of furniture-grade particleboard to derive relationships between internal bond parameters from density profile, and the respective failure position. They reported that the correlation between mean density and internal bond is high ($r=0.81$), but that the correlation between minimum density and internal bond is lower. Schulte and Früwald (1996b) also investigated the relationship between failure position and density profile of MDF panels and pointed out that most MDF specimens fail in a region between 15 to 35% and 65 to 85% of the panel thickness.

Wong *et al.* (1998) explored the effect of mat moisture content and press closing speed on the formation of density profiles and properties of isocyanate bonded Lauan (*Shorea* spp.) particleboard. They defined several features of density profile in detail; those were peak density (mean of the highest densities measured within each half of the profile, PD), core density (mean of the central region located

within 20% of total board thickness, CD), peak distance (distance of peak density from the board surface, Pdi), peak base (distance between intersections of the density profile contour, Pb), and gradient factor (horizontal distance between the center line, from the mid point to the profile contour, GF). Not surprisingly, they found that the peak density could be increased by combining high moisture content particles at the surface and low moisture content particles at the center. They also pointed out that higher press closing speed reduces Pdi and Pb, with an increase in GF. At lower mean density, the PD could be increased by applying a faster press closing speed, but the effect diminished as the mean density increased. The MOE of the particleboards with high MC near the surface were higher than those with uniform MC, whereas MOR is subjected to the effect of many other factors including PD. Internal bond strength is largely dependant on the CD.

Wong and her co-workers (1999) explored the effects of density profile on the physical and mechanical properties of particleboards bonded using Lauan (*Shorea* spp.) with isocyanates. They produced two-types of particleboard; flat density profile and conventional "U" shaped density profile. Wong and her co-workers found that in homo-profile boards, the MOR and MOE, internal bond strength, and screw withdrawal resistance are highly correlated to the board mean density. They also reported that at equal mean density level, the MOR and MOE of the conventional particleboards were higher than the homo-profile boards because of the high density near the face.

Wong and her co-workers (2000) also investigated the effects of the hot pressing method and mat moisture distribution on the formation of density profile. Statistical analysis indicated that there was a large variation in peak and core density. They also found that the difference between peak and core density of the boards produced using a two-step hot pressing method was substantially high.

Song and Ellis (1997) explored heat transfer, bond strength, and dimensional stability in terms of numbers of flakes in specific uniaxially compressed columns (24, 30, and 40 flakes), face flake moisture contents (5 and

15%), and press closing time (15 and 45seconds to reach target thickness). Aspen flakes (55.0mm in length, 17.5mm in width, and 0.69mm in thickness) mixed with powder PF resin was used to make the flake assemblies. It was found that heat transfer to the core of the assembly was accelerated by a short press closing time, higher moisture content in face flakes, and a lower number of flakes in an assembly. Also, relative density differences between face and core layers were greatest for low numbers of flakes. Bond strength and thickness swelling were highest in face layers and decreased with density profile. The conventional fiberboard with "U" shape density profile showed higher MOR values than homo-profile boards but MOE values were similar. The internal bond strength and screw withdrawal resistance were entirely dependent upon the core density and mean density, respectively.

Suo and Bowyer (1995) reported a model to predict bending properties (MOR and MOE) and internal bond strength of nonoriented structural flakeboard. In the model, each layer of a panel was considered as a plane and to be orthotropic. Overall panel MOE and MOR were calculated based on panel layer properties. They verified their model by experimental results and mentioned that the predicted MOE and MOR were reasonably accurate.

Hata *et al.* (1989) studied the effects of steam injection time and timing on the properties of particleboards. They found that in conventional hot pressing, the "U" shape density gradient was prominent whereas in steam injection pressing the density distribution was rather uniform. The flexure properties of the higher mean density board made with steam injection pressing had smaller values than those made with conventional hot pressing. The internal bond strength of the boards, however, was much greater than conventionally pressed boards. They also indicated that the properties of the boards were almost independent to the steam injection time.

Wang and Winistorfer (2000) used a *in-situ* density measurement system in order to monitor changes in density of wood composite mats during consolidation.

This study was done in order to directly monitor material behavior during the hot pressing process. They found that the stress-strain response of flakeboard mats in hot and cold pressing were similar, characterized by a long stress plateau followed by a sharp increase in stress and an immediate decrease after the press reached final position. The stress relaxation, however, was much faster during hot pressing than that of cold pressing.

Wang *et al.* (2001a) explored multi-step press closing strategies. They found that closing the press up to a certain position and heating up the center layer before closing to the target thickness provided a more uniform density profile. The multi-step press closing results in multiple densification peaks rather than the two peaks that appeared in conventional hot pressed board.

Wang *et al.* (2001b) further explored the effect of step-closing pressing of MDF on panel performance. They reported that the step-closing pressing enhanced internal bond strength by increasing core density and decreasing surface density, which resulted in decrease of bending properties. They also found that greater core density did not result in higher internal bond strength. They also measured layer thickness swell, water absorption, total thickness swell and total edge swell using a nondestructive optical technique. They found that layer thickness swell is significantly and positively related to density of all layers. Thus, they suggested that efforts to improve dimensional stability of MDF should be focused on stabilizing high-density surface layers.

Kawai and Sasaki (1986) produced a low-density particleboard ($400Kg/m^3$) using isocyanate resin and strand type lauan (*Shorea* spp.) to explore the effect of pressure and pressing time on the density profile and related physical properties of the board. They found that the density in the face layer tended to increase with increasing pressing pressure and time. A steep density gradient did not increase MOR because horizontal shear failure occurred prematurely. Thickness swelling and water absorption tended to increase with increasing pressing pressure.

Winistorfer *et al.* (1996) used nonparametric regression analysis to model the vertical density profile of aspen oriented strandboard. They compared vertical density profile curves among different furnish moisture levels and press closing time. It was revealed that a 4% moisture content mat was significantly different from other levels (8 and 12% moisture content). However, the 8% level was not significantly different from the 12% level. Vertical density profile curves for all press closing times (20, 60, and 100 seconds) were significantly different.

Xu and Winistorfer (1996) applied Fourier analysis to fit a mathematical expression to the vertical density profile of flakeboard. They first performed Fourier transformation of the density profile data, and then synthesized the mathematical equation in the form of a cosine based on the transform output. They found that the fitting equation well agreed with the vertical density profile data obtained from two sets of flakeboards.

Xu and Suchsland (1998) developed an analytical model to understand and predict the development of MOE of wood composite panels with a uniform vertical density profile. The simulated model indicated that the MOE of particleboards decreased as average out-of-plane orientation angle of particles increased, yet was not influenced by particle size. The result also showed that the boards made with high-density wood species had higher MOE than that of low-density species when the same compaction ratio was used on both species. At the same board density level, however, the MOE was lower for boards with high-density species. They also indicated that MOE in the orientation direction increased continuously as percent alignment increased but MOE across the orientation decreased and leveled off after the percent alignment exceeded approximately 60%.

Xu (1999) studied the effect of vertical density distribution on bending modulus of elasticity of wood composite panels. Their theoretical analysis revealed that there was a linear relationship between MOE and peak density, but maximum MOE occurs when the peak density is at some distance from board surface.

3. OBJECTIVES

In order to synthesize composite materials which have controlled internal structure, a wide range of fibers, adhesives, and matrices used for composites was reviewed in chapter 2. From the review, it was concluded that natural fibers have specific strength and elastic specific moduli that compare favorably with a number of synthetic fibers. In addition, natural fibers can be easily modified by various chemical treatments (especially polar ones). However, these advantageous properties are not fully utilized in current composite manufacturing technologies. It is believed that useful composite materials and molded engineering objects can be synthesized by using well-chosen natural fibers, specially tailored adhesives, orientation of fibers in the pre-form fiber network, and consolidation approaches which offer high levels of control. A long-term objective of the research of which the present thesis is a part is to synthesize natural fiber-based composite objects whose internal structure and outer shapes are optimized for specific engineering applications.

In this research, natural fiber composite beams will be synthesized to demonstrate the potential benefit of controlling internal structure within a composite object. The emphasis in the present research is on development of techniques to aid in the synthesis of miniature load-bearing beams, using gaseous reactive chemical injection pressing. A miniature rectangular pressing system which can inject and remove gaseous chemicals under controlled chemical, thermal, and mechanical conditions will be developed. The device will be used for sequential gas injection within hemp and wood pre-forms. This will affect localized softening followed by activation of adhesive curing. Such sequencing will ensure that the final structure of the beam is established before adhesion takes place, thereby minimizing residual stress and maximizing adhesion.

Property control within the proposed objects may be affected by manipulating the spatial distribution of fiber type, spatial distribution of fiber orientation, and process-induced structure. Thus, selection of fiber type from a variety of available natural fibers may be the first work in the present study. From the literature review, hemp fibers were selected mainly because of their long length which simplifies the manual formation of highly oriented pre-forms. Anatomical features and mechanical properties of hemp fibers are therefore explored in the present research. However, it must be stated here that hemp fibers were selected primarily for their ease of manipulation; they are used as a tool to investigate the effect of orientation on the properties of the composites made from them. Wood fibers are also used in the present research and a range of other fiber types may be employed in future development of the approaches established here.

A variety of chemical treatment methods were analyzed by Chowdhury (1999). He identified gaseous ammonia as one of the easiest and simplest treatment methods to affect chemical softening of natural fibers at near-ambient temperatures. In the present study, gaseous ammonia will be used to soften natural fiber pre-forms and eventually create internal structure gradients.

Adhesives and matrices that may be used to bond natural fibers were also discussed in chapter 2 and Appendix A. Among them, phenolic resin (Phenol formaldehyde) is widely used for the manufacture of wood-based composites because of its good bonding properties and water resistance. Pizzi and Stephanou (1994a) found that gel time of the alkaline catalyzed resole PF resin noticeably slows down above a pH of approximately 9 and may therefore be little effected by ammonia. Furthermore, the same researchers (Pizzi and Stephanou , 1994b) found that the curing rate of resole PF resin can be accelerated at near-ambient temperatures by adding esters such as propylene carbonate and methyl formate. This chemical combination will be employed in the present research.

Heat and moisture together influence the densification process of conventionally hot pressed panel products. In this research, the role played by heat

and moisture in densifying natural fiber pre-forms will be replaced by gaseous ammonia. Natural fiber mats will be densified at 50°C (above the boiling temperature of methyl formate). It is the softening action of gaseous ammonia which will be used to create internal structure at such a low temperature. After gaseous ammonia injection, vapor phase methyl formate will be injected to replace the role of heat to accelerate curing of PF resin. X-ray densitometry will be used to evaluate the density gradients created. A technique will be developed to investigate the effect of methyl formate injection on the adhesion of PF resin-to-hemp interfaces. A miniature pressing device will be designed for this purpose.

It has been widely assumed that the strength of thermosetting adhesive bonds is dictated solely by curing temperature. In the present research, the dynamics of testing temperature on the strength of partially cured PF-to-wood bonds will be explored. For this purpose, a miniature computer-controlled bond forming and cooling system will be developed. This study may provide opportunities to maximize bond strengths before press opening and alternative approaches to stabilizing panels and molded objects after leaving the presses.

The natural fiber composite beams to be created will be tested to explore the relationship between localized internal density and corresponding mechanical properties. The resulting mathematical relationships will be used for stress analysis of a hypothetical beam during flexure. The transformed-section method will be used to analyze stress within the composite beam. This analysis will be used to demonstrate the potential increase in specific (density corrected) performance that may be obtained by use of process-induced property control in engineered structural components.

Objectives of present research may be summarized as follows:

A. Explore anatomical and tensile strength properties of hemp fiber slivers used to make oriented fiber beams.

B. Explore the bond strength development characteristics of hemp fibers and wood fibers and the effect that methyl formate injection has on this behavior. Particular attention will be given to the effect of combinations of hemp bonding surface on bond strength development.

C. Techniques will be developed to enable the effect of testing temperature on the strength of partially cured PF-to-wood bonds to be explored. This is with a view to optimizing adhesion mechanisms operative both within sealed pressing systems and more conventional industrial hot pressing operations.

D. A miniature rectangular gas injection pressing system which can inject and remove reactive chemicals on pre-formed fiber network will be designed and constructed.

E. Trial sample beams will be synthesized with oriented hemp- and randomly formed-wood fiber networks. Various pressing conditions will be explored and internal conditions (gas pressure and temperature) will be sensed.

F. Tensile strength distributions within fabricated sample beams will be measured and correlated with localized density. This information will be further used for stress analysis of a hypothetical density-graded beam loaded in flexure.

4. MATERIALS AND METHODS

4.1. INTRODUCTION

An important objective of this thesis was to develop means of making natural fiber composite beams in a gas injection pressing system. Recently, Chowdhury (1999) designed a cylindrical sealed pressing system in which pre-formed wood fiber networks were consolidated under controlled thermodynamic and chemical environments. That work emphasized the selection of treatment chemicals, but did not deal with the internal structure of the materials created – which were themselves very different in nature from those created in the present work. Since an important aspect of the present research was to investigate links between synthesis methods and structure (section 5.6), a new type of gas injection pressing system was designed and constructed. This system enables sequential injection and removal of gaseous reactive chemicals to be affected within rectangular pre-forms under controlled thermal and mechanical conditions. The system was designed to accommodate a wide range of pre-form configurations and fiber types, though focus in the present work was on oriented hemp fibers and non-oriented wood fibers. The design of the system is described in Section 4.3.4.

The bonding kinetics of adhesives used to form the above-mentioned composite beams were also investigated. An Automated Bonding Evaluation System (ABES) was modified and then used to explore both the bonding properties of individual hemp strand pairs and those of networks of overlaying hemp fibers (described in sections 4.3.3. and 4.3.4. respectively). In addition, an automated computer-controlled forced–air cooling system for miniature ABES bonds was also developed and then used to explore the temperature dependencies of properties of partially formed miniature bonds (section 4.3.5.). This system was further modified with the addition of stainless steel pressing heads to enable gases and liquids to be

injected into miniature bonds during their formation at elevated temperatures (section 4.3.4). This innovation enabled the responsiveness of miniature bonds to temperature to be evaluated under chemical conditions related to those pertaining during fiber composite formation in the sealed pressing system.

A selection of miniature beam samples formed in the pressing system was evaluated physically and mechanically. Of principal concern was the characterization of pressing-induced density gradients and their influence on the strength and stiffness of the beam.

4.2. MATERIALS

In this research, wood fibers and hemp fibers were selected for use in trial beams. The hemp fibers are long and easy to manipulate (as described in section 4.2.1) and, compared to most other natural fibers, they have high specific strength and stiffness. Hemp fiber was used as a vehicle to develop methods to investigate relationships between structure and properties of natural fiber composites because high levels of orientation could be affected with relative ease. Wood fibers were also used as the material to explore the possibility of manipulating density profiles within beams by sequential gas injection and removal. Wood fibers (unbleached Kraft pulp) were employed both due to their availability in industrial quantities (and consequent economic importance) and because assemblages of such fibers have predictable and controllable consolidation characteristics compared to those of the parallel oriented hemp networks. Sliced Maple veneers were used to explore the effect of testing temperature on PF bond strength and also as supports during bonding studies for hemp fibers.

Preparation and properties of each of the above material types used in the research are considered in turn below.

4.2.1. Hemp fiber yarn

Highly processed and pre-oriented hemp sliver yarns were obtained from a commercial operation (Ohio Hempery; Guysville, Ohio). These yarns were mechanically processed from the retted stalk such that they contained a minimum of pithy material and dust. In general, once the hemp material is cut in the field, it is allowed to ret in order to decompose the stalk and ease fiber separation. While the stalks lay in the field, much of the nutrients extracted from the soil by the plant are returned as they decompose. The stalks are turned and then baled with conventional hay harvesting equipment and further processed into fine yarns through several steps often termed scutching, hackling, and drawing. No chemicals were employed in the production of the hemp slivers used in the present research. Some hemp sliver yarn is shown in Figure 4.1.

The yarn consists of linear assemblages of hemp slivers forming continuous staples. The weight per unit length of the yarn was approximately 8.5g/m. The yarn was stored at 20°C and 65% relative humidity (RH) before being used, and its conditioned moisture content was 8%.

Figure 4.1. Hemp sliver yarn used in this research.

4.2.2. Hemp strand material

In addition to the above material, hemp strands were obtained directly from dried hemp stalks (Figure 4.2). Under the dissecting microscope, the bast portion was carefully separated from the pithy material. Typical width and thickness of the separated hemp strands ranged from 2.0 to 5.0 mm, and 0.08 to 0.1mm respectively. The hemp strands were then cut into 2.5-mm (width) × 15.0-mm (length) using a single-edge razor blade. The cut pieces were stored at 20°C and 65% RH before being used. The conditioned moisture content was again 8%.

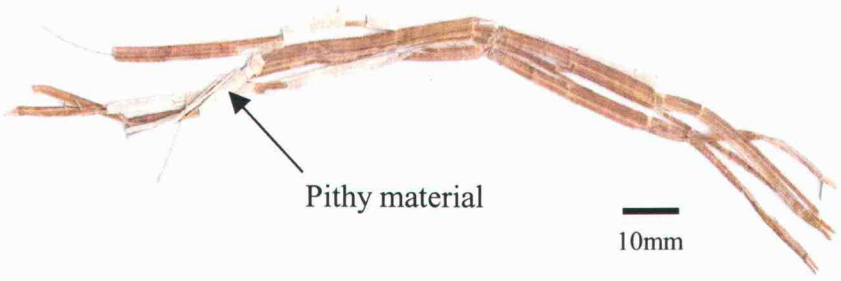

Figure 4.2. Hemp strand used in this research.

4.2.3. Wood Kraft pulp fibers

Unbleached Kraft pulp was obtained from a local mill (Halsey, OR). The fibers were processed from Douglas fir (*Pseudotsuga menziesii* (Mirb.) Franco) chips and were specially extracted before the bleaching stage in the plant. The concentration (solids content) of the pulp slurry at the point of extraction was about 10%. The fiber was washed in water, dried (while thinly spread and fanned to avoid

the onset of fungal attack) and conditioned in a standard room at 20°C and 65% RH before being used. The conditioned moisture content was 6%.

4.2.4. Wood veneer

Peeled Maple (*Acer marcrophyllum* Pursh.) wood veneer strips of 0.8-mm thickness were used to explore the effect of testing temperature on the strength of partially cured PF bonds. Maple is a diffuse porous species and thus provides surfaces of even texture compared to many other species. It also has a relatively low extractive content, which may effect adhesion mechanisms and consequent bond strength development. The veneers were cut into a fixed length and width (120mm × 20mm plus or minus 0.1 mm) by means of a specially designed automated pneumatic cutting device. These pieces were conditioned at 65% RH and 20°C to a moisture content of 7%. Figure 4.3 shows the automatic sample cutting device.

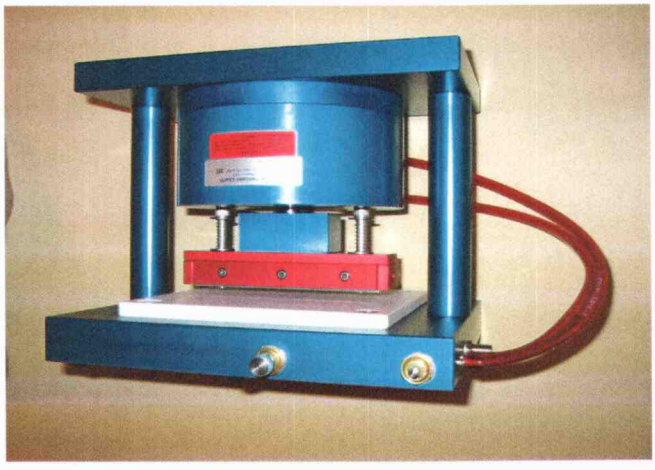

Figure 4.3. Automated ABES sample cutting device

4.2.5. Adhesive

Pre-catalized and filled resole type PF adhesive (donated by Georgia Pacific Resins, Inc.) was used for the research (pH 11.5, solids content 48%). The reasons for selecting this particular type of adhesive were discussed in section 2.4.4 and 2.7.2. The PF resin was diluted with de-ionized water to reduce its viscosity when using it in a miniature spray system to apply adhesives to hemp or wood fibers (see section 4.3.4. and 4.3.6.).

4.3.EXPERIMENTAL METHODS

4.3.1. Evaluation of anatomical and mechanical properties of hemp

4.3.1.1. Anatomical features

Hemp fibers were observed using optical microscopy (Nikon Type118) and a dissecting microscope (Nikon SMZ 2T) equipped with an image analysis system (NIH IMAGE® software), and scanning electron microscopy (AmRay 3300 FE field emission scanning electron microscope). The width of individual hemp fibers and width, thickness and length of hemp slivers were measured with the image analysis system, while the surface morphology of hemp slivers and hemp strands were observed using the SEM.

In order to measure the width of individual hemp fibers under the light microscope, a small amount (approximately 0.5g) of hemp slivers were macerated for 2 hours in hydrogen peroxide/acetic acid (1:1 v/v), and then carefully washed

with distilled water. Macerated fibers were then laid on a slide glass and a cover glass was placed on top. The widths of 50 individual hemp fibers were then measured under the light microscope. Since the length of slivers was much larger than their thickness or width, thickness and width were measured at three to five different positions along the length. The lengths of 50 individual slivers were measured.

In order to explore the surface morphology of hemp slivers and hemp strands, each were sectioned transversely using single-edged razor blades. The samples were then air-dried, mounted on aluminum stubs, and platinum-palladium coated. Then they were examined in the AmRay 3300 FE field emission scanning electron microscope.

4.3.1.2. Tensile strength and stiffness of hemp slivers

The tensile strength of single hemp slivers was measured using the Automated Bonding Evaluation System (ABES) device without activating its hot pressing function. Details of ABES are given in section 4.3.2. For this purpose, a small number of conditioned hemp slivers were randomly selected from hemp yarn.

Paper mounting strips measuring 230mm × 15mm were prepared and a transverse center-line was marked on them. Single slivers were carefully isolated from the yarn and inspected under the dissecting microscope to avoid regions with obvious irregularities. The slivers were then cut to 20mm length using a single-edge razor blade and mounted on the paper strip so that the sliver was aligned perpendicular to the centerline. Individual slivers were then secured on the paper strips by applying a small bead of epoxy resin (Epoxy Plus^{TM}) to each end. The separation of the beads affected a span of 3mm. The above-mentioned manipulations were carried out under a dissecting microscope and, at all stages, hemp slivers were handled with forceps in order to avoid damaging them.

After 24 hours of conditioning and adhesive cure, the paper strip was cut into two pieces at the center. The prepared sample was then carefully mounted on the ABES system; the ends of the paper strips being held by the pneumatic gripping system of ABES.

There were two ways to pull the samples mounted on the ABES device: by activating the computer controlled pneumatic pulling piston, or by manually turning the pull head adjuster (Figure 4.4). After some preliminary trials, it was elected to pull the samples by turning the pull head adjuster because it was difficult to affect small amounts of deformation when using the pneumatic loading system. The deformation of the sample was calculated by the scale marked on the pull head adjuster (63 units/full turn) and pitch of the thread (1.61mm pitch) that is connected to the gripping head. The samples were carefully pulled at a speed of approximately 0.025mm/s by manually rotating the adjuster (Figure 4.4). This corresponded to an axial strain rate of 8.3 microstrain/sec.

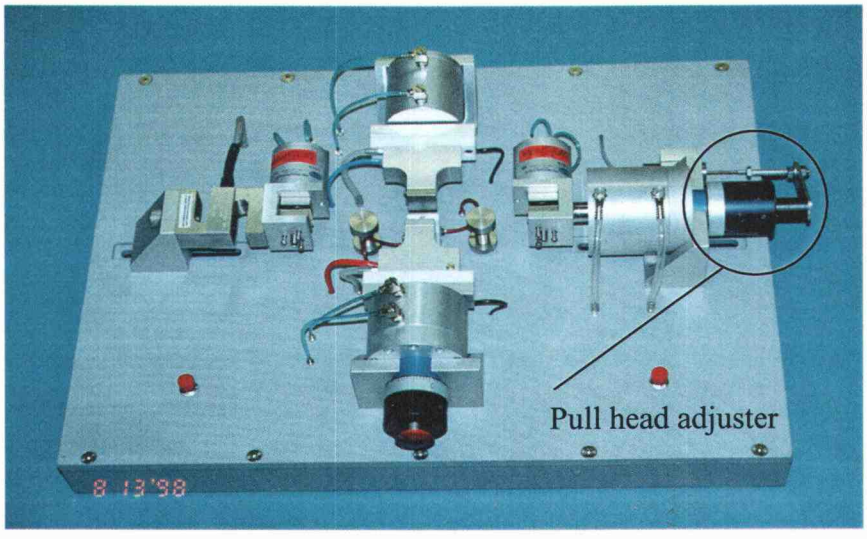

Figure 4.4. Pull head adjuster of ABES

The values of force to fiber failure were measured and electronically recorded using the data acquisition system that is part of ABES. The cross-sectional area of the sliver at the failure location was then calculated by measuring width and thickness under a dissecting microscope with the image analysis system. Based on the maximum force prior to failure and cross-sectional area, the strength of the hemp slivers were calculated. A total of 20 samples were tested in this manner. Figure 4.5 shows a schematic diagram of the tensile strength test.

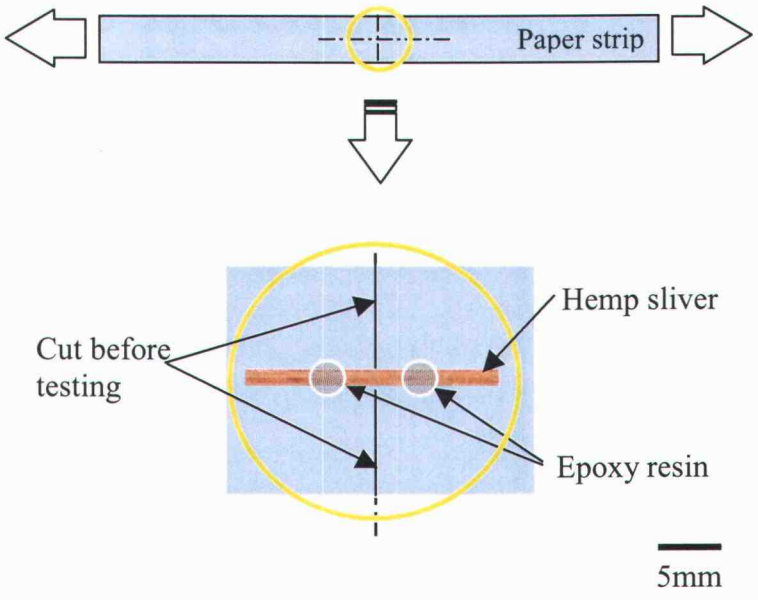

Figure 4.5. Schematic diagram of tensile tests of hemp slivers

4.3.2. The automated bonding evaluation system

The Automated Bonding Evaluation System (ABES) has been used for a number of experiments in the present work. Its functions in standard format will be summarized before discussing the modifications that were made for special testing.

The ABES enables the bond strength development characteristics of a variety of adhesives and adherend combinations to be explored under highly controlled temperature and pressure conditions. The system allows miniature bonds to be formed and tested in lap-shear mode immediately after their being partially cured to a pre-selected level. Performing these tests for a variety of forming times and temperatures allows series of bond strength development plots to be constructed. An overview of the bond forming and testing zone of ABES is shown in Figure 4.6.

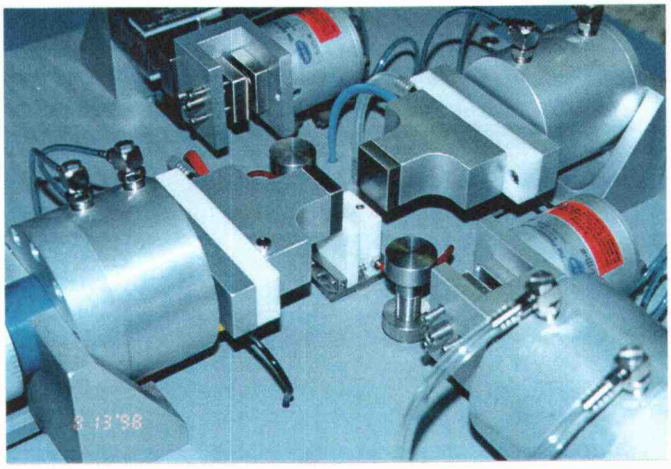

Figure 4.6. The bond forming and testing zone of the Automated Bonding Evaluation System

By using relatively thin adherend strips (typically 0.8mm for wood bonding studies), a broad range of target temperatures may be achieved at the glue-line shortly after the beginning of bond forming periods. In this way, near-isothermal bond strength development may be achieved right after the beginning of each bond forming period.

Repetition of the bond forming and testing procedure for a range of pressing times (while holding hot pressing temperature constant) enables near-isothermal bond strength development with time to be plotted. Each point on such a plot therefore corresponds to a similar glue bond that has been cured under controlled conditions of temperature and pressure and almost immediately thereafter pulled to measure its accumulated shear strength. Repeating this procedure for a number of different pressing temperatures enables a set of isothermal bond strength development plots to be constructed. These data enable the effect of temperature on rates of isothermal bond strength development to be explored.

The modifications to ABES will be summarized here before being described in detail. Firstly, it has been modified so that it may be used to explore thermoplastic characteristics of adhesive systems, including those that are predominantly thermosetting. A computer controlled cooling system which can cool selected bonds immediately prior to their being pulled was designed and incorporated into ABES. Details of the cooling system will be further explained in section 4.3.5. Secondly, stainless steel gas injection blocks were made and used as a means of injecting chemicals into bonds during hot pressing (Section 4.3.4). To explore the bonding characteristics of overlapping hemp strand pairs, which need very small but accurate bond pressing force, a spring-loaded miniature hot pressing block also was designed and added to ABES (section 4.3.3).

4.3.3. Evaluation of bond strength development between hemp strand pairs

The bonding characteristics of hemp strands were investigated to explore the effect of bonding surface combinations on adhesion rates and final strengths. It was pointed out in Chapter 2 that such strands have surfaces of contrasting structure which may play an important role in effecting the production and properties of composites made from them.

4.3.3.1. Miniature hot pressing blocks for forming bonds between hemp strand pairs

ABES in its normal format is designed to apply pressing forces in the order of 100 to 500 Newtons. Bonding areas normally range from 100 to 625mm^2. However, the bonding area of pairs of hemp strands is very small (approximately 5mm^2) compared to that of the normal test. Thus, a miniature hot pressing block which can exert small but controlled amounts of pressing force to the minute bonding area was designed. This is shown schematically in Figure 4.7.

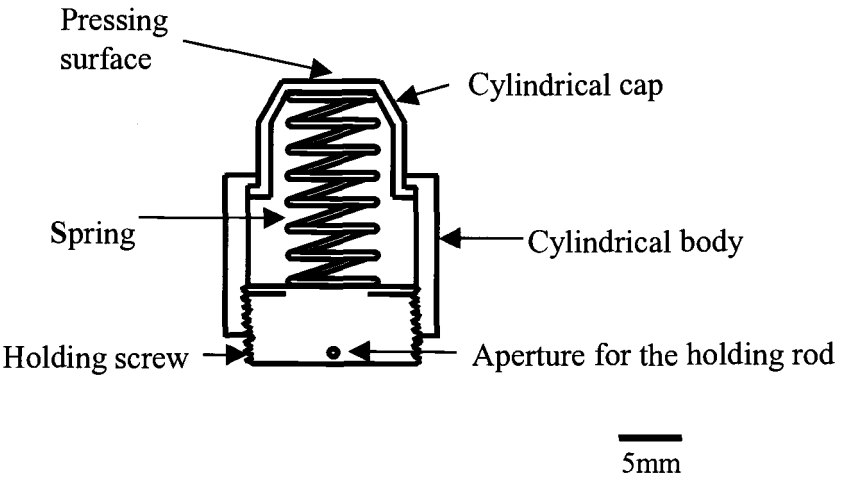

Figure 4.7. Schematic cross-sectional diagram of the miniature hot pressing block.

The hot pressing block consists of a cylindrical cap which contacts and transmits heat to the hemp strand, a cylindrical body which holds the cylindrical cap and spring, and a holding screw. All these parts, except the spring, were made of aluminum because of the ease of heat transfer from the hot press of ABES. Four stainless steel rods (1.6mm diameter and 40mm long) and four tension springs were

used to connect the hot pressing block to the pressing anvil of the ABES. In addition to the spring-loaded block, a single stationary block was designed and mounted on the rear anvil of ABES. Figure 4.8 shows the miniature hot pressing blocks installed.

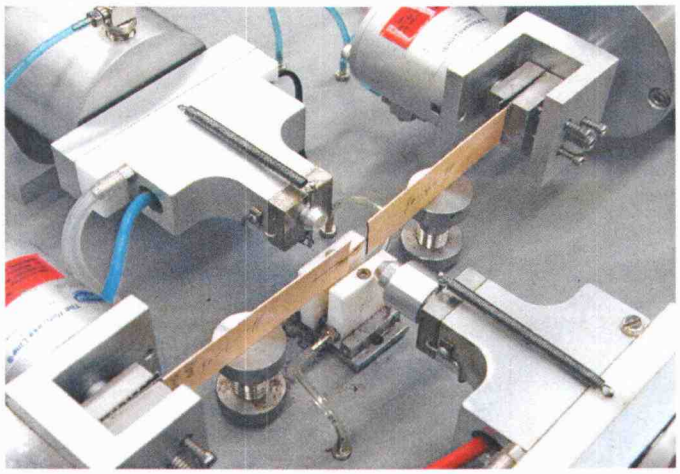

Figure 4.8. The miniature hot pressing blocks and installed samples on the ABES.

Force was applied to the lap-shear bond of hemp strands by compressing the spring inside the hot pressing block by a controlled distance between the two hot pressing blocks of ABES. The spring constant used for the hot pressing block was 1.8N/mm, with a maximum force of 20N. The amount of force may be controlled either by adjusting the spring-holding screw or the travel distance of the hot press in the ABES. For this research, the mechanism was adjusted to affect a hot pressing pressure of 1.1MPa. A bonding area of approximately 5mm^2 was employed and this necessitated a pressing force of 5.5 Newtons. This pressure value was selected because in most particulate wood-based composites

manufacturing, the hot pressing pressure ranges from 0.7 (for plywood) to 8 MPa (fiberboard). Especially in plywood manufacturing, the pressing pressure typically ranges between 0.7 and 1.5MPa. The effect of pressing pressure on adhesion mechanisms may be the subject of future investigations once the basic principle of synthesizing structural composite beams has been established; it was, however, beyond the scope of the present investigation.

4.3.3.2. Bond test sample preparation

Hemp strands were obtained from the bast portion of crumpled hemp stalk by removing the pithy starch material. Strand surfaces interfacing with the pithy material are here termed "inner surfaces" and the opposite surfaces are termed "outer surfaces". Small pieces of hemp strand (approximately 2mm × 15mm) were prepared and conditioned at 20°C and 65% RH. Before mounting them on the wood supporting strips, the strands were examined under a dissecting microscope and those with any gross damage and irregularities were avoided. Pieces of sliced Maple (*Acer marcrophyllum* Pursh) veneer (0.8mm thick) were cut into strips 20.0mm × 85.0mm to mount the hemp strands. A center-line was drawn on one end of the wood strip to align the hemp strand at the center of the endmost portion of the strip. Hemp strand sections were carefully mounted on the endmost edge of wood strips so that the strands protruded by 5.0mm. A small amount of epoxy resin (Epoxy Plus^{TM}) was used to secure the hemp strands on the wood strips. Preparation and mounting of the strands were performed under a dissecting microscope. Figure 4.9 shows the dried and crumbled hemp stalk material and a pair of mounted hemp strand test specimens.

Figure 4.9. Dried and crumbled hemp stalk and a pair of hemp strand test specimens.

A very small amount of PF adhesive was carefully applied onto one surface of a hemp strand using a glass rod. The bonding area was only approximately 5mm^2. However, in order to calculate accurate bond strength values, the exact bonding areas were measured by using a dissecting microscope and image analysis system after testing. Residual adhesive could be identified and used to locate the limits of the bonding area.

After applying PF adhesive, the specimens were installed on the ABES and hot pressed at 90°C for various times (from 30 to 600 seconds). The temperature of 90°C was selected because it lies within the wide range of temperatures that are generated within natural fiber composites during industrial hot pressing. In future investigations, a range of temperatures may be employed to characterize the kinetics of adhesion. The present tests were performed preliminarily to establish the difference in bonding between contrasting surfaces.

Isothermal bond strength development plots for the different combinations of surface topography were then constructed. In addition, the failure surfaces of the

test specimens were examined under the SEM. Table 4.1 shows the ranges of tests preformed.

Table 4.1. Hemp strand bonds formed and tested with different surface pairs

Surface combination	Range of pressing time (s)	Number of bonds formed and tested
Inner-Inner	30-600	10
Inner-Outer	30-600	15
Outer-Outer	30-600	14

4.3.4. Evaluation of bond strength development between hemp sliver networks

This study was carried out to explore the PF bond strength development between parallel oriented hemp fibers and also to investigate the effect of the injection of reactive chemicals (methyl formate) on such strength development. For the gas injection studies, injection pressing heads were specially designed and constructed.

4.3.4.1. Gas injection pressing heads

Figure 4.10 shows a cross-sectional schematic diagram of the heads during bond forming (not to scale).

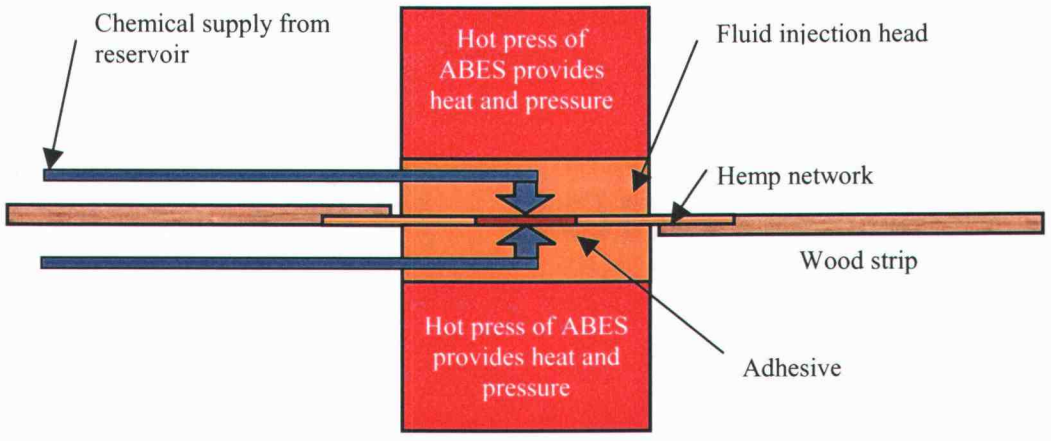

Figure 4.10. Schematic representation of the gas injection pressing system used to inject reactive chemicals into bonds as they are being pressed.

The heads were attached to the hot pressing blocks of ABES by four locking screws. Inside each head, a vertical hole (3mm diameter and 20 mm height) was drilled and a series of smaller lateral apertures (total of 6 holes of 1mm diameter) was used to convey chemicals to the bonds. The head was made of stainless steel to prevent corrosion by reactive chemicals and to convey heat from the hot pressing blocks (aluminum would have conducted heat more effectively but lacks the necessary chemical resistance). Figure 4.11 shows the gas injection pressing heads installed on the ABES.

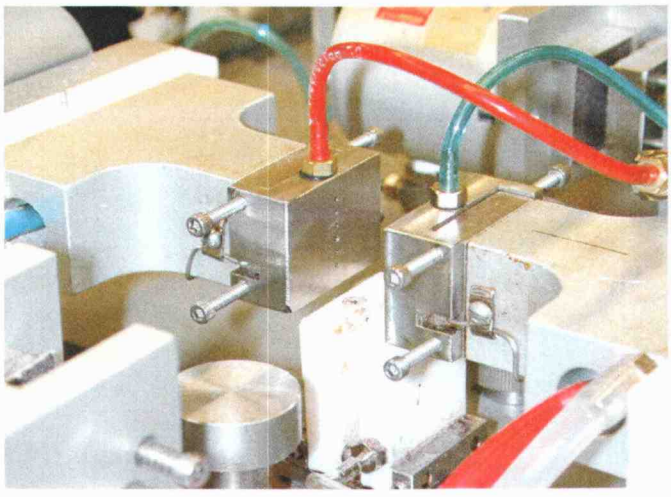

Figure 4.11. Gas injection pressing heads attached on the hot pressing blocks of the ABES

4.3.4.2. Sample preparation for bond strength testing of hemp sliver networks

Long hemp sliver yarns were cut into pieces of 50.0mm length. The yarns were then divided into two portions of approximately equal weight. The mass of prepared hemp sliver material was 20.0g/m^2 with 3mm thickness. Thus, the unconsolidated density of the hemp sliver network was approximately 6.67Kg/m^3. Each sliver network was mounted on one end of a sliced maple veneer strip measuring 20.0- × 85.0-mm such that the mounted hemp slivers were evenly distributed over the width and protruded 30.0-mm from the end of each strip. The number of hemp slivers per unit width that was mounted on the wood strips was approximately 20-30/mm. Epoxy resin was used to secure the hemp slivers on the strips. The prepared specimens were then stored at 20°C and 65% RH for 24 hours. Figure 4.12 shows a typical pair of specimens.

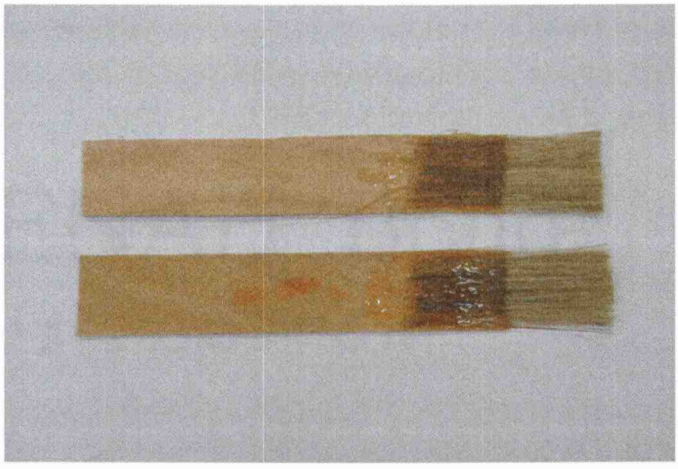

Figure 4.12. A pair of hemp sliver networks attached to wood strips

Phenol formaldehyde adhesive was applied to the network of hemp slivers (bonding area of 20.0mm × 10.0mm) using a specially designed precision spraying system. A fixed size of plastic tube (1.6mm in inner diameter and 50.0mm length) filled with PF resin was connected to a miniature spray device for this purpose. The plastic tube reserved a set amount of PF resin (approximately 0.1g) for spraying a batch of specimen pairs. The bonding area was defined by a steel masking plate such that only the bonding area (20.0- × 10.0-mm) was exposed during spraying. The amount of PF resin applied was approximately 0.03g per sample pair. This is equivalent to an adhesive content of 20% of the total miniature composite formed. A schematic diagram of the resin spray device on the test specimens is shown in Figure 4.13.

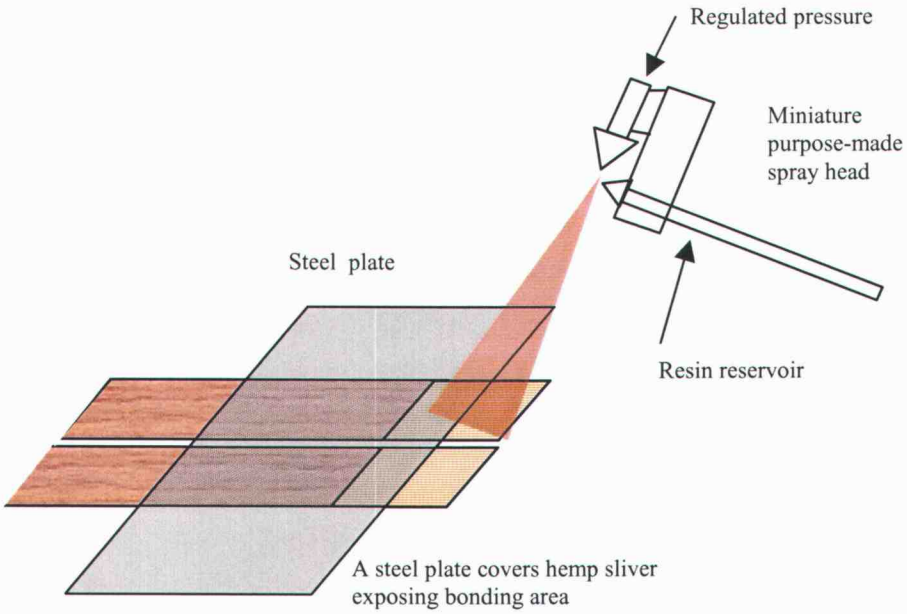

Figure 4.13. Schematic diagram of the miniature resin spray device for hemp sliver networks

Pairs of glued specimens were placed in the ABES device with 10mm of overlap. The glued areas were then pressed at 50°C for a variety of times (from 30 to 600 seconds) with a pressure of 1.1MPa. The pressing temperature and times were selected to explore bond strength development rates at low temperature, and also to investigate the effect of methyl formate on PF bonds cured at such a low temperature. This temperature is above the boiling point of the methyl formate that may be used in the synthesis of composite beams.

When investigating the effect of methyl formate on adhesion, approximately 2ml of the liquid was put in a plastic syringe. The needle of the syringe was inserted and tightly fit to the plastic tube that is connected to the gas injection pressing blocks. Approximately 10 seconds after press closure, methyl formate was injected into the bond. The large (excessive) amount of methyl

formate (2ml) was selected to ensure that the bonds were fully exposed to the chemical.

After pre-selected curing times, bond forming pressure was reduced, the free ends of the wood mounting strips were gripped pneumatically and the miniature oriented hemp fiber samples were pulled in tensile mode to failure. Forming time and tensile force were automatically recorded for each test. The ranges of tests conducted are summarized in Table 4.2.

Table 4.2. Experimental plan for the hemp sliver tests

Treatment	Range of pressing time (sec)	Number of bonds formed and tested
Control	25-600	17
Methyl formate (injected 10 sec. after press closure)	25-600	15

4.3.5. Modification of ABES to explore the effect of temperature on the strength of partially cured bonds

ABES was modified to explore the effect of temperature on the strength of partially cured PF adhesive bonds. A pneumatically driven and spring-loaded cooling head was developed and mounted on the ABES system for this purpose. The cooling head enables selected bonds to be rapidly cooled down immediately after press opening, yet before being pulled. The system was calibrated to enable any target testing temperature (lying between pressing and ambient temperatures) to be achieved from any starting temperature within the operating range of ABES (ambient to 150°C).

4.3.5.1. Concept of the bond cooling test

The importance of bond testing condition on bond strength was considered earlier in section 2.3. The main requisite of the bond cooling function was to decrease the temperature of selected bonds formed under various temperature and time conditions as quickly as possible down to pre-selected target bond testing temperatures. In this action, it was also necessary to maintain the bond at target temperatures during pulling. One important reason for the need for fast initial cooling was to minimize further curing during cooling.

4.3.5.2. Design issues for the cooling system

A retractable cooling system was developed. The head resides under the hot pressing zone of ABES to enable bonds to be formed in the normal way prior to cooling. Figure 4.14 shows the computer controlled cooling system.

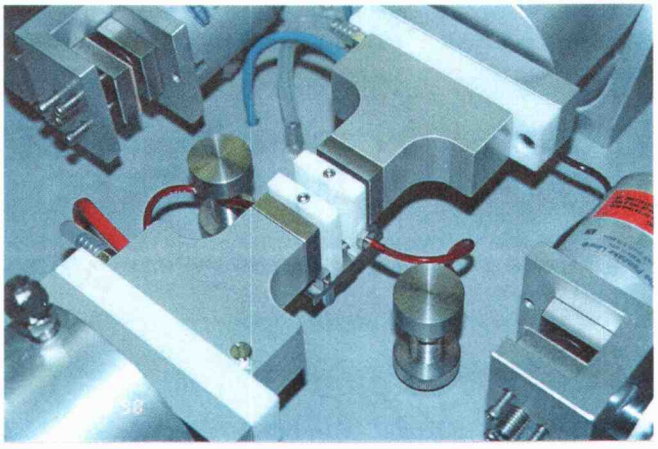

Figure 4.14. A computer controlled cooling head system in ABES. Cooling head is in cooling position.

The cooling head was elevated by a pneumatic cylinder when needed. In the retracted (lowered) position, the cooling head stays away from the path of the hot press. The movement of the cooling head was controlled digitally by slightly modifying the control software developed for ABES.

4.3.5.3. Design details

The cooling head consists of two rectangular plastic blocks mounted on an adjustable supporting platform. The thickness of the blocks was such that when the cooling head was elevated, each block fitted between the neighboring retracted hot pressing block and test bond. In order to prevent heat transfer from the hot pressing blocks, the cooling heads needed to have high heat and chemical resistance together with reasonably good machinability. Polytetrafluoroethylene (PTFE) was therefore selected.

The cooling head blocks have 4.0mm diameter passageways for fluid supply. Six lateral pin-holes of 1mm diameter were evenly spaced along the

vertical supply passage-way so that the air jet coming through the pinholes may cool down the bond evenly.

The PTFE blocks sit upright on a stainless steel bed block and slide on the bed block surface. Two spring-loaded rods pass through the two PTFE blocks to guide this movement. The guide rods are connected to stainless steel stopper blocks, which are, again, connected to the bed block. The gap between the two PTFE blocks may be adjusted by changing the position of the stopper blocks.

The PTFE blocks, stopper blocks, bed block, and spring-loaded rods comprise the cooling head (Figure 4.15). The head was then connected to the pneumatically driven piston and positioned at the center of the ABES so that the cooling head rises up through the spaces between overlapped surface and hot pressing block. The operation of the cooling head and associated regulated air supply is computer controlled.

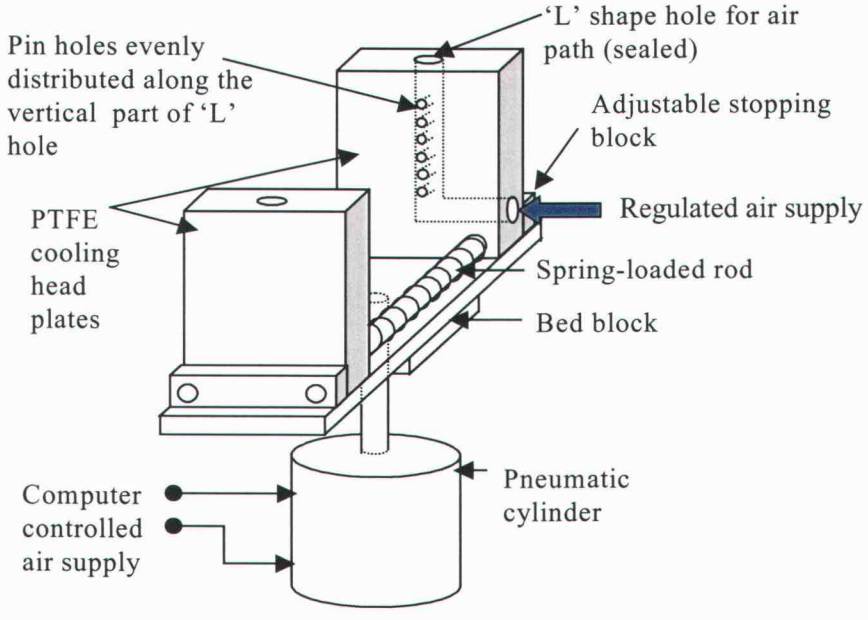

Figure 4.15. Schematic diagram of the cooling head with pneumatic cylinder

The cooling process is established at the end of the hot pressing stage in a test sequence (Figure 4.16). The steel hot pressing blocks are first retracted. Immediately after the retraction, the pneumatic piston is activated, the piston pushes up the cooling head, and the regulated air-jet is directed on the wood surface for a time set by the computer program. The time lapse between retraction of the hot pressing block to the start of the air jet cooling action is less than 1.5 seconds. A single temperature of the air jet was used throughout the experiment presented here. However, the temperature and pressure may be varied if necessary in future applications of the system. After cooling, the cooling head was held in its elevated position until the bond was pulled and failed. The cooling blocks in this position prevent radiant heating of the bonds after cooling and before failure.

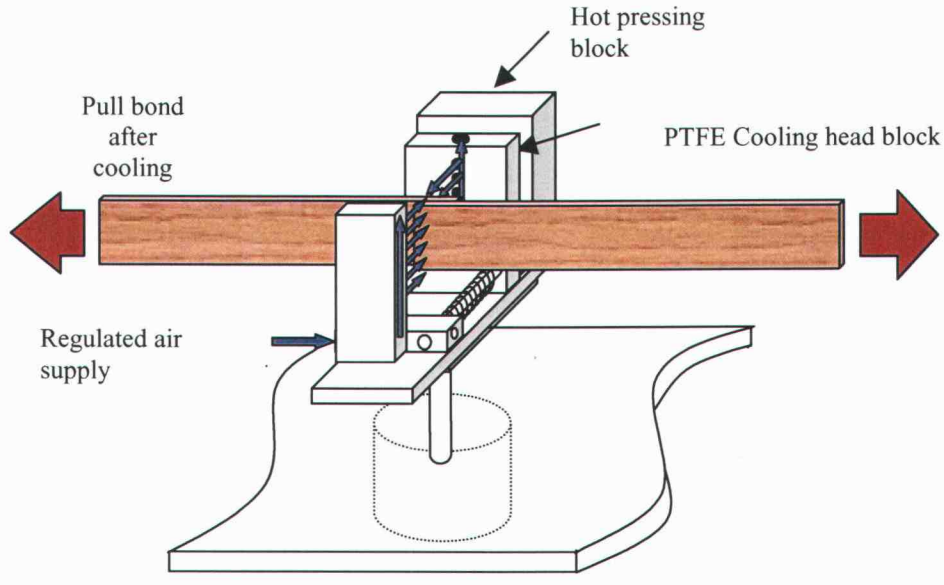

Figure 4.16. Schematic diagram of bond cooling and testing.

4.3.5.4. Calibration of the cooling system

In order to reach target bond temperatures immediately prior to bond pulling, two different approaches to bond cooling with the system were explored. In both cases, the extent of bond cooling prior to pulling was monitored by inserting miniature thermocouple (PTFE insulated, 0.25mm. diameter.) into the center of supplemental test bonds which were formed and cooled under various conditions but not tested.

In the first approach, air jet pressure was varied in the hopes of achieving a series of stabilized target bond testing temperatures (Figure 4.17).

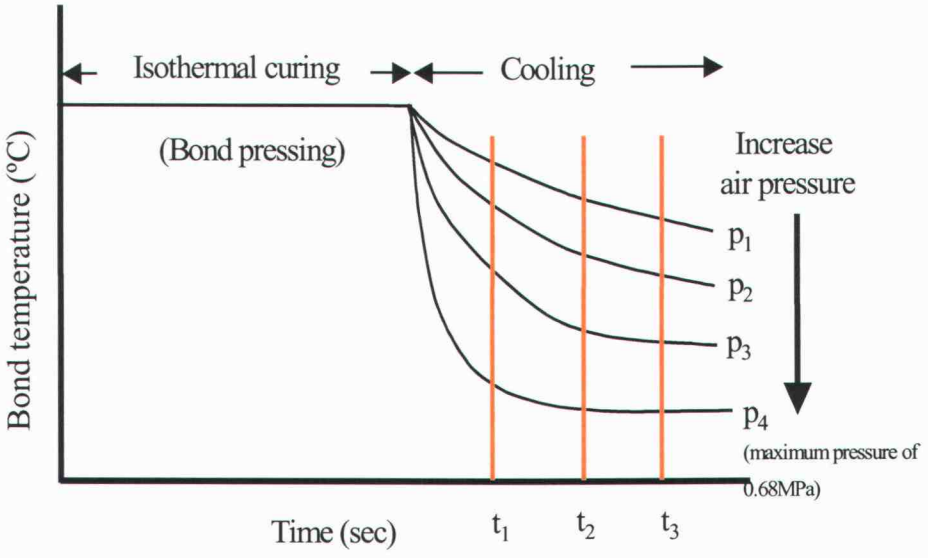

Figure 4.17. Schematic diagram of bond cooling by controlling air pressure. Glue-line temperature was decreased by directing air-jets with different pressures on to the bond (p_1,p_2,p_3, and p_4) for various cooling times (t_1, t_2, and t_3)

Since the rate of temperature drop was dependent on the air pressure, the cooling path varied with starting (pressing block) temperature (Fig. 4.17). This was not ideal since the cooling path may influence structural transitions of the

polymers. If a fixed minimum cooling time with maximum air pressure is used to minimize further curing of the bonds, then the range of target testing temperatures becomes narrow. If the bond is tested at different times along with maximum air pressure, then it may be difficult to maintain high target testing temperature because of the rapid temperature decrease of the bond at the early stage of cooling. Such analysis led to a more elaborate and satisfactory way to obtain series of target testing temperatures as follows.

The enhanced cooling approach involves the use of a combination of fast initial cooling (with high air pressure) followed by a stabilization period during which relatively slow cooling without any air blowing (Figure 4.18). Fast initial cooling for various amounts of time (from 0.1 to 10 seconds) enabled all bonds to follow the same cooling path and then to stabilize to the target testing temperature by means of ambient cooling (without air blowing) for short periods. A value of 1 second for the latter was found optimal after a range of trials. Immediately after the slow ambient cooling period, the bond was tested. This cooling process was effective because it cooled down the bond quickly to minimize further curing of the resin after press opening and held the test temperature fairly constant at the target temperature. This approach is represented in Figure 4.18.

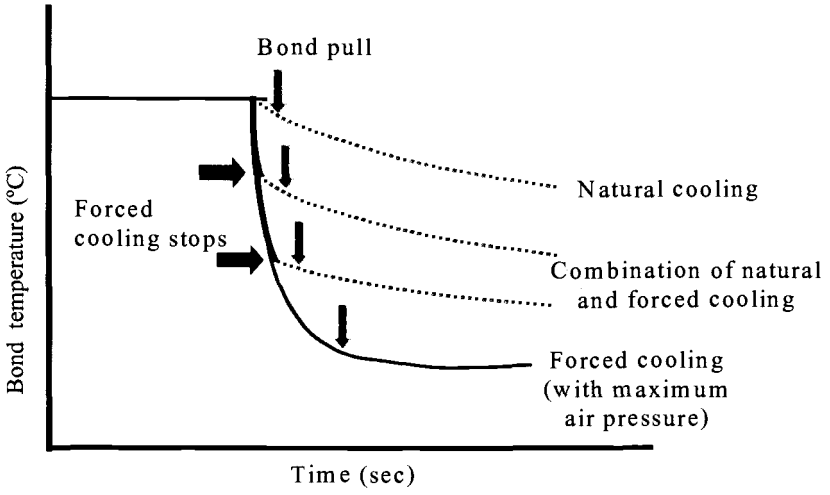

Figure 4.18. Schematic diagram of combined forced and natural cooling used to obtain any target bond testing temperature from any starting temperature.

In order to calibrate the system, a mathematical relationship between cooling time and temperature drop was derived. This provides bond temperature for given combinations of forced (with high pressure air jet) and natural (without air jet) cooling. The analysis is based on Newton's law of cooling and the derived equations included the following assumptions:

1. Heated body was confined to the volume of the bond.
2. During forced cooling, only convective heat transfer occurred due to high-pressure air-jet (radiant losses were assumed negligible).
3. Initial temperature was uniform throughout the body.

Newton's law of cooling may be expressed as:

$$q = hA(T_b - T_a) = -c\rho V(dT/d\tau) \tag{4.1}$$

where:

q heat transfer rate (kJ/s)

h	convective heat transfer coefficient (W/m^2·°C)
A	surface area of the body (m^2)
T_a	fluid temperature (°C)
T_b	temperature of the body (°C)
c	specific heat (kJ/kg·°C)
ρ	density of the body (kg/m^3)
V	volume of the body (m^3)
τ	time (sec)

Given an initial condition of:

$$T_b=T_0 \text{ at } \tau = 0 \tag{4.2}$$

The solution to equation (4.1) is:

$$T_\tau = (T_0 - T_a)e^{-[hA/c\rho V]\tau} + T_a \tag{4.3}$$

In the case of the bond cooling, T_a is the temperature of high pressure air that blows onto the bond, T_b is the temperature of the bond before being cooled and T_τ is the bond temperature after τ seconds of cooling. For forced cooling, the temperature afterτ seconds of cooling can be calculated by:

$$T_f = (T_0 - T_a)e^{-[h_1A/c\rho V]\tau} + T_a \tag{4.4}$$

and for natural cooling, the temperature after τ seconds of cooling can be calculated by:

$$T_n = (T_0 - T_a)e^{-[h_2A/c\rho V]\tau} + T_a \tag{4.5}$$

The right side of the equations 4.4 and 4.5 can be rewritten as:

$$T_f = (T_0 - T_a)e^{-k_1\tau_1} + T_a \tag{4.6}$$

$$T_n = (T_0 - T_a)e^{-k_2\tau_2} + T_a \tag{4.7}$$

where k_1 and k_2 are $(h_1 A/\rho cV)$ and $(h_2 A/\rho cV)$, and τ_1 andτ_2 are forced and natural cooling time, respectively. With the exception of the convective heat transfer coefficients for forced and natural cooling (h_1 and h_2), other terms inside the parenthesis are constant.

If a combination of forced cooling for τ_1 followed by natural cooling modes for τ_2 is used, then the temperature after a combination of cooling can be obtained by:

$$T_t = (T_f - T_a)e^{-k_2\tau_2} + T_a \tag{4.8}$$

$$T_t = [\{(T_0 - T_a)e^{-k_1\tau_1} + T_a\} - T_a\}e^{-k_2\tau_2} + T_a] \tag{4.9}$$

where T_t is the target testing temperature after τ_1 seconds of forced cooling followed by τ_2 seconds of natural cooling.

Upon simplification:

$$T_t = \{(T_0 - T_a)e^{-k_1\tau_1}\}e^{-k_2\tau_2} + T_a \tag{4.10}$$

The values for k_1 and k_2, which are associated with convective heat transfer coefficients for forced and natural cooling, h_1 and h_2 respectively, are system-specific and were derived from temperature-versus-time calibration data (Figure 4.19).

The decrease of glue-line temperature of bonds pressed at 90°C were measured by inserting small diameter thermocouple probes.

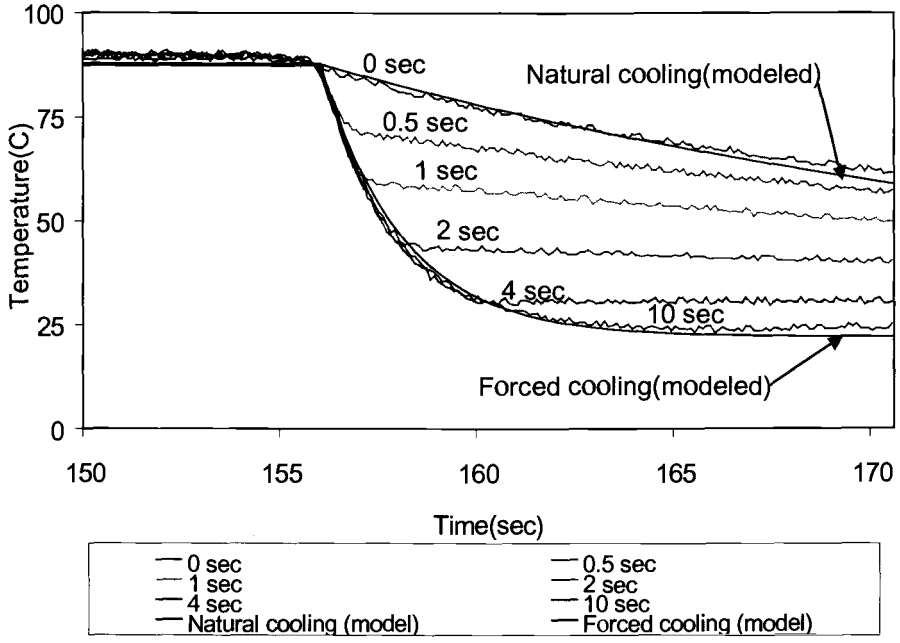

Figure 4.19. Measured glue-line temperature decrease depending on combination of forced and natural cooling. These curves were used to calibrate the system.

From Figure 4.19, initial conditions and coefficients are shown in Table 4.3. Initial temperature of the body (T_0) was decided from the measured glue-line temperature immediately prior to cooling. The air temperature (T_a) was also measured at the cooling head. Values for temperature (T_b) were measured after 5 seconds of cooling time (τ). This value was arbitrarily selected. From equations 4.6 and 4.7, values of coefficients k_1 and k_2, were derived respectively. The resultant fit was good (deviation were within ±2°C) and repeated calculations with other time values proved unnecessary. After the calculation, the modeled temperature decrease

for forced and natural cooling was incorporated in Figure 4.19. The modeled temperature decrease was well agreed to the measured ones.

Table 4.3. Coefficient derived from Figure 4.19.

	Natural Cooling	Forced Cooling
Initial temperature of the body, T_0 at $\tau = 0$	87.5	87.3
Fluid temperature, T_a	22	22
Cooling time, τ	5	5
Temperature of the body, afterτ seconds of cooling, T_b	76.0	28.5
Coefficient, k	0.0397	0.4613

The derived coefficients (k_1 and k_2) used to reach target temperature using equation 4.10.

4.3.5.5. Bond formation and testing sequence

Sliced maple (*Acer macrophyllum* Pursh) veneers (0.8mm thick) were cut into strips of 20.0 × 105.0mm. These pieces were conditioned to 7% moisture content (± 0.5%). Wood cells were longitudinally oriented though no attempt was made to control orientation of growth ring on the strip surface.

Pre-catalyzed and filled resol type phenol formaldehyde (PF) adhesive was used in this research. PF adhesive was applied to the endmost 8mm of one piece of a bonding pair immediately prior to their being mounted in the ABES system.

The bond area measuring 20mm(width) by 8mm(overlap) were placed in the A.B.E.S. device. The pneumatically driven and computer controlled A.B.E.S. device simultaneously applied heat and pressure to the overlapping region via heated steal blocks. Hot pressing temperature, pressure, and time were controlled by A.B.E.S. control box and computer program.

At the end of hot pressing, the steel hot pressing blocks were retracted. Immediately after the retraction, the pneumatic piston was activated and the piston pushes up the cooling head in cooling position and blew air-jet on the wood surface for the time set by computer program. The time that took from the retraction of hot pressing block to the start of the air jet cooling was less than 1.5 seconds. The pressure and temperature of the air jet was constant over the experiment.

Three different bond forming temperatures were used and for each bond forming temperature, at least five level of different cooling temperature was tested for various bond curing times.

4.3.6. Forming hemp and wood fiber mats for miniature beams

4.3.6.1. Mat forming with hemp slivers

The highly processed and pre-oriented hemp sliver yarns were conditioned at 20°C, 65% RH before being used and they stabilized to a moisture content of 8% (± 1%). In order to form rectangular pre-forms, the yarns were first precision cut into pieces of 220.0mm length. The quantity of slivers was metered to form beams with target densities of 800 to 1200Kg/m^3 when compressed to thickness of 10 to 13mm. The yarns were carefully and uniformly unraveled so that the orientation was not disturbed. The unraveled yarns were at about 120.0mm width and 0.15mm thickness. Metered amounts of unraveled hemp sliver yarns

(approximately 20 to 30 pieces) were put on the floor such that each piece was regularly and evenly distributed. Liquid resole PF adhesive (see section 4.2.2) was diluted to 40% solids content with de-ionized water to reduce viscosity and applied at a rate of 10% based on the dry weight of the slivers. The adhesive was sprayed with a single-action air spray (seeFigure 4.20). After one side of the unraveled yarns had been sprayed, the yarns were turned over and the other side was sprayed. The adhesive spraying process was manually but carefully operated. The thinly-spread and loosely packed yarns were sufficiently accessible to enable the adhesive droplets to penetrate among the slivers. The applied adhesive was measured and recorded. Resinated yarns were then carefully put together to create a pre-formed in a forming box.

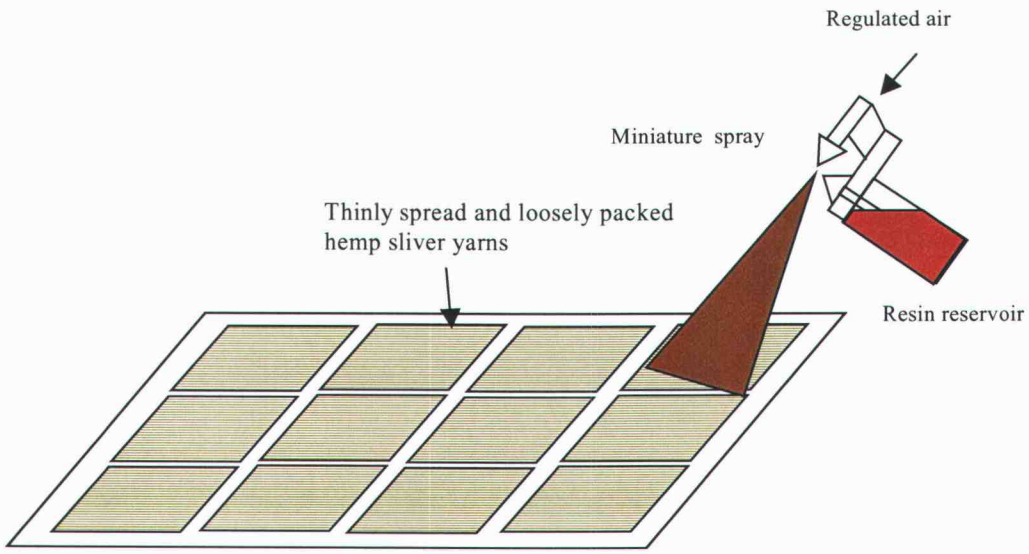

Figure 4.20. Schematic diagram of the resin spray on the unraveled hemp sliver yarns.

4.3.6.2. Mat forming with wood fiber

The quantities of fiber were metered to make beams with target densities of 750Kg/m^3 to 1000kg/m^3. Liquid resole PF adhesive (see section 4.2.2.) was again diluted to 40% solids content with de-ionized water to reduce viscosity and applied at a rate of 10% based on the oven-dry weight of fibers. Adhesive was sprayed using the single action air spray (Figure 4.21) as the fibers were tumbled inside a container by the agitation of an impeller to produce a uniform mixture. After spraying, tumbling was continued for 30 seconds to affect dispersion of adhesive as well as to break up agglomerations (balls) of fibers. The blended furnish was then hand formed by sprinkling it into a forming box, and manually pre-pressed with a rectangular plunger.

The specially developed adhesive spraying system consists of a motor with variable speed controller, an impeller, a pressurized spray tank, spray head, and resin reservoir. The impeller was specially designed; one end had a series of small holes to accommodate plastic tubes (2.95mm diameter and 150.0mm length) which vigorously agitate. The impeller passed through the center of the lid of the fiber container, and connected to the variable speed drive.

The resin was measured and kept in the reservoir under a slightly pressurized condition. Air pressure at the spray gun and resin reservoir were both activated simultaneously by a pilot valve. Variables, including the spray mist (spray nozzle setting, air pressure, etc.) were optimized experimentally to yield the finest mist possible and to avoid sputtering. After each batch of spraying, the spray gun was cleaned.

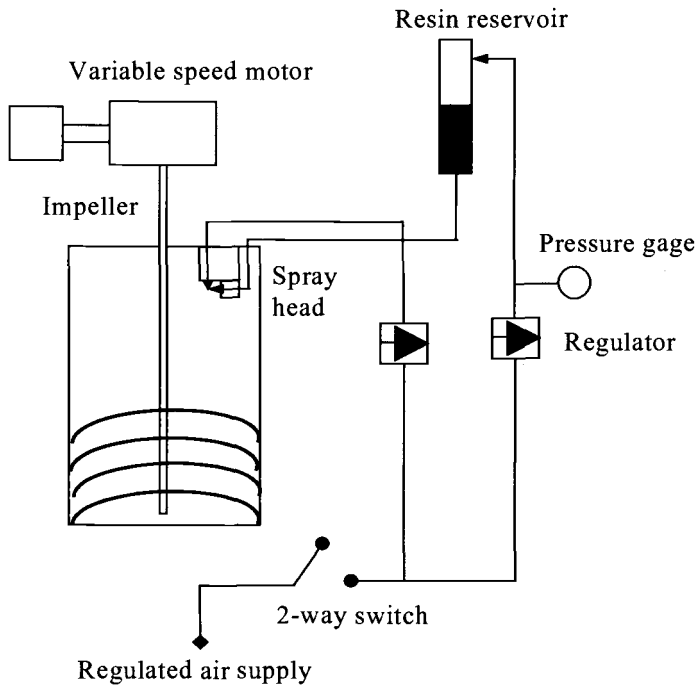

Figure 4.21. Adhesive spraying device for wood fibers

4.3.7. Gas injection pressing system for the synthesis of small rectangular beams

A laboratory-scale gas injection pressing system was designed and manufactured to synthesize miniature rectangular beams with internal structure gradients. This pressing system is connected to a servo-hydraulically driven pressing frame press (VersaTeste, model 30M). An associated gas injection system was also developed. This allows for the sequential injection and/or removal of chemical reactants in the vapor phase during pre-form consolidation.

4.3.7.1. Design strategies

The pressing system had to have provision for the controlled application of compressive stress with options for dynamic stress or position control. Secondly, the system had to have provision for the injection and removal of gas-phase reactive chemicals during pressing. Internal sensing of material conditions during gas injection pressing was also necessary. Thirdly, the system had to be capable of controlling the temperature of the platens. Lastly, the system had to be capable of computer controlled and digitized data acquisition. Peripheral sealing also had to be feasible for selected tests. Preliminary tests were conducted on hemp and wood pre-forms to ascertain the pressure necessary to achieve target densities in the order of $900kg/m^3$. The maximum size of the gas injection pressing platens was dictated by the load capacity of the servo-hydraulic press system (approximately 100kN) in concert with pressing pressure requirements.

4.3.7.2. Mechanical design

An overview of the system is shown in Figure 4.22. This system consists of upper and lower platens attached to the servo-hydraulic press. Each platen has 4 embedded cartridge heaters to transfer heat to the mat being formed, together with a gas injection plate where the reactive gases are injected from the perforated surface. The system was built from stainless steel.

Figure 4.22. The gas injection pressing system

4.3.7.2.1. *Upper and lower platens*

The upper platen consists of a top piece, a slide-in piece, and two end pieces (Figure 4.23). Each piece is connected by stainless-steel socket-head screws. The top and slide-in pieces have 4 holes (12.6mm diameter and 45.0mm depth) to accommodate cartridge heaters (75Watt, 120Volt of 12.5mm diameter and 38.0mm length with stainless steel sheath). The wires of the heaters exit from the top piece and are coated with heat-resistant PTFE plastic sheathing. A small (0.2-mm diameter) hole was drilled to accommodate a thermocouple.

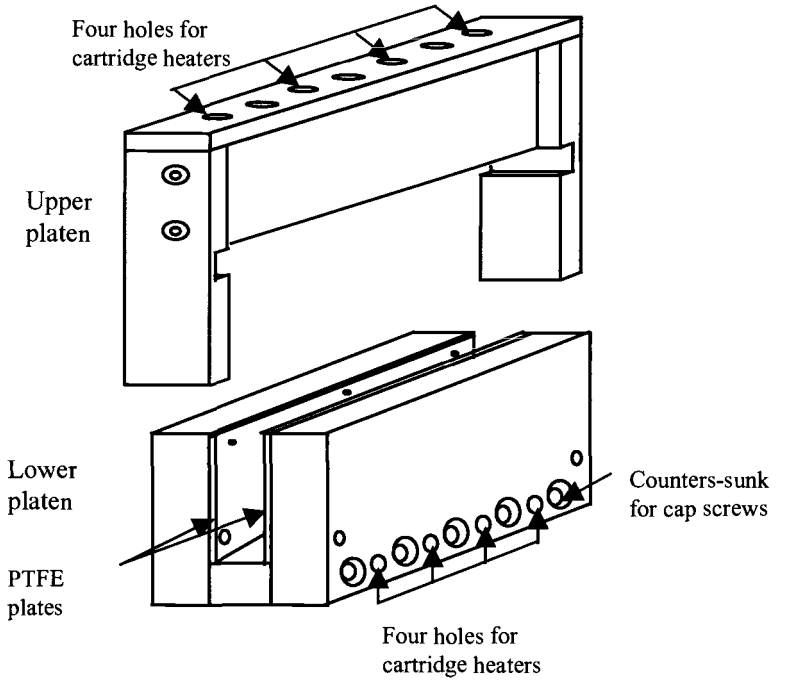

Figure 4.23. Upper and lower platens of the gas injection press

Two interchangeable sets of end-pieces have been made: long ones for use when fully sealed pressing is required, and short ones for partially-sealed pressing (where the ends of the sample are exposed to the atmosphere). Both sets of end-pieces have slots for the slide-fit of the gas injection plate. Also, a PTFE gas sealing plate (3.1mm thickness) was attached on the faces of both sets of end-pieces that contact the lower platen. For long end pieces, the PTFE plates provide a tight sliding fit to the end surface of the lower platens to generate a sealed environment. However, it was difficult with the long end pieces to sense physical conditions during gas injection pressing because access for sensors such as stainless steel tubes and thermocouple probes was impeded. The short end-pieces provide open space at the end of the platens for easy access of the sensors.

The lower platen consists of two side pieces and a bottom piece (Figure 4.23). Five holes were drilled to connect all three pieces using socket head cap screws; five holes in one of the side-pieces were threaded. Another four holes were drilled to accommodate the same type of cartridge heaters used in the upper platen. On the inside walls of the bottom platen, 3.1mm thick PTFE plates were attached with small flat-head cap screws. These PTFE plates provided a smooth gas-tight fit with the upper platens while contributing a minimum of frictional drag (important when operating the system in load control mode and when sensing load when operating in position control).

Although most experiments in this research were carried out at relatively low temperatures (at 50°C), the pressing system has the capability to be run at much higher temperatures for use in future applications. The number, location and power-density of the cartridge heaters employed (specified above) was selected after considering the thermal mass and shape of the pressing platens and the need for uniformity of heat transfer to the pressing surfaces. Two self-tuning temperature controllers with proportional, integral and derivative functions (PID) were used to control the temperature of the platens. Temperature control, with an accuracy of ± 1°C, over a range from ambient to approximately 150°C could be achieved.

Both upper and lower platens were precision-mounted on the hydraulically driven materials testing machine. In order to prevent heat transfer from the platens into the loading frame, glass-epoxy thermal barriers were placed between the platens and the press. Figure 4.23b shows the upper and lower platens attached to the frame of the hydraulic press.

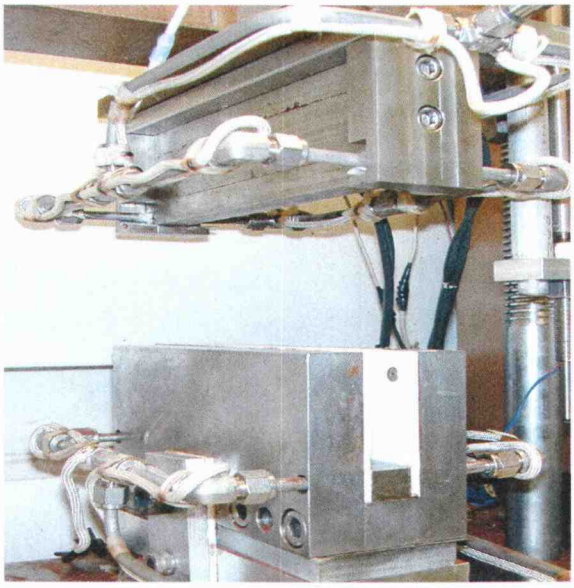

Figure 4.24. Upper and lower platens attached to the pressing system

4.3.7.2.2. *Gas injection plates*

A gas injection plate (19.1-mm wide, 15.9-mm thick and 209.6-mm or 238.8-mm long) was attached to each pressing platen. The plate for the upper platen was elongated in order to locate in the grooves of end-pieces affixed to the upper platen. The gas injection plates consisted of a thick perforated piece and thin cover piece. These pieces were connected by recessed socket head cap screws with a gasket interposed. The thick perforated piece had three evenly-spaced slots (2.5mm width, 7.0mm depth, and 232.4mm length) along their length. An arrangement of perforations within the slots provided pathways for fluid injection. The diameter and spacing of the holes was carefully selected, after some preliminary experimentation, in light of the following issues:

- maximize uniformity of fluid distribution at the platen-fiber interface;
- ensure sufficient freedom of flow to affect the required fluid mass transfer rate through the interface;
- ensure structural rigidity of the platen surface when high compressive pressures were applied to the fiber perform;
- avoid hole diameters which led to fiber ingress or excessive "dimpling"

The hole arrangement selected is shown in Figure 4.25, together with other aspects of the plate design. Cross-channels and end-access holes provided a means of circulating the treatment fluid through the injection heads.

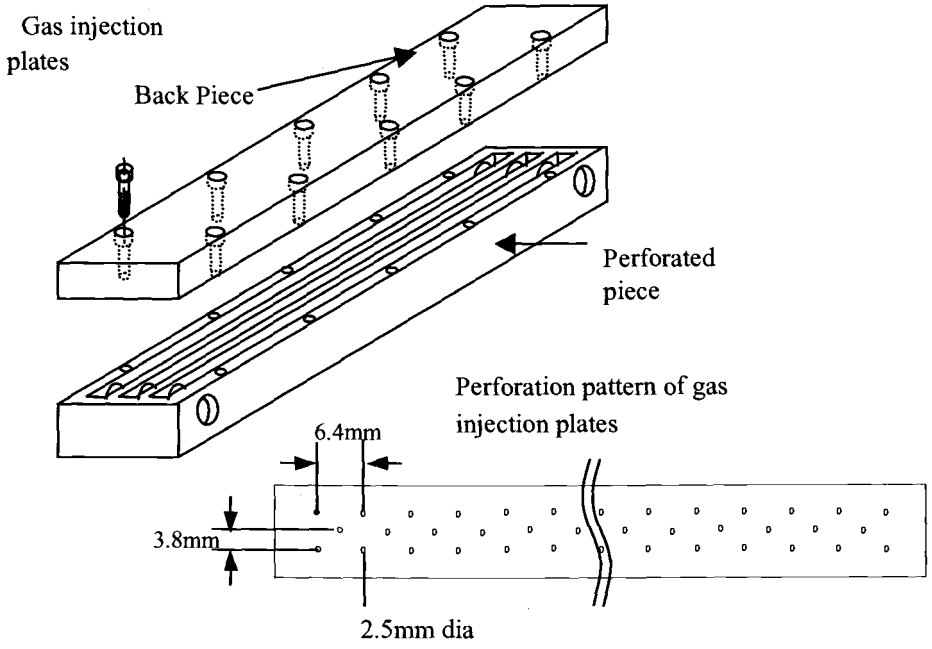

Figure 4.25. Diagram of gas injection plates

4.3.7.3. External gas supply system

The two fluid supply ports on the injection heads were connected to a stainless-steel tubing system. In order to avoid localized condensation of treatment chemicals (principally methyl formate), it was necessary to heat all external gas supply lines. Rope heaters (OMEGALUX, 400Watt, 120Volt) were wrapped around the stainless steel tubing system. The temperature of the tubing was monitored at a range of positions and controlled to approximately 50°C by means of solid-state AC voltage regulators.

A gas injection and removal system which was originally developed by Chowdhury (1999) was extensively modified and used to inject and remove reactive gases in the present system. Figure 4.26 schematically represents the external gas supply and removal system. The supply system was configured so that treatment fluids could be supplied and removed through either the upper or lower gas injection plates in a range of ways; this was in order to affect a wide range of treatment regimens. The external gas injection system is connected to external chemical container tanks with their own regulators. The pressure of the injected fluid gas was monitored by means of a pressure transducer (Omega PX212-300G5V) specially selected for its chemical and temperature resistance. In order to remove injected gases, an aspirator and vacuum tank was incorporated. The injection and removal of gases was affected and controlled manually by means of 2-way valves (with seals and bodies specially selected to resist methyl formate and anhydrous ammonia at elevated temperatures).

A cylindrical gas bomb (160.0-mm length and 62000mm^3 volume) was connected at the very end of the gas injection system to facilitate the direct injection of a desired gas of limited source volume or mobility (in this research methyl formate). An electrical band heater was mounted around the gas bomb and a temperature controller was used to control its temperature. A pressure gage and a 2-

way valve were also connected to the gas bomb. The entire gas injection pressing system is shown in Figure 4.22.

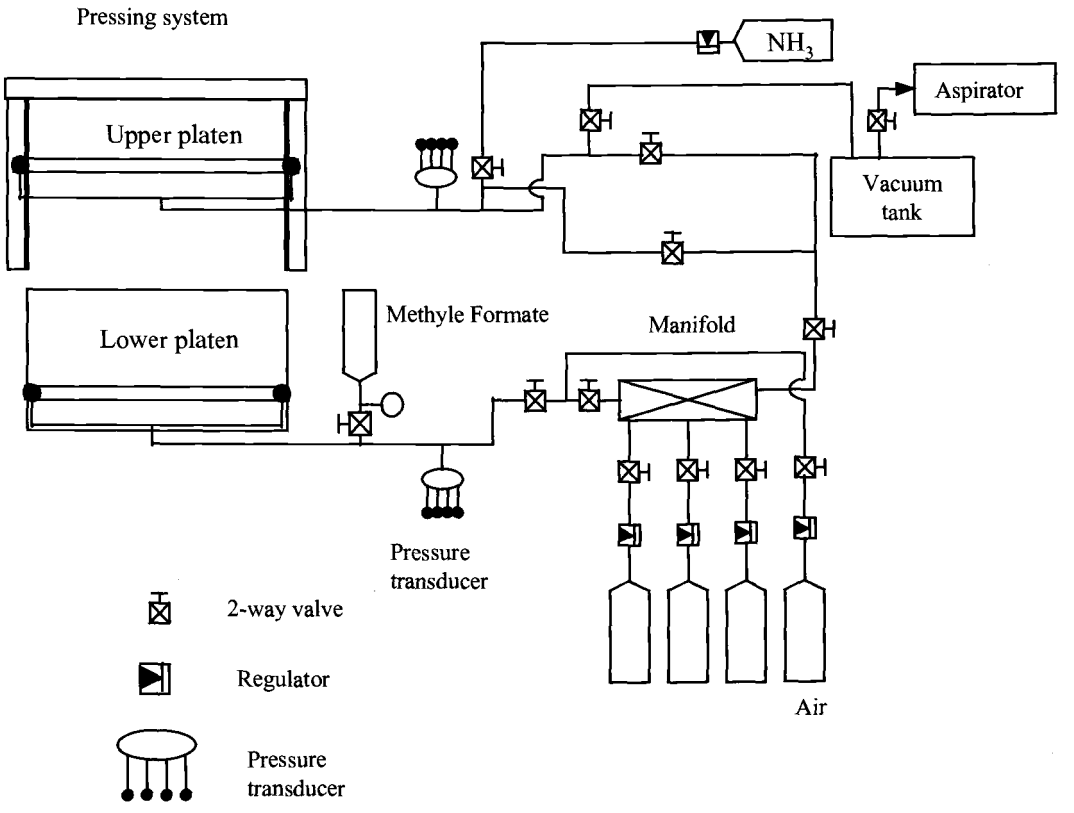

Figure 4.26. Schematic diagram of the gas injection and removal system

4.3.7.4. Platen position control and load measurement

In order to measure the position of the platen, an LVDT (Macrosensors model GHSD 750-1000) of 50-mm range was mounted beside the upper platen. This was connected beyond the thermal barriers of the upper platen to minimize the influence of heat. The thickness of the mat was dictated by the position of the platen. A pressure transducer (Omega PX3031KG5V) was mounted in the

hydraulic pressing system in order to monitor pressing force during sample consolidation. The analog signals from both the LVDT and oil pressure transducer, together with those from a number of other temperature and pressure sensors, were connected to the digital data acquisition system (Campbell 21X) to monitor and record the thickness of the mat and the pressing pressure.

4.3.7.5. Monitoring gas pressures and temperatures inside selected mats

After adhesive application with the specially designed miniature spraying system, fiber pre-forms were created using a miniature forming box. During the formation of selected mats, two miniature stainless steel tubes (0.58mm ID and 0.81mm OD) were inserted at a range of cross-sectional and longitudinal locations. The tubes were subsequently connected to pressure transducers (Omega PX176050A5V) in order to explore gas pressure gradients inside mats during gas injection and removal. Cross-sectional measurement locations were controlled by sub-dividing the total mass of resinated fibers into quarters and inserting the tubes and thermocouple probes in between those divided portions during lay-up. Figure 4.27 shows a schematic diagram of the pressure and temperature measurement locations inside the mat.

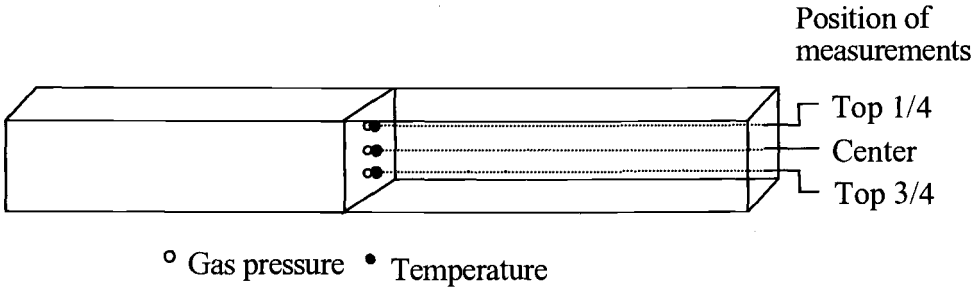

Figure 4.27. Position of gas pressure and temperature measurement inside the mat

The analogue to digital data acquisition system (Campbell 21X) was used to record the data from the following sensors:

- LVDT to measure platen separation
- Pressure transducer to measure hydraulic pressing pressure
- Pressure transducer to measure fluid injection/removal pressure
- Pressure transducers (two) to measure fluid pressures within mats during gas injection and removal
- Thermocouples (two) to measure temperature gradients inside mats during pressing

4.3.8. Chemical treatment and pressing sequences

As outlined in Chapter 3, the main objectives of the experiment were as follows:

I. Characterization of the softening action of gaseous ammonia on pre-formed wood and hemp fiber mats under a range of conditions.

II. Exploration of internal fluid pressure and thermodynamic behavior of mats during compaction.

III. Formation of trial composite sample beams by exposing pre-formed mats to gaseous ammonia followed by methyl formate vapor. The PF resin was catalyzed by the methyl formate after the mat had been softened.

IV. Creation of cross-sectional property gradients within sample beams by controlling pressure and sequencing of ammonia injection and removal.

4.3.8.1. Measurements of the softening action of anhydrous ammonia

The hemp fiber slivers were used in this experiment. Resin (10% based on dry sliver weight and 15% furnish moisture content) was sprayed on the hemp slivers as described in section 4.3.6. The pre-formed mat was placed in the pressing system and pressed at 50°C under thickness control mode. After the target thickness was reached (corresponding to a density of 1000kg/m^3), the press was held stationary until the decreasing pressing force (often termed counterpressure) stabilized. Anhydrous (gaseous) ammonia was then injected from the upper platen at a pressure of 0.62MPa. This test was conducted to ascertain whether gaseous ammonia softening could be affected in the gas injection pressing system.

In order to create a density gradient with gaseous ammonia, the maximum attainable softening was examined. This was done by compressing resinated pre-forms of wood fibers and hemp slivers by slowly increasing the pressing force with ammonia injection. Resinated (10% of dry weight of each constituent elements and 15% of furnish moisture content) hemp slivers and wood fibers were placed in the pressing system. The pre-formed mats were then pre-pressed to a thickness to 50mm. Then, gaseous ammonia was injected from the upper platen at 0.62MPa for 3 minutes. The pre-formed mat was then compressed at a rate of approximately 222.5N/s up to 6.8MN. This process was employed to minimize the elastic response of the pre-formed mat. After it reached maximum pressing force, the pressure was held for another 120 seconds. Thickness and pressing force was measured and recorded. Data for control samples which were formed without ammonia treatment were also collected and recorded.

Experiments were performed to check how deeply the ammonia gas penetrated through the hemp sliver pre-form. For this purpose, a measured amount of the hemp sliver was divided into four smaller parts with equal weight. Resin was not applied. Small pieces (5.0mm × 5.0mm) of litmus paper with a response range of pH 10 to 12 were then prepared and placed between the four parts of hemp

slivers. The pieces were placed at three different locations along the length. The pre-forms were placed in the pressing system and compressed to a density of 1000kg/m^3. Ammonia gas was injected from the upper platen at a range of pressures (from 0.14 to 0.41MPa) and times (from 5 to 30 seconds). Immediately after the ammonia injection, the press was opened and the color change of the litmus paper was checked and recorded.

4.3.8.2. Control of ammonia gas for the hemp sliver composite

One of the objectives of this research was to create a property gradient at low temperature using gaseous ammonia. The use of various gas pressures and treatment times were explored along with differing injection methods. Gas pressures explored ranged from 0.14 to 0.41MPa and the treatment time ranged from 5 seconds to 200 seconds.

For this purpose, resinated hemp sliver and wood fiber pre-forms (9% based on dry sliver weight and 15% of furnish moisture content) were prepared as described in section 4.3.6. The pre-formed mats were placed in the pressing system and pressed at 50°C under load control. Load control, rather than position control, was selected in order to maximize the differential densification of material within the cross-section. After the thickness had largely stabilized, ammonia gas was injected from the upper platen for a set amount of time. Immediately after the ammonia injection, high-pressure air (approximately 0.7MPa) was injected from the bottom platen and vacuum (0.14Mpa) was applied from the upper platen. This strategy was adopted in order to limit the penetration of ammonia. After flushing with air, methyl formate was injected from the pre-heated bomb into the bottom platen. After various amounts of pressing time, methyl formate was washed out using high pressure air from the bottom platen and vacuum from the upper platen before the press was opened.

Another injection method employed involved simultaneous injection of gaseous ammonia from one platen and air from the other. This was done to prevent the gaseous ammonia, which was found to be highly mobile, from penetrating fully through the mat. Instead of injecting gaseous ammonia from the upper platen, the equal pressure of air was also applied simultaneously from the bottom platen.

4.4. CHARACTERIZATION OF SAMPLE BEAMS

A range of sample beams were produced and all were placed in a standard room at 20°C and 65% RH for at least 24 hours prior to being tested. Internal densification due to the NH_3 gas injection was explored by x-ray densitometry. Also, the sample beams were cut into smaller pieces using a specially designed miniature circular saw to explore tensile strength and stiffness. The tensile strength and stiffness data, along with density gradient data, was used to model the stiffness of a hypothetical beam using the transformed cross-section method (section 5.7.1).

4.4.1. X-ray densitometry

An in-house x-ray densitometer system was used to measure density gradients within the created beams. This system can measure and record density-related x-ray beam attenuation data for wood and wood-based composite samples. The system is fully automated and computer controlled with custom-made software. A copper-targeted x-ray tube is employed as the x-ray source. The emissions include copper's characteristic K-alpha line at 8.05KeV. This energy level shows a wide range of attenuation over wood's typical density range. Consequently, small variations in wood density evoke large variations in detected x-ray beam intensity, which yields very good resolution for quantifying density

differentials. During the measurement the samples mounted on a tray were moved in discrete steps through the x-ray beam by means of an x-y table that is driven by electric servo-motors. The pulse rate of photons passing through the sample at each new point was counted.

The x-ray tube current and voltage were set at 30kV and 20mA respectively. The spot size of the beam and step size of the x-y table was set as 0.1mm. For each sample beam, the measurement was made at least three different places. To derive the density gradient of the sample, the measured changes in transmission were analyzed based on Lambert-Beer's Law (eq 4.11).

$$I_z = I_0 \exp^{-k\rho z} \tag{4.11}$$

where

I_z	intensity of measured x-ray beam
I_0	intensity of incident x-ray beam
k	extinction coefficient
ρ	density of the sample (g/cm^3)
z	thickness of the sample (cm)

4.4.2. Tensile strength and stiffness, and thickness swelling tests

Sample beams were cut into pieces to explore tensile strength and stiffness and thickness swelling characteristics of the material (Figure 4.28). Only one half-length of each beam was used for the tensile tests because of the possible defects due to the inserted thermocouple and small stainless steel tube used for the internal temperature and pressure measurements made during sample manufacture. The central parts of the test beams were used for thickness swelling tests. The tensile

test material was further cut into three smaller pieces along the y-z plane so that each piece had the same thickness (13.5mm) but had 1/3 of the width of the original beam. A specially designed miniature precision air-cooled circular saw was made and used for this purpose. Then, each smaller piece was further cut into five or six smaller specimens of equal thickness along the x-z plane.

A standard screw-driven universal testing machine with a pneumatic gripping system was used to perform the mechanical tests. Before each test, width, thickness, and density of the each specimen were recorded. During the test, 10 data points (load and elongation) were collected per second with an analog to digital data acquisition system (Campbell 21X). Maximum force to failure was also recorded. From the head speed of 1mm/min.and span of 25.0mm, deflection per data point and tensile modulus were calculated.

Prepared samples (see Figure 4.28) were soaked in water at 21°C. Changes in thickness were measured at various lapsed times (from 30 seconds to 24 hours). The percentage increase in thickness was calculated based on the initial thickness.

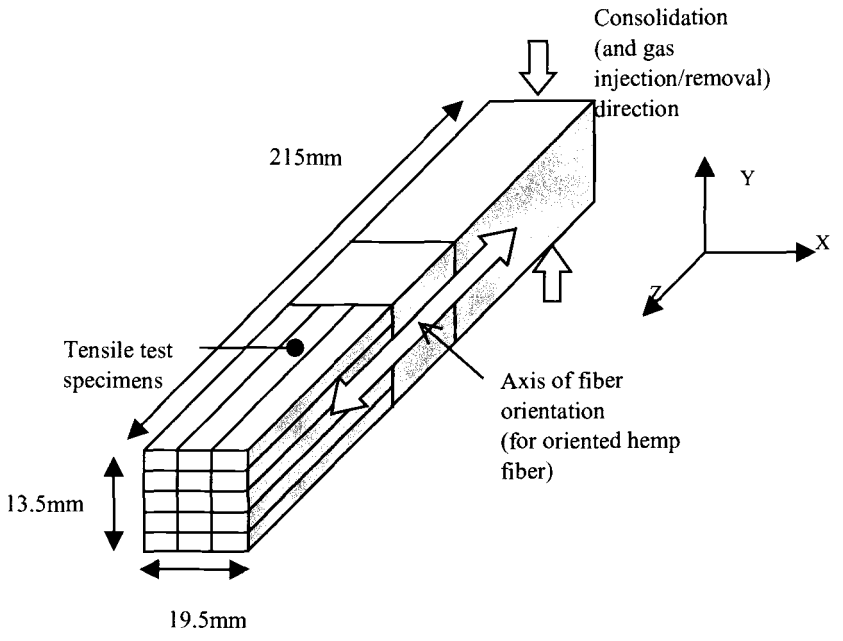

Figure 4.28. Diagram of manufactured beam prepared for tensile strength and stiffness and thickness swelling tests.

5. RESULTS AND DISCUSSION

5.1. ANATOMICAL AND MECHANICAL PROPERTIES OF HEMP FIBERS

5.1.1. Anatomical features of hemp

The anatomical features of hemp fibers used to form oriented fiber composite beams were observed in order to anticipate and eventually optimize the bonding and rheological behavior of assemblages of such fibers during composite formation. Electron (SEM) as well as light and dissecting microscopy was used to explore the surface morphology of hemp strands and slivers. Size (width, thickness and length) of single slivers was also measured.

Figure 5.1 shows an SEM cross-section of a piece of hemp stalk of the type used in the present research.

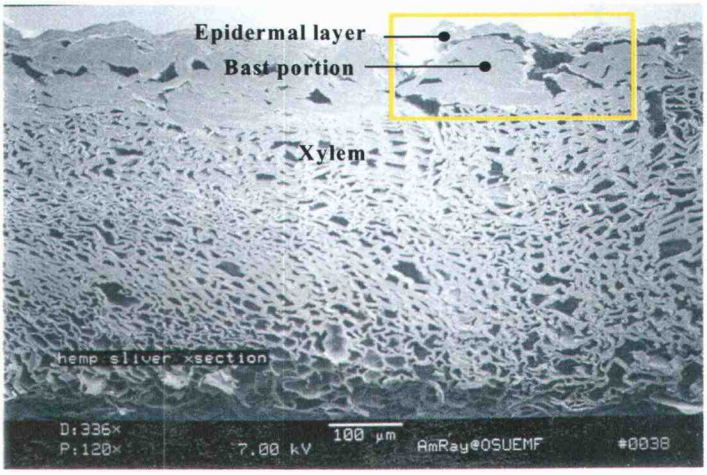

Figure 5.1. Cross -section of dried hemp stalk (120×)

Bast fibers are located at the upper portion of the figure, above the xylem cells. It was found that the outer portion of the bast fiber zone is covered with epidermal cells. Figure 5.2 is an enlargement of the rectangular area in Figure 5.1. The size and cell wall thickness of bast fibers are evidently greater than those of xylem cells. In addition, the transitions from xylem to bast and bast to epidermal cells are abrupt and may well lead to high levels of stress concentration when such bonded elements are subjected to load.

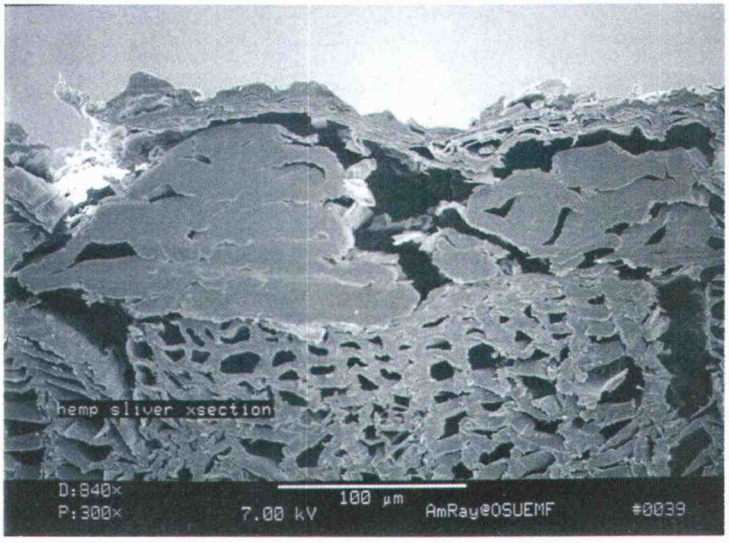

Figure 5.2. Enlarged portion shown in Figure 5.1 (300×)

Figure 5.3 shows an epidermal surface of a dried hemp strand portion which is covered with waxy material. The effect of such epidermal surface characteristics on inter-fiber bond strength development is critical and is discussed in section 5.2

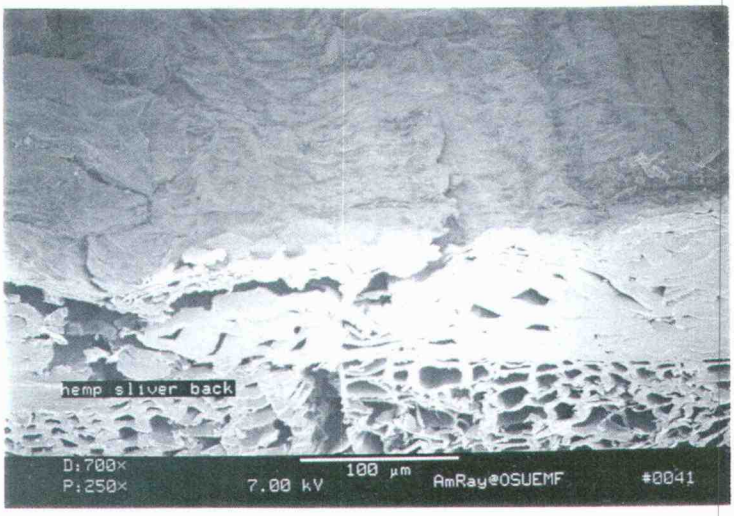

Figure 5.3. Epidermal surface of dried hemp (250×)

Figures 5.4 and 5.5 show the surface morphology and cross-section of hemp slivers used for synthesizing the hemp fiber composite beams in the present study.

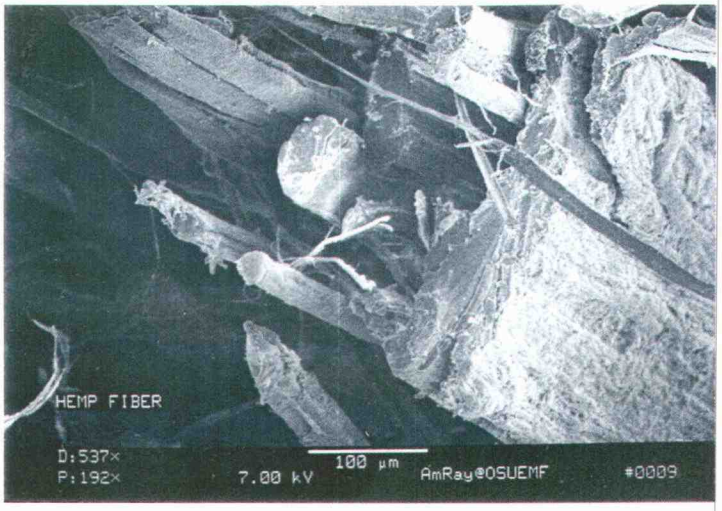

Figure 5.4. Isometric view of hemp slivers (192×)

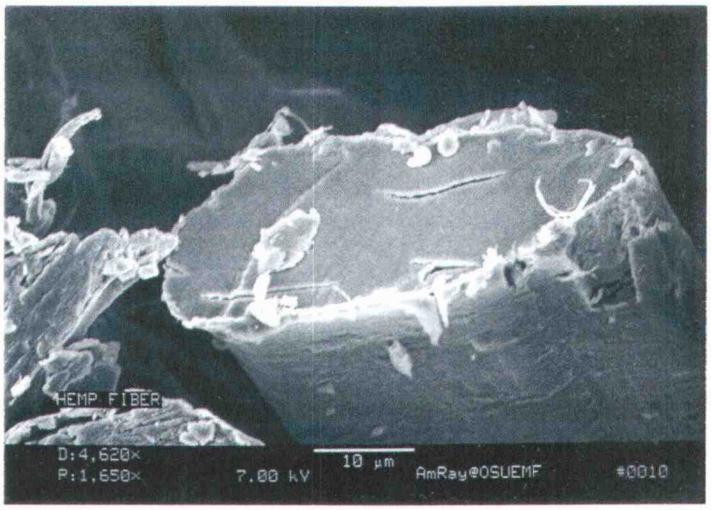

Figure 5.5. Cross -section of an individual hemp fiber (1650×)

The observed hemp slivers have very small lumens compared to those of typical wood fibers (Figure 5.5). This almost certainly influences compaction properties of hemp fiber mats during their consolidation since the void fraction is consequently small and density is high. This is likely to be especially relevant when trying to establish cross-sectional density profiles during the consolidation of oriented strand pre-forms. Density profiles are established in conventionally pressed randomly oriented wood fiber pre-forms (MDF and the like) both by virtue of the diametric flexure of cell-wall material about the lumen, and bending longitudinally due to bridging from one fiber cross-over point to another. Further, the uniaxial orientation of the hemp fiber pre-forms reduces the magnitude of bridging since the fibers pack efficiently when so arranged.

Typical dimensions of hemp slivers were measured using a dissecting microscope and image analysis system. The results are shown in Table 5.1.

Table 5.1. Typical dimensions of hemp slivers

Feature	Number of observations	Mean	Standard Deviation
Individual fiber width	50	21.3μm	3.69μm
Single sliver length	50	305.4mm	155.2mm
Single sliver width	197	249.2μm	154.3μm
Single sliver thickness	197	35.4μm	9.6μm
Individual fiber length*		5-55mm (Ilvessalo-Pfäffli,1994) 1-34mm (Catling and Grayson, 1982)	

* Value from the literature

The observational results indicate that hemp slivers consist of several individual hemp fibers connected side by side but longitudinally offset. The mean length of single hemp slivers used in the present research was about 305mm, while width and thickness were 249μm and 35μm respectively. The width of individual hemp fiber was about 21μm. Measurements made by other workers (Ilvessalo-Pfäffli,1994; Catling and Grayson, 1982) suggest that the length of single hemp fibers range from 1.0 to 55.0 -mm; they also confirm that single slivers consist of individual fibers connected in the length direction. Thus, single hemp slivers used in this study were an aggregation of individual hemp fibers connected in the width and length directions.

5.1.2. Tensile strength of hemp slivers

The tensile strength of single hemp slivers was measured as described in section 4.3.1. The cross-sectional area of each tested sliver was measured using a dissecting microscope and digital image analysis system. From the anatomical

features observed in section 5.1.1, it was found that the lumens of single hemp fibers are very small. Therefore the cross-sectional area was calculated from the width and thickness of each sliver tested and the contribution of the lumen ignored. Table 5.2 shows the slivers' tensile strength and stiffness; values are in stress units since they are cross-section corrected.

Table 5.2. Tensile strength of hemp slivers

Tensile Strength (MPa)	Source of Data
819.2 (mean) / 372.1 (SD)	
630 –1080	Rials and Wolcott, 1996 Robson and Hague, 1996 Snell *et al.*, 1997 Seber and Lloyd, 1995

The tensile strength values for hemp slivers obtained in this study are within the range previously published by many researchers (Rowell *et al.*, 1996). In the absence of a viable micro-mechanical model of the slivers and constituent fibers, it is difficult to identify the source of the large variability in tensile load-bearing properties observed here and by other workers. Cross-sectional size effects almost certainly play a role since crack initiation and propagation within cell walls depends on surface morphology. Variability in surface morphology, in turn, may be an inherent part of the natural structure, but is also introduced by the way the fibers are processed. Further, little information is available about variability in the chemical constituents of cell wall material between and within such fibers.

In spite of this variability, hemp fibers do exhibit very attractive properties. Indeed, variability is well within that of typical wood fiber bundles used for panel products, including MDF and the like (Jane, 1960; Snell et al., 1997).

5.2. BOND STRENGTH DEVELOPMENT BETWEEN HEMP STRANDS

This part of study was carried out to explore the effect of epidermal and xylem-contacting surface characteristics on the strength development of bonds between PF adhesive and hemp strands. When raw material derived from various sources such as bast fibers like hemp and cereal straw are used in composite manufacturing, these fibers may contain epidermal surfaces depending on the fibers' origin and production process. It has long been known that the waxy epidermal surface adversely affects the final properties of composites made from them, but these effects have not been evaluated quantitatively. In this study, pairs of hemp strand surfaces were prepared as described in section 4.3.3 in order to directly assess bond strength development with PF adhesive. Figures 5.6 is SEM images of inner and outer surfaces at two levels of magnification. The inner surface adjacent to the xylem is shown in Figure 5.6A and B and the outer layer that contains an epidermal surface is shown in Figure 5.6C and D. No clear differences in visible surface characteristics are evident, however.

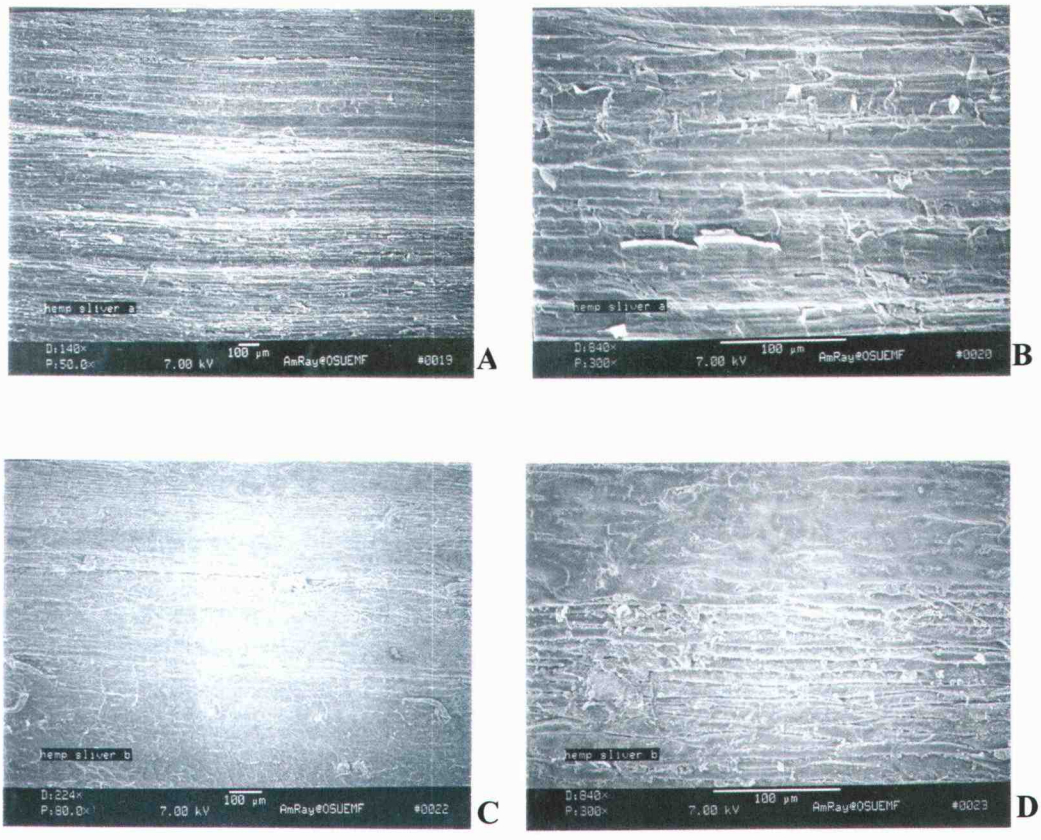

Figure 5.6. SEM micrographs of different surfaces of a hemp strand. A: inner surface ×50; B: inner surface ×300; C: outer surface ×50; D: outer surface ×300)

Isothermal shear strength development data are shown as Figure 5.7. Each point corresponds to the shear strength of a strand-pair pressed at a temperature of 50°C and pressure of 1.1MPa using the miniature pressing heads described in section 4.3.3. These strength values were calculated by dividing the shear force-to-failure by the bond area (measured accurately by microscopic observation of each sample individually).

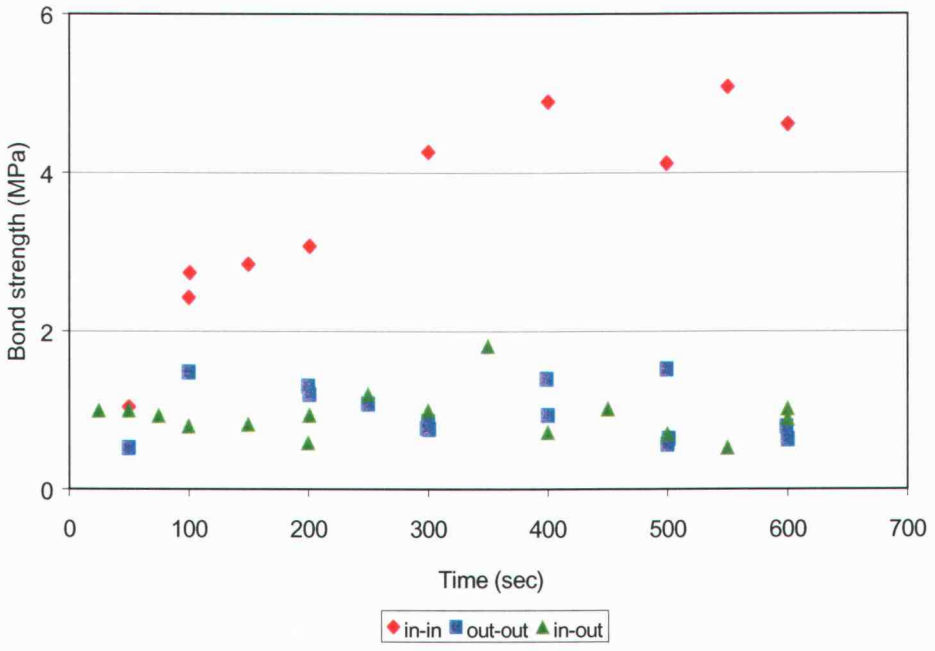

Figure 5.7. Phenol formaldehyde bond strength development between variously combined hemp strand surfaces (overlap area nominally 5mm^2, pressed at 1.1MPa and 50°C).

No account has been taken of the parabolic distribution of shear stress that is generated along the overlap of lap-shear test bonds. Such non-uniformity of stress becomes small as overlap is reduced and when shear strength values are small compared to the elastic moduli of the adherends (hemp strands). In the absence of an accurate estimate of glue-line thickness, numerical analysis of such stress distribution is unreliable (Humphrey and Zavala, 1989; Lindner, 2000; River, 1981). Future development of fiber and strand testing techniques may enable such corrections to be applied.

It was found that the presence of an epidermal surface in a bonding pair greatly reduced bond strength (Figure 5.7). It is also evident from the data that bond strengths between inner surfaces of hemp strands develop as the curing time

increases whereas the bond strength between inner-outer, and outer-outer surfaces remain low regardless of curing time. Bonds formed between inner surfaces increased linearly at a speed of 9.6kPa/sec up to 400 seconds (R^2=0.84). Bonds formed with epidermal surfaces exhibit no significant correlation with elapsed pressing time. The bond strength data between inner-outer and outer-outer surfaces were statistically analyzed; p-values for outer-outer and inner-outer combinations were 0.98 and 0.36 respectively which, in turn, indicated that bond curing time had no effect on bond strength development between such combinations. The mean values (for all times combined) are, however, 0.96MPa for outer-outer and 1.05MPa for inner-outer combinations. Bonds formed for 20 seconds fall near this value suggesting that the initial rate of bond strength accumulation is as fast as that for non-epidermal surfaces which eventually attain high strength. This finding indicates that the presence of epidermal surfaces in PF resin bonding does indeed adversely effect bond strength regardless of degree of curing. Thus, when natural fibers which contain epidermal surfaces are used, other types of adhesives must be explored. Alternatively, means of chemically removing the waxy layer may be developed.

Matched pairs of fracture surfaces for an inner-outer combination and inner-inner combination is shown as Figure 5.8.

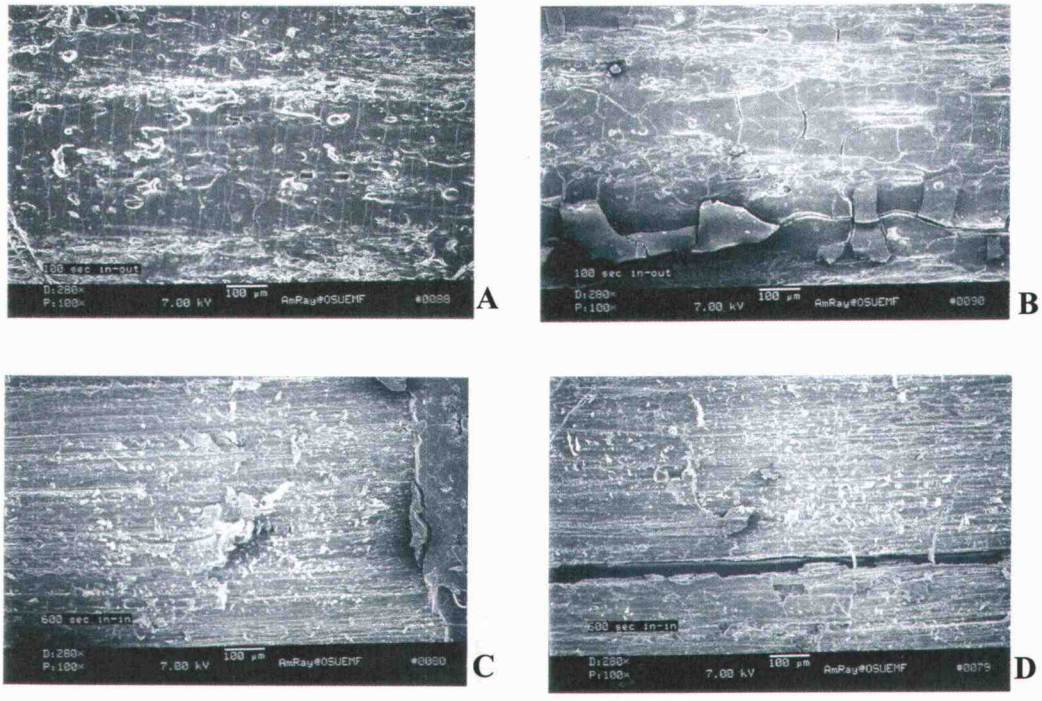

Figure 5.8. Fracture surfaces of PF-to-hemp bonds. Pressed at 1.1MPa for 100 seconds (A and B) and 600 seconds (C and D). Frames A and B are inner and outer surfaces of a single bond of 0.98MPa of strength Frames C and D are inner surfaces of an inner-inner pair of 5.1MPa strength.

5.3. BOND STRENGTH DEVELOPMENT OF ORIENTED HEMP SLIVER NETWORKS

Adhesion was explored between oriented hemp slivers configured in a form similar to that in beams consolidated in the gas injection pressing system. Small portions of fiber network were treated with 10% (by weight) liquid PF adhesive and laid over one another with an overlap of 10mm before being pressed at 1.1MPa at 50°C. When compressed, the samples reached a thickness of 0.05mm. This corresponded to a density of approximately 950kg/m^3. Densities within the miniature beams (section 5.6) ranged from 917 to 1190kg/m^3.

Further investigations will involve exploration of adhesion kinetics and failure mechanisms of fiber assemblages compressed to a range of densities with a diversity of fiber types and adhesive formulations and concentrations. The objective of the present study was to develop a single testing technique and use it with a single combination of material and pressing parameters. The combined data for tests conducted both with and without the injection of methyl formate are shown as Figure 5.9.

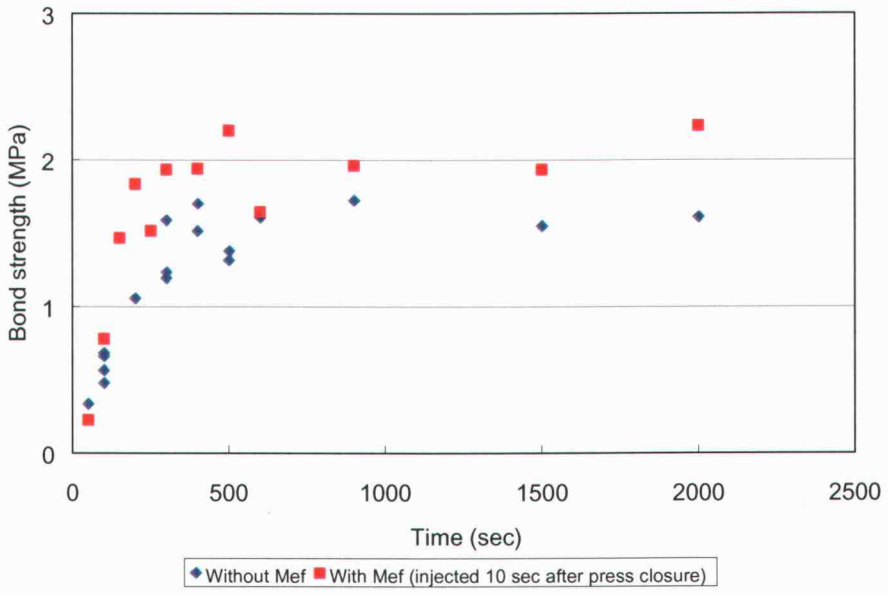

Figure 5.9. Bond strength development between hemp sliver networks formed at 50°C both with and without methyl formate injection.

Load values have been converted to stress by dividing by the overlap area of the networks. This was done because all test samples failed principally by fiber-pull-out and all fibers overlapped by the same distance. Indeed, the overlap was

limited to 10mm, after preliminary trials, in order to avoid the introduction of significant levels of fiber breakage both within and beyond the bonding area.

It is evident from Figure 5.9 that bonding progressed rapidly at the outset for both data sets and leveled off at values between 1.5 MPa and 2.25 MPa. The introduction of methyl formate hastened bond strength development rate and fully cured bonding values were also enhanced. For the purpose of this discussion, the data sets have been divided into two parts. That period when strength values rose rapidly (0-500 seconds) have been linearly regressed, while beyond 500 seconds strength development was not significant and values were averaged.

Linearly regressed bonding rates based on the first 500 seconds of pressing have gradients of 2.5kPa/sec (R^2=0.77) for untreated bonds and 3.8kPa/sec (R^2=0.74) for the ones treated with methyl formate. Statistical analysis indicated that the bond strength development rate of hemp slivers with methyl formate injection was different from that without mehyl formate (p-value of 0.012). The bond strength values after 500 seconds for both cases were not affected by curing time (p-value is 0.23 for without methyl formate and 0.41 for with methyl formate). The mean bond strength of the sliver networks was 1.62MPa without methyl formate and 1.94MPa with methyl formate respectively. It was also found that the mean bond strength with methyl formate was significantly different from that without methyl formate (p-value=0.002). Based on these data, methyl formate injection increased linearly regressed strength development rate by 51% and final values (beyond 500 sec) by 22%. As described earlier (section 2.7.2), methyl formate has tri-functional groups (compared to the di-functionality of formaldehyde) which increases the number of functional groups in the methylol phenol. The addition of methyl formate also represents an increase in the concentration of reagents.

The fully cured strengths of the bonded networks may usefully be compared to the bond strength of individual hemp sliver pairs presented in section 5.2 (mean values of 5.1MPa, 1.05MPa, and 0.96MPa for inner-inner, inner-outer, and outer-

outer combinations respectively). Bonding sites in the networks contain all three combinations of surface interface. Failure mechanisms associated with such a diversity are likely highly complex. Using a simple weighted mean, and assuming each fiber has an equal partition of inner and outer surface area, then a network shear strength of 2.1MPa is derived. This compares quite favorably with the network value of 1.62MPa measured without methyl formate injection.

Table 5.3 Hemp fiber and network shear strength.

Orientation	Regressed Bonding rate	Mean strength after 500 seconds
Inner-inner	9.557kPa/sec	4.60MPa
Inner-outer		1.05MPa
Outer-outer		0.96MPa
Network	2.499kPa/sec	1.62MPa
Network with methyl formate	3.771kPa/sec	1.94MPa

This result suggests that the measurement of bonding characteristics for individual sliver pairs may provide information useful in estimating how they will perform in fiber-based composite materials. No account has, however, been taken of the strength and stiffness of strands and their influence on the distribution of shear stress along the length of bonding interfaces. Such analysis will be conducted in future investigations. Figure 5.10 shows part of the hemp sliver network after testing. There were no discernible differences between surfaces formed with and without methyl formate injection.

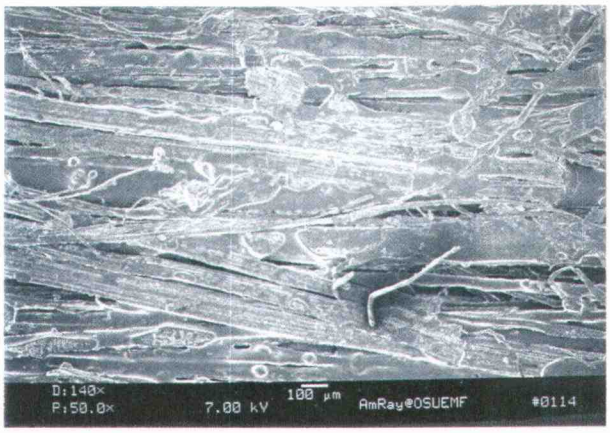

Figure 5.10. Failure surface of hemp sliver network after testing.

5.4. EFFECT OF TEMPERATURE ON THE STRENGTH OF PARTIALLY CURED PF-TO-WOOD BONDS

It has already been pointed out (section 2.5.1) that bond strength development within natural fiber-based composite materials during the consolidation process influences the efficiency of production and quality of products. In both conventional and unconventional sealed pressing techniques, adhesives are subjected to varying temperatures. Temperatures generally rise during conventional pressing processes and decline as the source of heat and surface sealing (platen) is removed. Adiabatic cooling is known to result from surface venting of entrapped water vapor. Such venting occurs during press opening and its sequencing and that of resultant internal cooling with the concomitant transfer of loads to glue-bonds is highly dependent on the rheological properties of the composite. Composite pressing simulation algorithms which include the press-opening stage (Thömen, 2000; Thömen and Humphrey, 2002) do, however, suggest that for industrially produced MDF, particleboard, and flakeboards, unacceptable levels of stress (and consequent damage) are transferred

to the components' microstructure before surface gas venting and associated potentially advantageous temperature decrease occur.

Temperatures within composites may, however, be artificially manipulated. Use of perforated pressing platens and sealed pressing of the type used in the present work offer the opportunity not only to inject gases (including high temperature air or water vapor) at the beginning of pressing cycles but also to vent internal gases prior to press opening. Pressing simulation runs executed by Thömen and Humphrey (2002) for industrial steam-injections panel presses suggest that significant reductions in internal temperature may thereby be affected.

Pressing temperature employed in the formation of miniature beams in the present study were however low (50°C) since an alternative means of stimulating adhesive polymerization (methyl formate injection) has been employed. Significant increase in internal temperature (in excess of 70°C) have, however, been measured and attributed to heat of sorption of ammonia. Removal of ammonia by venting and evacuation has also been found to effect rapid cooling. These mechanisms are addressed in section 5.5 below. The influence of such cooling on bond properties may thereby also be of importance in future development of sealed pressing apparatus for beam and related molded composite objects.

The technique described in section 4.3.5 was developed with a view to characterizing the effect of temperature on the ability of bonds to transfer stress and thus hold components together during the transition from full to zero platen restraint at the end of industrial cycles.

5.4.1. Isothermal strength development

As described in section 4.3.5, standardized bonds (Maple adherends, phenol formaldehyde adhesive with spread rate of $80g/m^2$, bonding area 20mm wide by 8mm overlap pressed at 1.1MPa) were formed at 70°C, 90°C, and 100°C and

variously cooled immediately before being pulled. Before describing cooling effects, isothermal strength development without cooling will be described. Strength values for bonds pressed for times ranging between 20 and 200 seconds and tested without cooling are therefore shown in Figure 5.11.

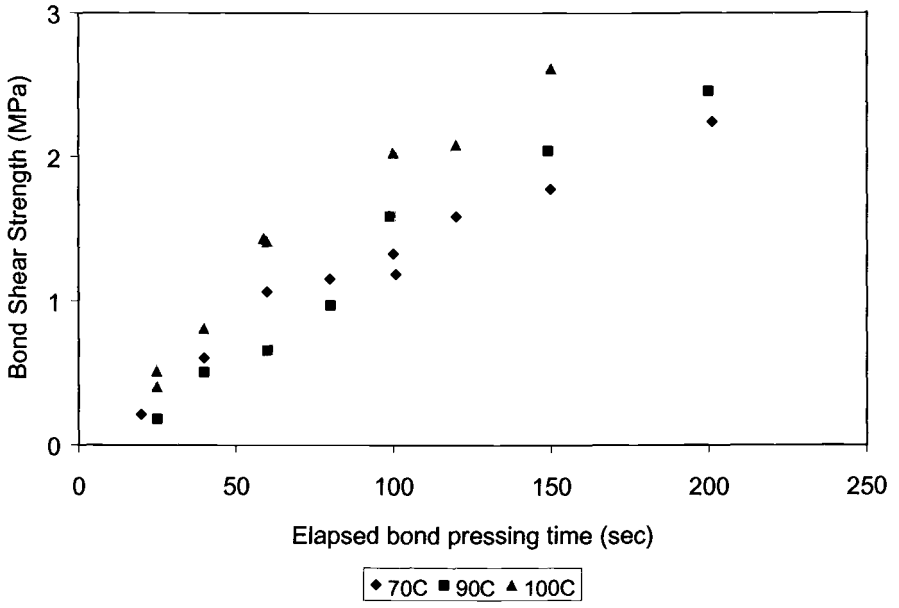

Figure 5.11. Bond strength development without cooling at three different temperatures.

Linear regression of strength versus time for each temperature suggest a near linear relationship. Resultant coefficients and R^2 values are show in Table 5.4.

Table 5.4. Strength data for uncooled bonds formed at three temperatures.

Pressing temperature (°C)	Linearly regressed isothermal bonding rate (kPa/sec)	R^2
70	10.6	0.95
90	13.3	0.96
100	16.9	0.95

The thermosetting nature of the adhesive is clearly evident in Figure 5.11. Figure 5.12 shows an Arrhenious plot of bonding rate.

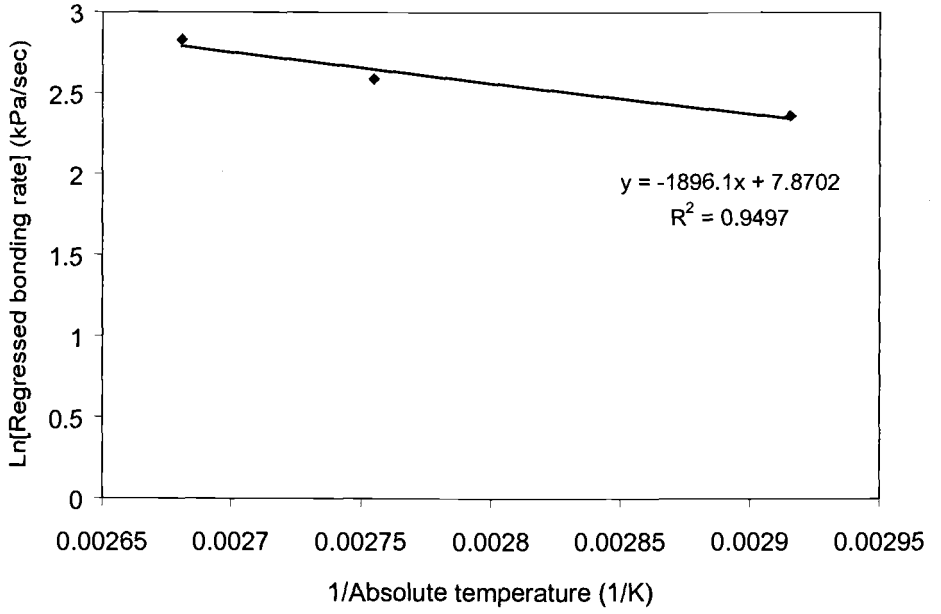

Figure 5.12. Natural logarithm of regressed bonding rate vs reciprocal of absolute temperature.

The alignment of the points of the Arrhenious plot of Figure 5.12 combined with that based on corresponding isothermal tests conducted with identical adhesive in complementary tests (Humphrey, 2001) suggest that the strength development is the consequence of a first-order chemical reaction. Humphrey and Ren (1989) coined the term reactivity index (Ri) to describe the responsiveness of such physical systems to temperature, such that:

$$Ri = -T \cdot \ln A$$

where Ri = reactivity index (K)
T = absolute temperature (K)
A = isothermal rate of bond-strength development (Pa/sec),

An Ri value of 1896.1K has been derived from the data of Figure 5.12. This value may be used as a guide as to how the adhesive's bonding rate will respond to changing temperatures within composites during consolidation.

5.4.2. Bond cooling effects

Shear strength values for bonds pressed at 90°C but cooled to six temperatures ranging between 87°C and 24°C are shown as Figure 5.13. Bond pressing times used in Figure 5.13 are defined as the lapse of time from when the pressing blocks close on the bond to when the blocks are retracted. Forced cooling was initiated within one second of press opening and the polymerization rate was greatly reduced. Inaccuracies due to time delays between press opening and bond failure were therefore minimized.

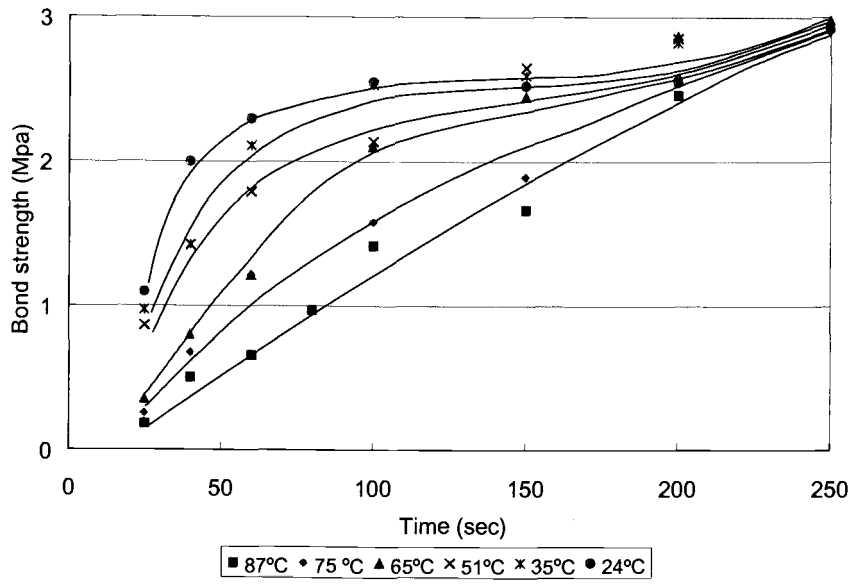

Figure 5.13. Strength versus forming time for PF-to-wood bonds formed at 90°C and variously cooled prior to being tested

Lines of bond strength versus forming time for constant testing temperature have been added manually to the data in Figure 5.13. It is evident that cooling of partially cured bonds greatly increased their shear strength and that the effect declines as cure progresses. For example, after 75 seconds of pressing at 90°C, the differential of bond strength between 24 °C and 87 °C was 1.4Mpa; this corresponds to a cooling-induced strength increase of 142%. However, after 250 seconds of isothermal pressing at 90°C (Fig. 5.14), the effect of cooling had almost entirely ceased. The behavior of adhesive between press closing and 25 seconds of pressing could not be reliably resolved because curing temperatures were transient during that period (rising from ambient to block temperature).

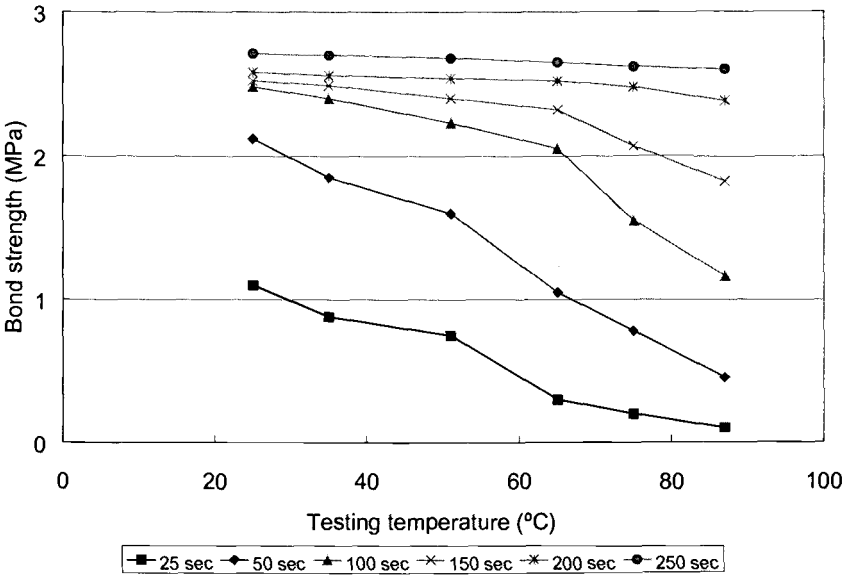

Figure 5.14. Strength versus testing temperature for a range of six elapsed pressing times (derived from the data in Figure 5.13)

Strength development data for bonds formed at all three temperatures are combined as Figure 5.15 (A, B, and C). Alongside each of these (Fig. 5.15 B, D, and F) are corresponding plots showing the temperature dependency of bond strength at a range of six elapsed isothermal pressing times. These data have been derived from the fitted curves of Figure 5.15A, B, and C.

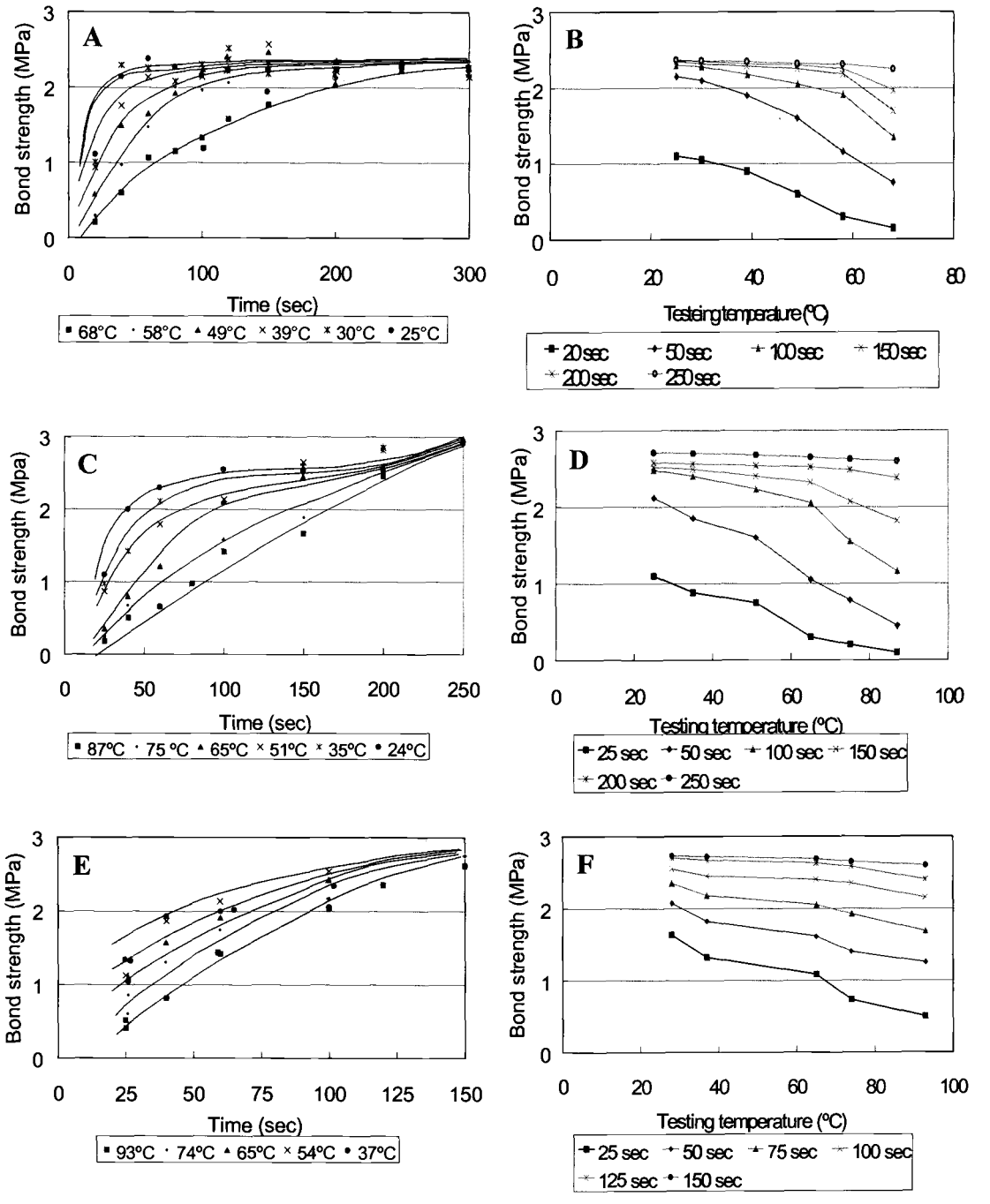

Figure 5.15. Effect of cooling on partially cured PF-to-wood bond strength pressed at 70°C (A and B), 90°C (C and D), and 100°C (E and F).

Evidently, the little-cured bonds display high temperature dependency and this progressively decreases as bonds reach intermediate levels of strength. It seems reasonable to suggest that the polymer passes through a transition in structure that renders it resistant to temperature. Glass transitions in polymers do, however, normally occur at well-defined temperatures (T_g). In this case, the strengths exhibit progressive changes in strength with no discrete transition.

Application of the conversion-temperature-transformation (CTT) concept to these data is not therefore possible because transitions in bond strength with temperature (at fixed cure level) are gradual rather than stepwise and glass (T_g) or rubber (T_r) transition temperature cannot therefore be extracted. The lack of clear transformation may be the result of complex interactions of the adhesive with wood.

The above results imply that the strength of partially cured thermosetting bonds may be increased by lowering their temperature. With the advent of gas injection presses, a diversity of new pressing technologies may enable cooling prior to press opening and thus reduce pressing time.

5.5. SYNTHESIS OF NATURAL FIBER COMPOSITE BEAMS

The miniature pressing system described in Chapter 4 has provision for the sequential injection and removal of reactive chemicals in the vapor phase and thus offers opportunities for chemical treatment of natural fiber networks during pressing. The system may be used to make miniature samples under controlled chemical, mechanical, and thermal conditions as well as to evaluate the effects of specific conditions on the pre-form's structure and properties.

A number of preliminary trials were conducted to refine and calibrate the pressing and associated gas dosing and monitoring (transducer) systems. Beams were then synthesized using a range of pre-form configurations under controlled consolidation conditions. Tests were configured to address the following issues:

- How boundary conditions (particularly at the mat-platen interface) and mat attributes effect the spatial and time-based distribution of internal conditions during consolidation. Parameters of primary concern are:
    1. densification and stress relaxation
    2. gas pressure and constitution
    3. temperature
- How fluid transfer, thermodynamic, chemical, and rheological mechanisms contribute to the above measured behavior
- The feasibility of using anhydrous ammonia to effectively modify the rheological properties (viscoelastic parameters) of rectangular hemp and wood-fiber networks at near-room temperatures;
- The feasibility of using methyl formate injection to stimulate PF adhesive bonding at near-room temperatures;
- The feasibility of using judiciously injected ammonia to affect cross-sectional density gradients.

Most of the discussion to follow will revolve around time-based graphs of how conditions varied at selected locations within the beams during their consolidation. Both uniaxially oriented hemp and randomly formed wood fiber networks will be considered with and without phenol formaldehyde adhesive. Six samples produced during such tests were retained and some aspects of their structure and properties evaluated. Cross-sectional density profile (mass distribution in the consolidation direction) will be discussed together with spatial distributions of mechanical and swelling properties in Section 5.6 to follow.

Listed below are parameters that are pertinent to the discussion.

Time-based data for the following parameters:

- Internal conditions (at up to 3 cross-sectional positions):
  1. gas pressure (embedded hypodermic tubes)
  2. temperature (embedded thermocouples)
- Boundary conditions:
  1. compressive pressure (platen pressure)
  2. thickness (platen separation)
  3. injection fluid supply pressure (and fluid type)

Conditions measured after beam formation:

1. cross-sectional mass distribution (density profile)
2. tensile strength and swelling properties

Pre-form variables:

1. fiber type (hemp and wood)
2. adhesive type (none, liquid PF)
3. fiber orientation (random wood, oriented hemp)

Before considering the synthesis of beams with density profiles, the internal behavior of pre-forms at each stage of a selection of consolidation cycles will be considered. In order to show the overall nature of the system's behavior, representative data sets collected during the consolidation of hemp and wood fiber pre-forms using typical cycles of load are shown as Figure 5.16 and 5.17 respectively. The rheological, gas transfer, and thermal mechanisms that effect pre-form behavior are highly interdependent; each will be dealt with in the following discussion.

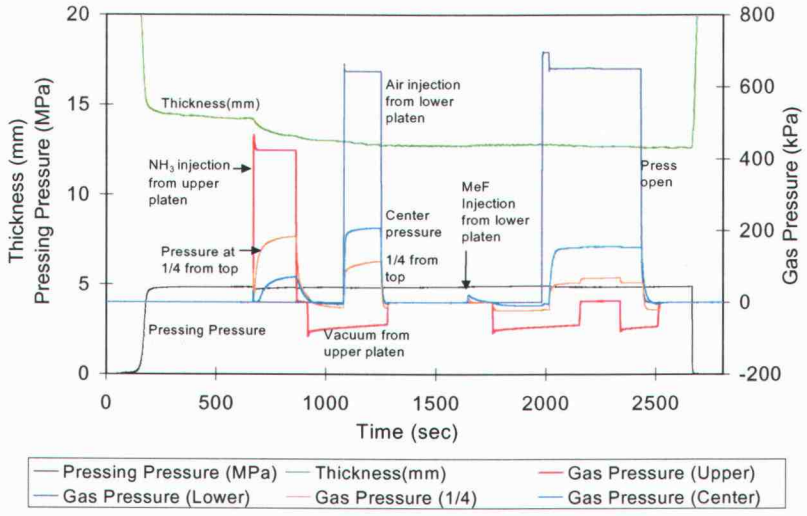

Figure 5.16. Combined data recorded during the consolidation of an oriented hemp fiber pre-form under load control. (Material: oriented hemp; initial closing speed: 0.3mm/sec; resin: 10% PF; pressing pressure: 4.85MPa; ammonia pressure and time: 413 kPa for 200 sec.; methyl formate: 25cc).

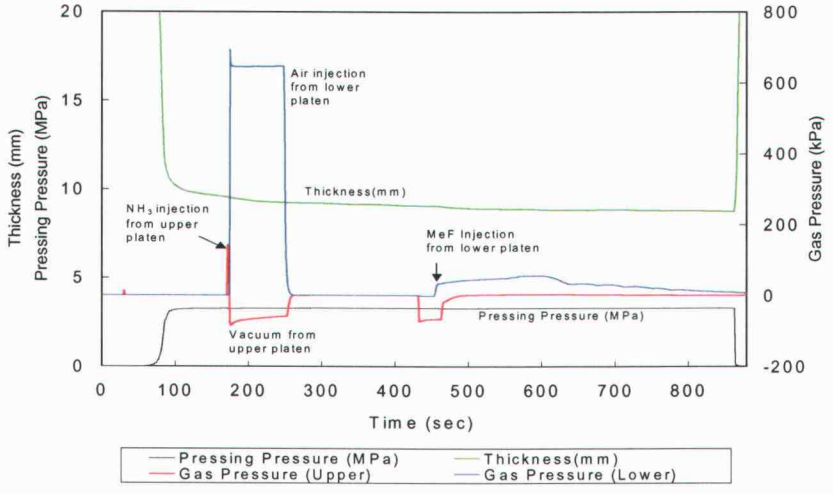

Figure 5.17. Combined data recorded during the consolidation of a randomly formed wood fiber pre-form under load control (material: wood; initial closing speed: 2.0mm/sec; resin: 9% PF resin; pressing pressure: 3.25MPa; ammonia pressure and time: 137.9kPa for 3 seconds; methyl formate:50cc).

5.5.1. Initial densification in the absence of ammonia

At the beginning of both pressing cycles (Figure 5.16 and 17), the press closed at a speed initially limited by the maximum pumping-rate of the hydraulic power unit of the system (2.0mm/sec). The system then progressively transitioned from being position-limited to being load controlled as the mats deformed in a highly non-linear fashion. Pressure-versus-time and thickness-versus-time plots for the initial rapid closure portions of cycles for both the oriented hemp fiber and similar (in terms of fiber mass) wood fiber pre-forms are shown as Figures 5.18 (A and B). Following these (Figure 5.19) are derived stress-versus-density curves for both materials.

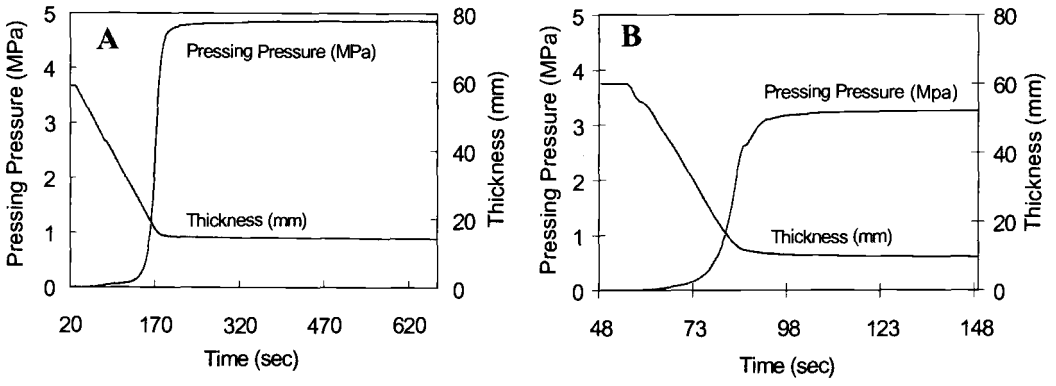

Figure 5.18. Pressing pressure- and thickness-versus time during the initial rapid ammonia-free compaction stage of A: oriented hemp; B: random wood fiber pre-forms (extracted from data for Figs. 5.16 and 5.17 respectively).

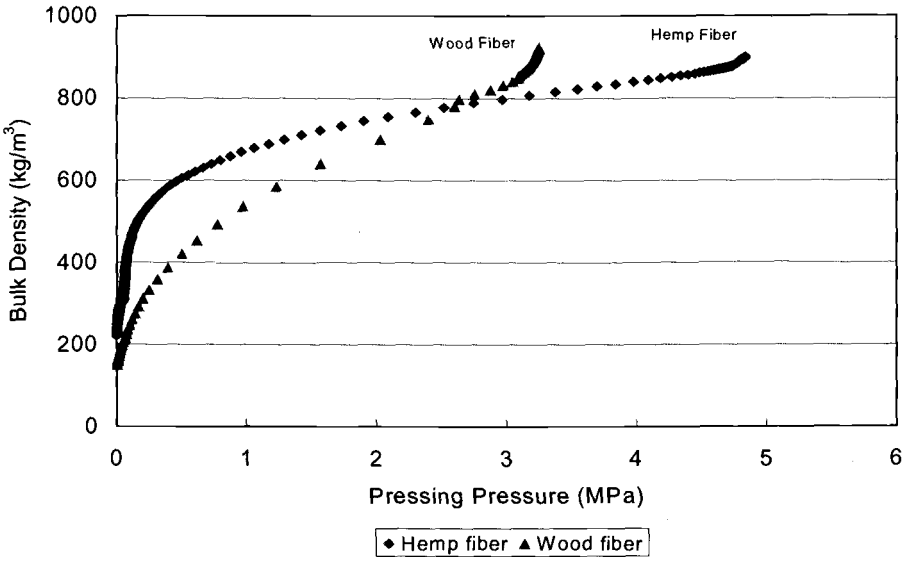

Figure 5.19. Density versus stress relationships for the initial rapid compaction stage of hemp and wood fiber pre-forms (derived from Fig. 5.18).

From the outset (at low bulk density), the oriented hemp network exhibits significantly greater non-linearity in compaction behavior than does the wood. Only small forces are needed to affect significant packing of the fibers. This may be attributable to both the efficient ordered spatial packing of the hemp fibers and their having small lumens and thick cell walls (as compared to the randomly formed wood mat with thin and collapsible cell walls). The wood fibers sustain a more complex sequence of deformation mechanisms as they are brought together. These mechanisms are dominated by axial fiber flexure and lateral re-location at low network densities; this is followed by complex and interdependent cell wall flexure and highly localized collapse at cross-over points between the randomly juxtaposed fibers as compaction pressures rise. These mechanisms, and the associated rheological characteristics of wood fiber networks, have been considered in related investigations (Ren, 1992; Thömen, 2001; Thömen and Humphrey,

2002). Pressure-versus-density curves (Fig. 5.19) for the two materials cross at a density of 790 kg/m^3 and pressure of 2.6 MPa. At high pressures the thin walls of the wood fibers evidently enable intra-fiber void spaces to be occluded whereupon the thick and consequently rigid walls of uniaxially oriented hemp fibers result in the creation of geometrically stable long and narrow voids between neighboring parallel fibers. The small lumens of hemp fibers require very high pressures to be obliterated. As a result, the hemp network requires a pressure of approximately 5MPa to reach a density of 925kg/m^3 whereupon the wood requires only 3.25MPa to reach the same density. These differences in compressibility will be discussed further (section 5.5.2) in the context of ammonia softening mechanisms.

5.5.2. The effect of ammonia on deformation and stress relaxation

It is evident from Figures 5.16 that the application of ammonia at the fiber-platen interface leads to internal gas pressure increases. In order to further explore the effects of ammonia on the rheological behavior of the fibers, some supplemental tests were conducted in which pre-forms without adhesive were compressed under a range of non-standard load and position regimens. Adhesive was left out so that the possible restraining effects of bonding on rheological behavior could be excluded.

5.5.2.1. Hemp networks

Data in Figure 5.20 is for hemp rapidly compressed and held at a thickness of 9.3mm (corresponding to a bulk density of 950kg/m^3), and counter-pressure (the reaction at the fiber-platen interface) recorded. Following closure, stress relaxation (at fixed bulk density) was allowed to progress for a period of 600 seconds until the

relaxation rate had decreased from its peak value of 386kPa/sec (just as target position was reached) down to a low and near-constant value of 2kPa/sec. At this stage, delayed-elastic and viscous components of the material's rheological profile had all but ceased (Ren, 1992). Ammonia was then applied through the upper platen boundary at a pressure of 620kPa for a period of 60 seconds – after which the supply was terminated and a vacuum pulled from the supply side in order to extract free ammonia from the system. After a further delay of 250 seconds, a second period of ammonia injection was initiated following a stepwise reduction in sample thickness. This was included in order to gauge the residual responsiveness of the ammonia-treated system to additional ammonia.

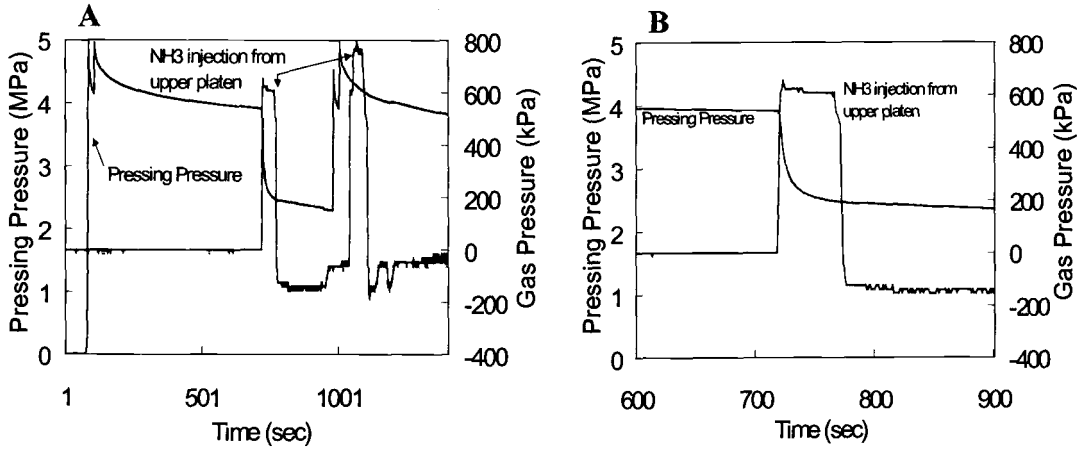

Figure 5.20. Behavior of a hemp fiber pre-form compressed under position control to a bulk density of 950kg/m^3 to explore stress relaxation due to two consecutive periods of ammonia injection. A: complete cycle; B: expanded graph during the first ammonia injection period.

Figure 5.20 shows that the stress relaxation rate for hemp was greatly hastened by the application of ammonia: beginning at a rate of 193kPa/sec and again leveling to a near-constant value of 2kPa/sec upon ammonia termination.

This behavior provides clear evidence that ammonia does indeed have a plasticising effect on hemp fibers and that the miniature beam-pressing system can be used to affect it.

5.5.2.2. Wood fiber networks

Load and thickness data for a randomly oriented wood fiber network are also presented as Figure 5.21 (A and B). A mat was rapidly compressed to a thickness of 10.1mm (corresponding to a bulk density of 874Kg/m^3) and counter-pressure was recorded. Stress relaxation was allowed to progress for a period of 250 seconds until the relaxation rate had decreased from its peak value of 117kPa/sec down to almost near constant value of 2kPa/sec. Ammonia was then injected through the upper platen boundary at a pressure of 137kPa for a period of 220 seconds – after which the supply was terminated and a vacuum pulled from the top platen and high pressure air injected from lower platen in order to extract free ammonia from the system. It is evident from Figure 5.21B that the stress relaxation rate was greatly hastened, as for hemp, by the application of ammonia - beginning at a rate of 22kPa/sec and leveling to a near-constant value of 2kPa/sec upon ammonia termination.

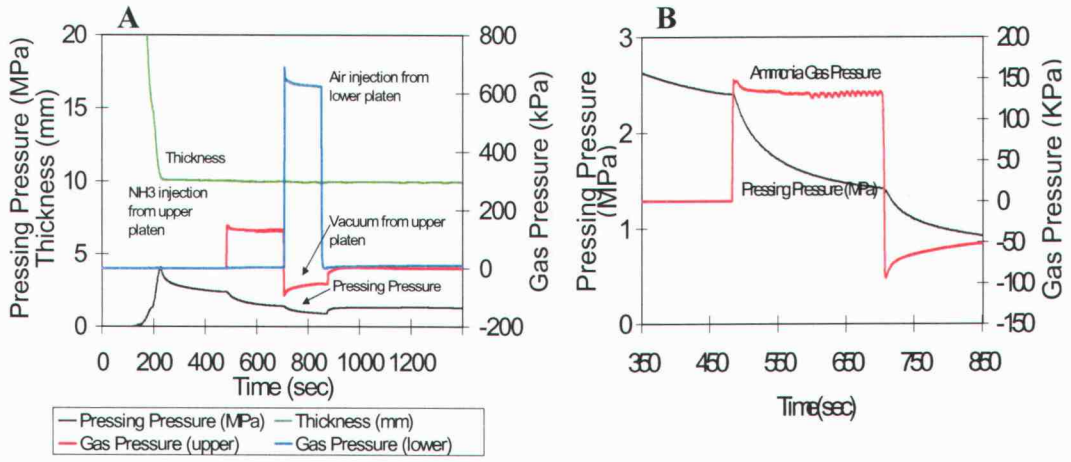

Figure 5.21. Behavior of a wood fiber pre-form compressed under thickness control to explore stress relaxation due to of ammonia injection (A) and expanded graph during ammonia injection (B).

It is well known that stress relaxation is important during industrial wood-based composite panel pressing since full press closure to a target position (bulk density) and the attainment of the conformity of wood elements necessary for efficient stress transfer in the final bonded product is not usually attainable without it. Such softening in conventional pressing depends upon the combined effects that temperature and moisture transfer have on the rheological properties of natural fibers (Humphrey *et al.*, 2000). The use of ammonia as an alternative means of softening may well have industrial potential. The effect appears to be rapid and significant energy savings may be possible by avoiding the need for high internal temperatures. Further, the large reduction of counter-pressure in the present test suggests the creation of a micro-structure which is largely stress-relaxed. Bonding within such a system could result in an efficient composite of high strength and dimensional stability; the bulk properties of conventionally pressed composites are compromised by the presence of substantial residual stress which has to be countered by the adhesive. Industrial use of ammonia for conventional panel

pressing is not, however, the primary concern of the present study; the focus here is on using ammonia to create spatial gradients of structure in non-panel products.

5.5.2.3. Densification under load control

The rapid decline in counter-pressure for a fixed platen position (pre-form thickness) detected in the present experiments (Fig. 5.20 and 5.21) does not enable one to quantitatively resolve the ammonia-induced softening effect either in terms of its spatial distribution or localized magnitude. This is due to the highly non-linear elasto-plastic characteristic of the fiber networks as a whole (evident in Fig. 5.19), combined with the small sample thickness (in the order of 10 mm). The declines in load evident in Figures 5.20 and 5.21 could be the result of a substantial level of ammonia-induced plasticisation and consequent yielding of only a small fraction of the sample's cross-section. Alternatively, the observed behavior could occur with a low level of plasicisation if the resistance to compression of the remaining portion of the cross-section rapidly declined with low levels of localized micro-stress relaxation and consequential densification.

In light of the above, a second hemp compaction study was conducted in which a load-control protocol was followed and consequent pressing-head movement (bulk densification) was monitored (Figure 5.22A and B). Compaction pressure was thus sustained throughout the cross-section as ammonia was applied. It is evident from Figure 5.22B that densification occurs progressively upon the application of ammonia and that the bulk strain rate has a maximum of 2.0 micro-strains per second and at the outset and progressively decreases to a value of 0.2 micro-strains per sec after 60 seconds. This result provided the first clear indication of the mobility of ammonia within the fiber network and the rate of its effect on the cell walls of hemp fibers.

After the rapid initial effect, plasicisation continued at an ever-decreasing rate. Indeed, upon ammonia removal, platen movement continued to occur. This residual effect is likely due to the increased viscose component of the yielding and micro-fracture of the cell wall system. Evacuation and flushing with air may not remove all ammonia and the residual is likely to maintain cell wall mobility. It may be that ammonia is entrapped in the hemp fibers due to their thick walls and very small lumens. Lumen size and shape (with sharp obtuse inner corners evident in Figure. 5.5) way also be sites for capillary condensation and retention of ammonia. Wood, on the other hand, has thin walls and large accessible lumens.

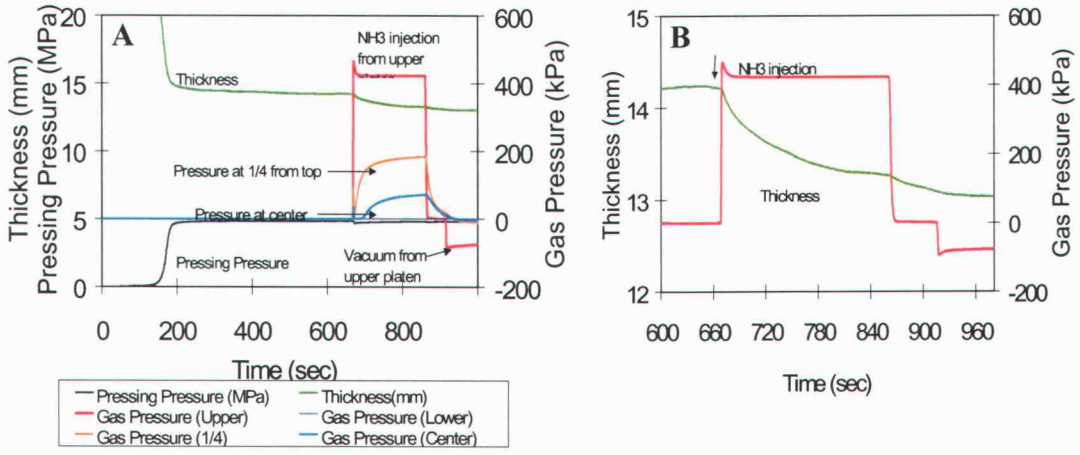

Figure 5.22. Behavior of a hemp fiber pre-form compressed under load control to explore deformation due to ammonia injection (A) and expanded graph during ammonia injection (B).

In the compaction cycle for wood fiber using a load-control protocol (Fig. 5.23A), compaction pressure of 1.6MPa was used. It is evident from Fig.5.23B that densification occurs rapidly upon the application of ammonia and that the bulk strain rate levels off from its peak value of 9.5 micro-strains per second to a value of 0.4 micro-strains per second within 50 seconds. This result suggests that the

gaseous ammonia is also highly mobile within the wood fiber network and that the effect on the cell walls of wood fibers is rapid.

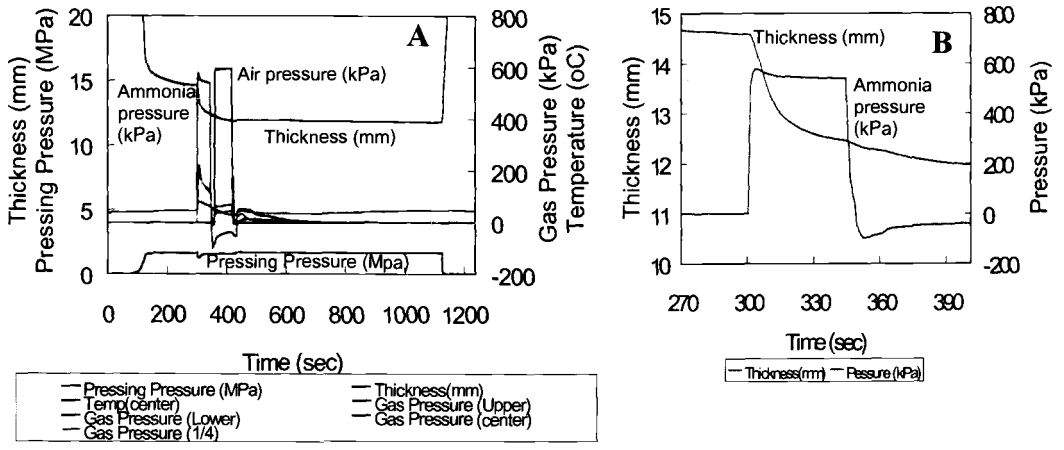

Figure 5.23 Behavior of a wood fiber pre-form compressed under load control to explore deformation due to ammonia injection (A) and expanded graph during ammonia injection (B).

The rapid compaction rate under constant load observed immediately following the application of ammonia implies one or a combination of the following:

1. The gas readily penetrates through the inter-fiber spaces of much of the beam and that the time-dependency of compaction is associated with local ammonia penetration and/or plasticisation of individual strands. If the system were limited by the rate of ammonia penetration through the whole sample cross-section, then platen movement under constant load would exhibit a progressive *increase* in rate as more and more of the section became plasticised -- which is clearly not the case.

2. Supply of ammonia to the interior of the sample is limited by its retention in the fibers near the platen boundary. Evidence for such an effect is provided by the cross-sectional distributions of temperature rise; these phenomena will be discussed in section 5.5.3. In that discussion it is hypothesized that measured internal temperature increases are due to heats of ammonia sorption.

5.5.2.4. Secondary ammonia softening

A second densification and ammonia injection cycle may be seen in Figure 5.20; this was affected following a period of evacuation and was carried out in order to explore its residual susceptibility to further plasticisation. Load was increased to its prior maximum (4.96MPa) by reducing thickness to 4.3mm (corresponding to a bulk density of 1120kg/m^3). Relaxation occurred at a similar rate to the prior maximum (approximately 187kPa/sec). However, upon re-application of ammonia, no significant increase in rate could be detected; the relaxation curve appears unaffected. This data suggests that the first application of ammonia resulted in near-complete softening and that little or no residual hydroxyl sites were readily available within the wall structure.

5.5.3. Gas penetration and internal heat generation

Figure 5.24 shows how gas pressures varied during a compression cycle of a hemp fiber mat. As ammonia gas was directed towards the upper platen at 420kPa, the gas pressure measured at the upper platen–mat interface almost instantly increased. At the very beginning, a small peak in internal gas pressure (of approximately 40 kPa and lasting about 9 seconds) was observed at the surface.

This peak may be due to the rapid reduction of internal pore volume caused by ammonia-induced densification. The effect may also be compounded by localized heat also generated by ammonia sorption.

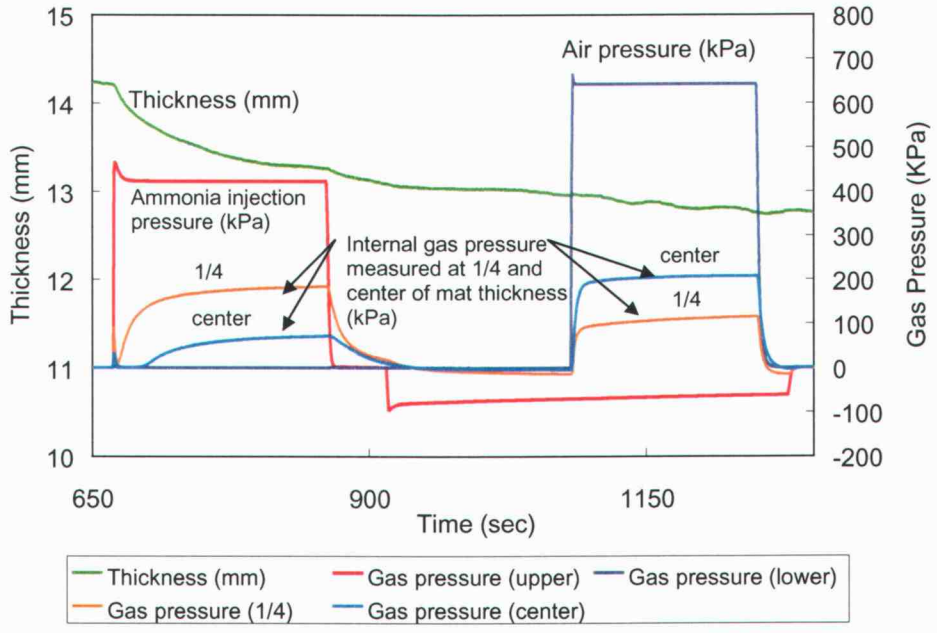

Figure 5.24. Internal gas pressures during ammonia injection of a hemp fiber mat.

Gas pressure 25% below the injection surface began to rise almost instantly. There was, however, a delay of 25 seconds before any rise occurred at the center of the sample. The delay may partly be the result of injected ammonia gas flowing axially (horizontally) towards the open ends of the sample) as well as in the transverse direction (through the thickness). It could, however, also be linked with sorption (and consequent retention) of ammonia in the surface layers of the sample.

Temperatures measured at the center of a wood fiber mat (750kg/m^3 and 14.5mm thickness) during ammonia injection (at a pressure of 0.62MPa) from the upper platen are shown in Figure 5.25. The temperature inside the mat almost

instantaneously increased upon ammonia injection. This rapid increase of internal temperature may be associated with the heat of sorption of ammonia by cell wall material.

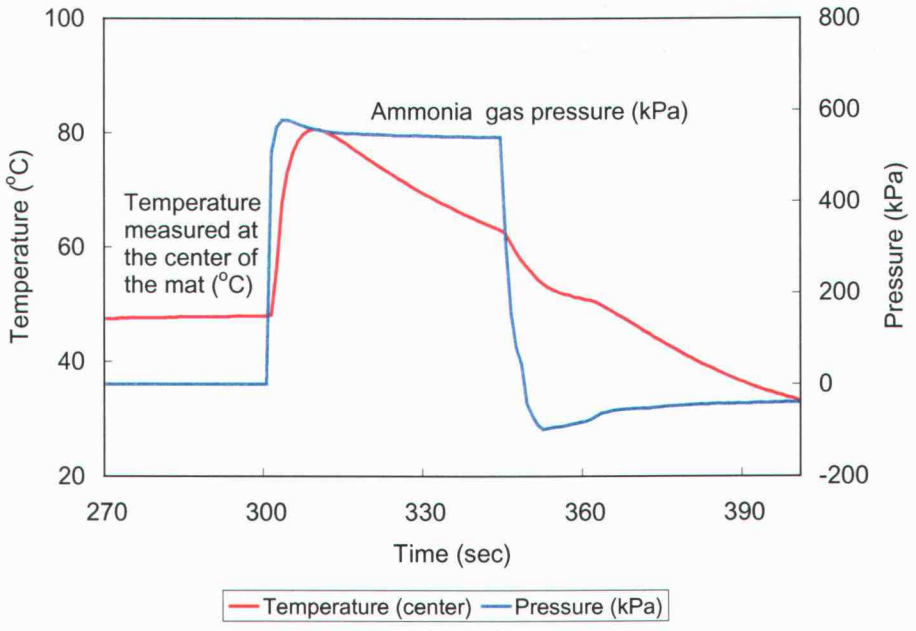

Figure 5.25. Temperature measured at the center of a wood fiber mat during ammonia injection (at a pressure of 620kPa)

Temperature and gas pressure distributions for a range of cross-sectional positions within wood-fiber mat are shown as Figure 5.26. Again, rapid increases of temperature about 1/4 of mat thickness below the platen injection and at the mat's center were observed. Temperature increases measured 3/4 of mat thickness below the injection platen were, however, small or unchanged. This may suggest that gaseous ammonia did not penetrate fully or, at last, the concentration (relative ammonia saturation) was low.

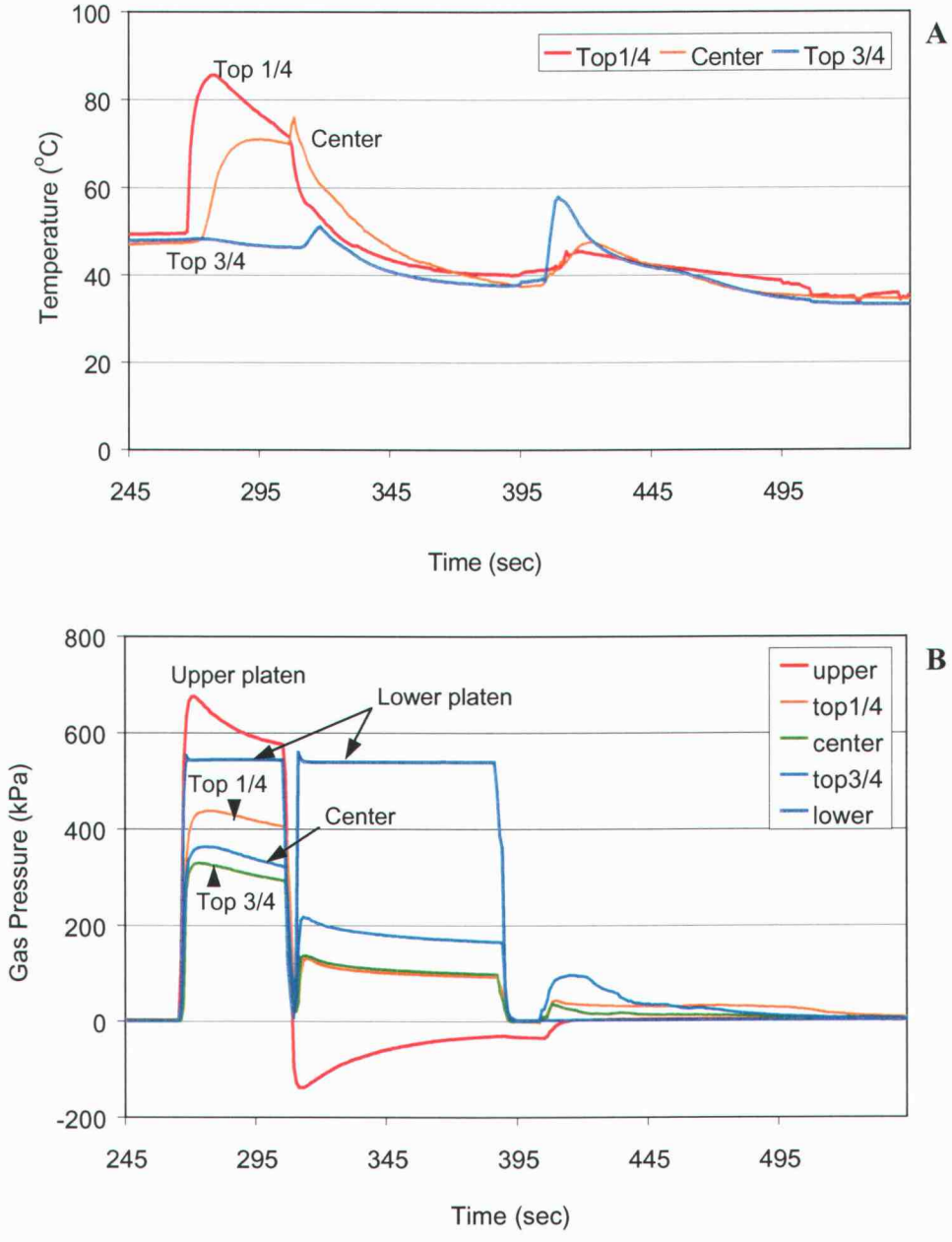

Figure 5.26. Temperature (A) and gas pressure (B) changes measured inside the wood fiber mat at a range of cross-sectional portions.

Temperature and gas pressure appear to be closely linked both during increases and decreases (ammonia injection and removal respectively). This effect suggests that temperature fluctuations are closely associated with the interaction of ammonia with cell wall material. The hypothesis of sorption being a source of energy is explored below.

5.5.3.1. Sorption analysis

Analytical estimates of heat generation and resultant temperature increases inside the wood fiber mat due to ammonia sorption have been made. A range of values for net heats of total sorption for anhydrous ammonia within plant fiber cell wall material (2260 – 3500 cal/mol) assembled by Bariska and Popper (1975) were used for this purpose. Values of specific heat of wood and ammonia (2135 J/kg/K) were obtained from Haselein (1998) and Bloomer (2000) and Chase (1998) respectively. Assuming that the temperature increase is only due to heat of sorption of ammonia by wood, supplied heat may be written as

$$E_s = H_{am} \times M_{a/w}$$

where E_s (J) is total heat supplied to the system, H_{am} (J/kg) is heat of sorption of ammonia, and $M_{a/w}$ (kg/kg) is mass of ammonia adsorbed per unit mass of wood until at equilibrium.

The heat capacity of the whole system may be written as

$$C_t = M_w \times C_w + M_{a/w}\, C_{am}$$

where C_t (J/Kg· K) is total heat capacity of the system, M_w (kg) is unit mass of wood, C_w (J/Kg· K) is specific heat capacity of wood, and C_{am} (J/kg· K) is

specific heat capacity of ammonia. Heat change due to a fixed mass of ammonia sorption by unit mass of wood can then be re-written as:

$$\Delta T = (H_{am} \times M_{a/w}) / (M_w \times C_w + M_{a/w} C_{am})$$

Temperature rise may be estimated for any level of ammonia sorption using the above analysis. Derived temperature rise versus ammonia sorption level (percent saturation) is shown as Figure 5.27.

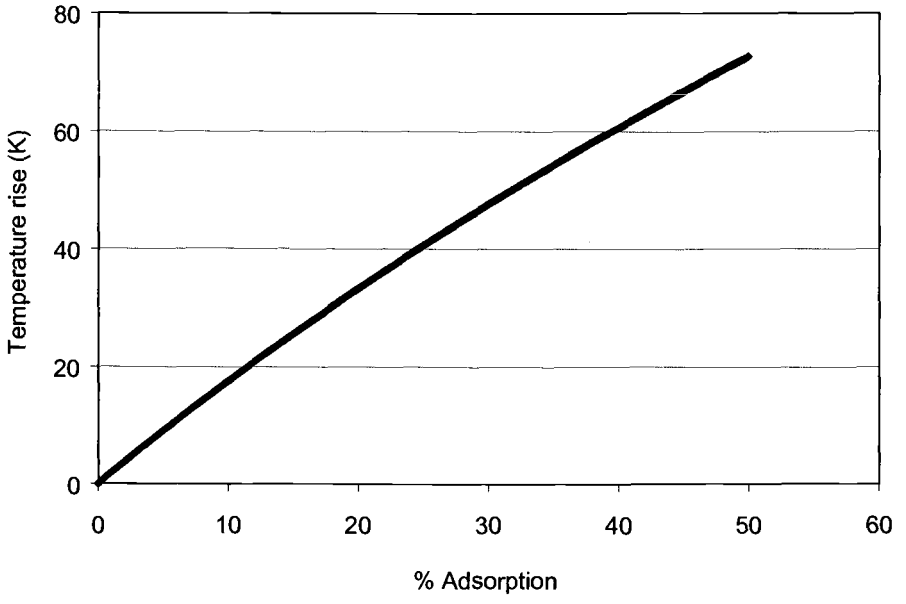

Figure 5.27. Effect of ammonia sorption on temperature increase, assuming a heat of sorption value of 3000 cal/mol.

The above calculations assume a value of 3000 cal/mol for the heat of sorption (at 100% ammonia saturation). Bariska and Popper (1975) calculated various values based on the BET model, the Bering-Sperpinsky theory, and a sorption potential theory developed by Polanyi (1975). They concluded that the value of heat of sorption of ammonia on wood and cotton cellulose ranges from 2260 to 3500

cal/mol. Based on the various values of the heat of sorption, temperature increase against % adsorption was plotted (Figure 5.28)

Figure 5.28.

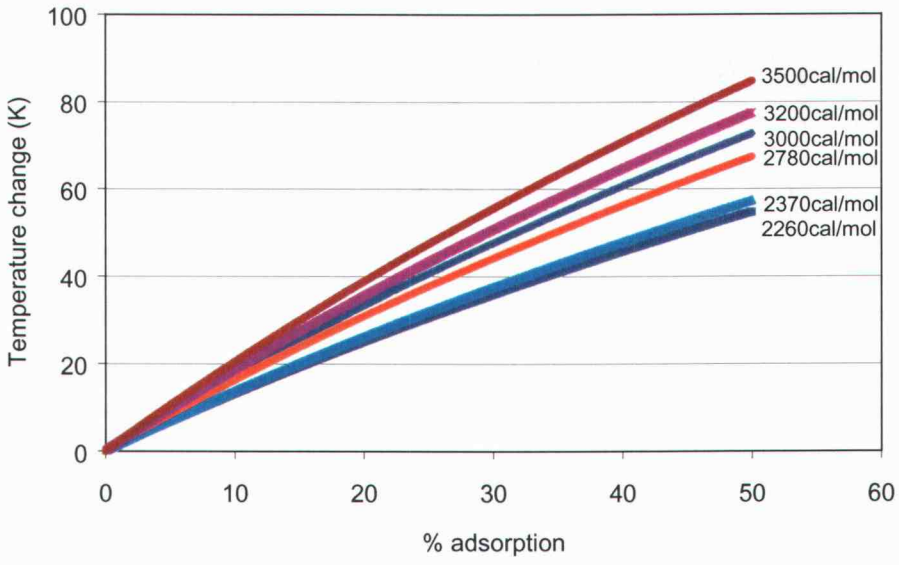

Figure 5.28. Effect of ammonia sorption on temperature change calculated from various heat of sorption values of ammonia.

Temperature increases measured within wood mats during ammonia injection in the pressing system (Figures 5.28) reached values as high as 70°C. This increase may, according to the above analysis, be affected by sorption of ammonia at saturation levels ranging between 38% and 72% depending upon which heat of sorption value is employed (ranging in the literature between 2260 and 3500 J/Kg). This supports the assertion that the heating effect is likely to be due to ammonia sorption. Future investigations will be directed towards assessing the impact of

such heating on rheological behavior of the fiber networks and adhesion between them, and how the effect may be used to gainfully control pressing methods.

5.5.3.2. Methyl formate injection

After excess ammonia gas had been purged by vacuum and opposing high-pressure air, methyl formate vapor (25 cc, at 690kPa) was injected from the heated vessel. Finite volumes of fluid were liquid loaded into the heated reservoir before it was heated to 80°C. When injection was activated, all the fluid in the vessel changed phase and vented through the platen surfaces into the sample (Figure 5.24). Pressure was therefore a maximum at the outset and decayed as the methyl formate gas dissipated in the system and penetrated the sample. Supply lines connecting the fluid vessel to the injection platens were heated to avoid condensation of methyl formate. Figure 5.29 shows internal gas pressure effects during the chemical's injection. The increase of measured gas pressure inside the mat indicates that methyl formate penetrated through the mat in spite of the very small increase at the upper platen (0.8kPa).

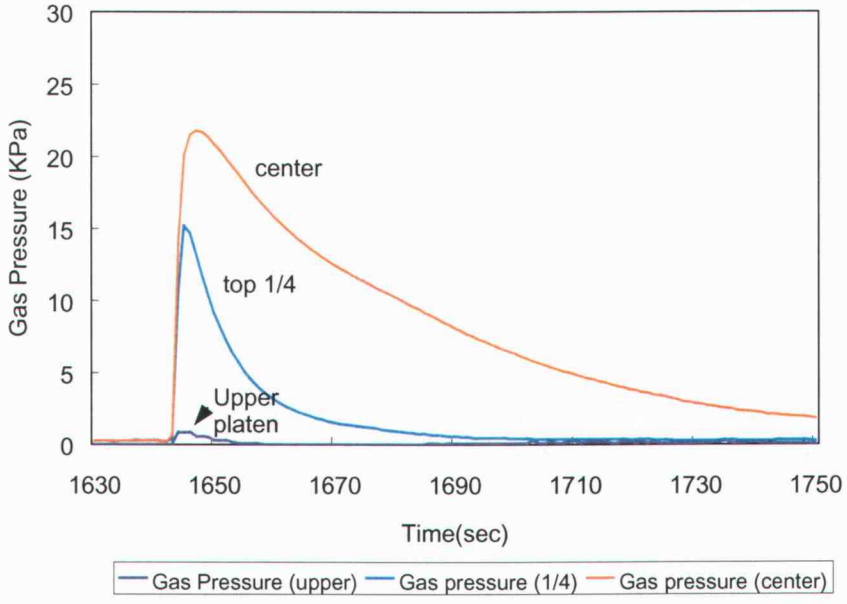

Figure 5.29. Methyl formate gas pressure measured inside a hemp fiber mat (extracted from the data from Fig. 5.16)

At the end of the pressing cycle, vacuum and high-pressure air were applied to the opposing sides of the sample in order to purge the methyl formate (which is toxic).

5.5.4. Creation of beams with density gradients

One of the objectives of this research is to verify the feasibility of creating density gradients through the cross-section of small rectangular beams. It has already been demonstrated that injection of gaseous ammonia can reduce internal stress and aid in the densification of natural fiber networks during pressing. However, in order to create a density gradient inside beams, gradients of ammonia-induced softening must be synchronized in concert with the application of platen

pressure. A first step to find such a combination was to explore density gradients of selected wood and hemp fiber beams that were made by injecting ammonia gas from the upper platen for a variety of pressure-time combinations. The density gradients were explored using the methods described in section 4.3.9.1.

Cross-sectional density distributions and corresponding treatment cycles for a range of exploratory trials are included in Appendix B. No prominent gradient in either pre-form type was evident however. Evidently, the high mobility of ammonia gas affected the entire cross-sections of each mat.

In order to gauge the maximum density difference that is attainable under ideal extremes of zoned softening, both wood and hemp fiber mats were slowly pressed up to a pressure of 17.9MPa at a rate of 0.029MPa/sec (Figure 5.30). This slow pressing pressure increase was selected in order to minimize the influence of the time-dependent component of the mat's rheological characteristic. For samples with ammonia saturation, 620.7kPa of gaseous ammonia was injected for about 100 seconds prior to the beginning.

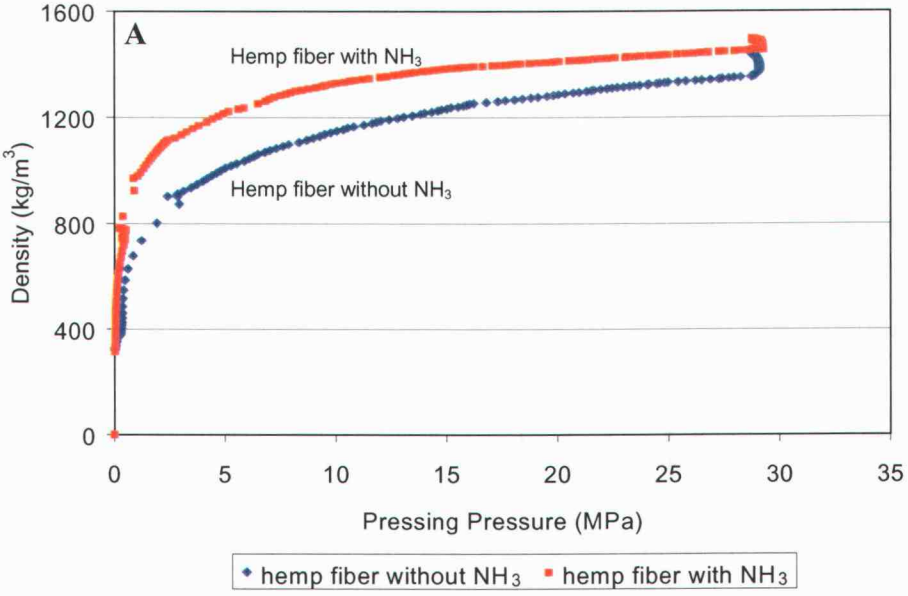

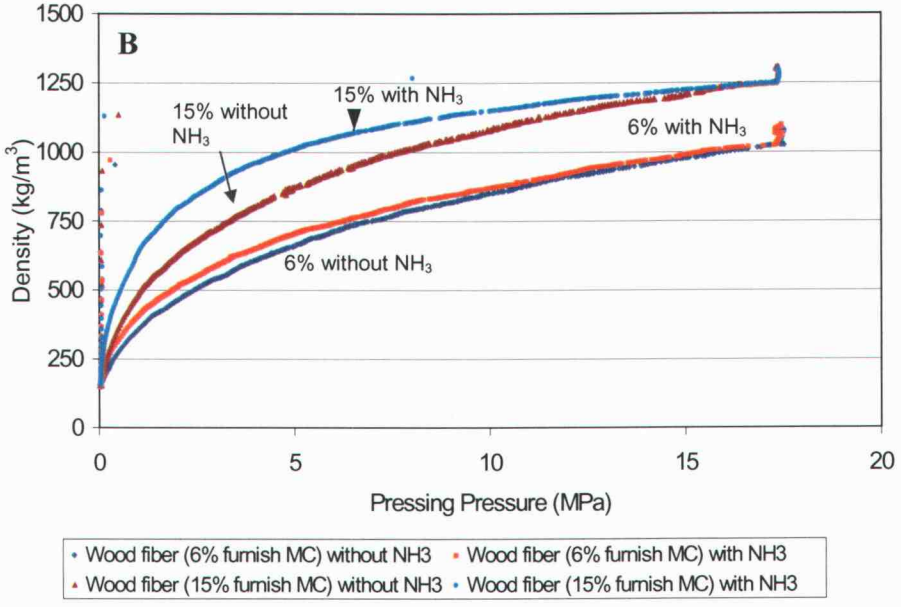

Figure 5.30. Comparison of the slow densification characteristic of ammonia-saturated and ammonia-free hemp (A) and wood fiber (B) mat

From the Figure 5.30, it may be inferred that the maximum density difference can be achieved when the hemp fiber mat is pressed between 2 and 10 MPa of pressure. For example, when the hemp fiber mat was pressed at 4MPa, the untreated mat attained a density of 958kg/m^3, while that of the ammonia-saturated mat was 1150Kg/m^3. For wood fibers, two sets of saturation test was performed; one set at 6% MC (without resin), and the other set at 15% MC (with 9% by weight of liquid PF resin). At 4MPa of pressing pressure, the difference of density between control at 6% MC and control at 15%MC was about 30%. Also from Figure 5.30B, it is clear that the overall compressibility was higher for 15% MC than 6%. For 4MPa of pressing pressure, the difference between control and ammonia saturated one at 15% MC was about 22% whereas those at 6% MC was about 9%. This result indicates that the presence of water aids in the softening effect of ammonia. This result is consistent with the findings of Davidson (1968).

If one can manipulate the gas injection process such that half of the beam is fully saturated and the other half is not affected by ammonia, the maximum difference of density would be over 20%.

In light of the above and following a number of preliminary trials (Appendix C) ammonia penetration was found to be restricted by the application of air (at 620kPa pressure) from the opposing platen. A pressing cycle that resulted in the cross-sectional density profile of Figure 5.32 is shown as Figure 5.31.

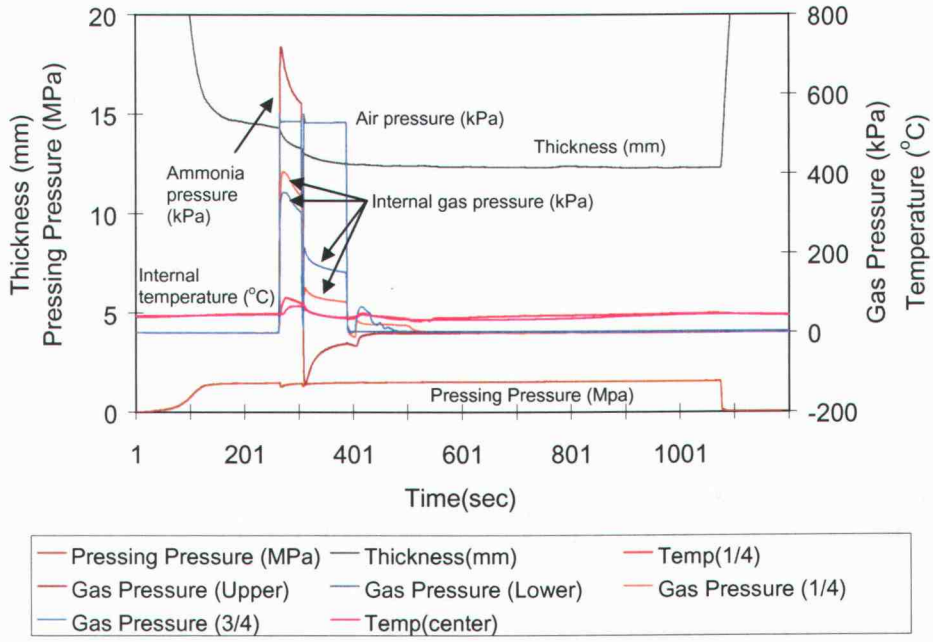

Figure 5.31. A pressing cycle used to create the density profile of Figure 5.32.

After manufacturing actual beams by sequential gas injection pressing, cross-sectional (in the consolidation direction) density profiles were measured using x-ray densitometry. A typical density profile is shown in Figure 5.32. It was clear that the density of the portion close to the surface where ammonia gas was injected is higher than the density of the portion where air was injected.

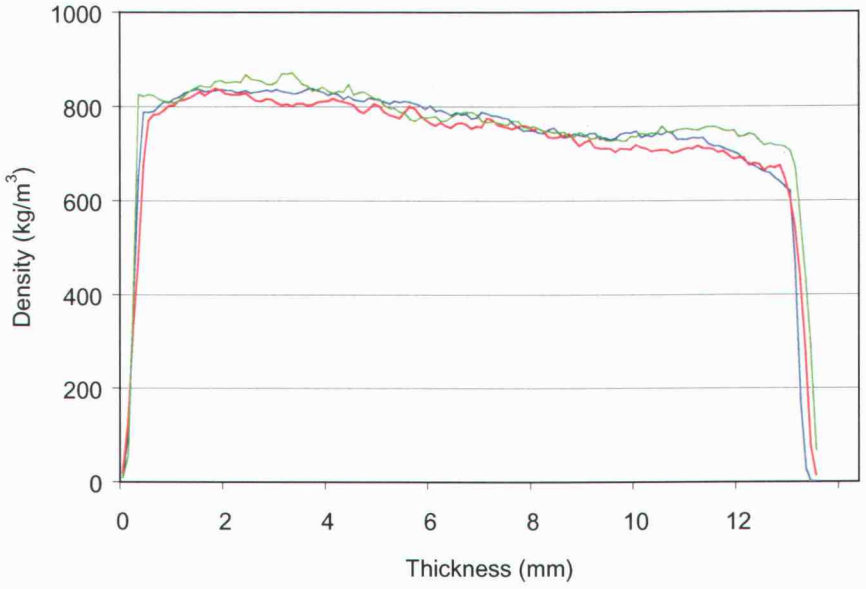

Figure 5.32 A typical density gradient of wood fiber beam object with simultaneous injection of ammonia and air (measured at three different places along the length).

5.6. CHARACTERIZATION OF A TRIAL BEAM

5.6.1. Effect of density on tensile strength and modulus

Tensile strength and modulus of wood fiber beam samples were tested as described in section 4.3.9. In order to then explore links between density and properties, the created beams were first cut into three pieces as shown in Figure 4.28. The resultant samples were used to explore tensile stiffness and strength and swelling characteristics of the material.

Data relating maximum tensile yield strength to density is plotted in Figure 5.33. The tensile strength increased with increasing density as expected, though the

correlation is clearly not very high. The cause of this scatter may lie in the local variability in composite structure due to the manual method used for mat formation. Miniature automatic mat formation techniques are presently under way and uniformity of pre-form structure is likely to be significantly improved. The present relationships will, however, be used to demonstrate the potential of gas injection pressing techniques to affect gradients of structure.

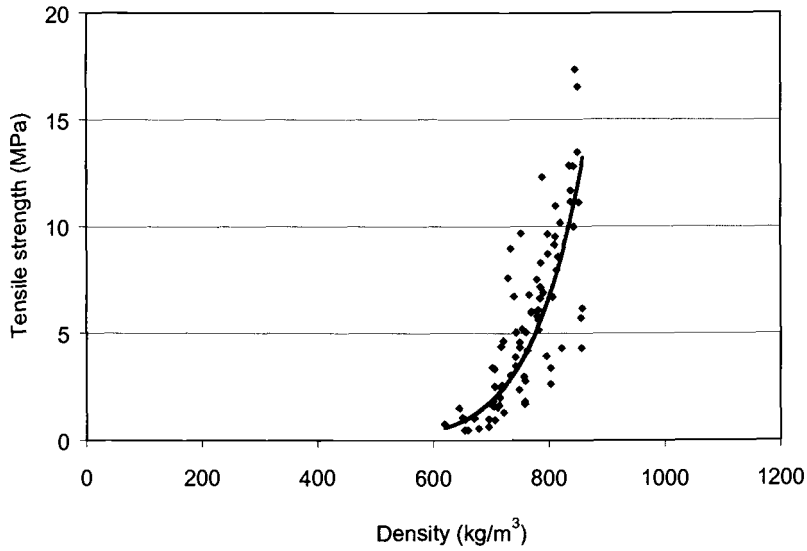

Figure 5.33. Relationship between density and maximum tensile yield strength for an ammonia-injected beam made from PF resinated MDF furnish.

The relationship between density and elastic modulus is as follows

$$\sigma = 9\times10^{-26}\rho^{8.9129} \qquad (5.1)$$

Where σ is maximum tensile yield strength (MPa) and ρ is density (kg/m^3).

Modulus of elasticity was also plotted against density (Figure 5.34.). Modulus of elasticity evidently increases with density though again, considerable scatter is evident.

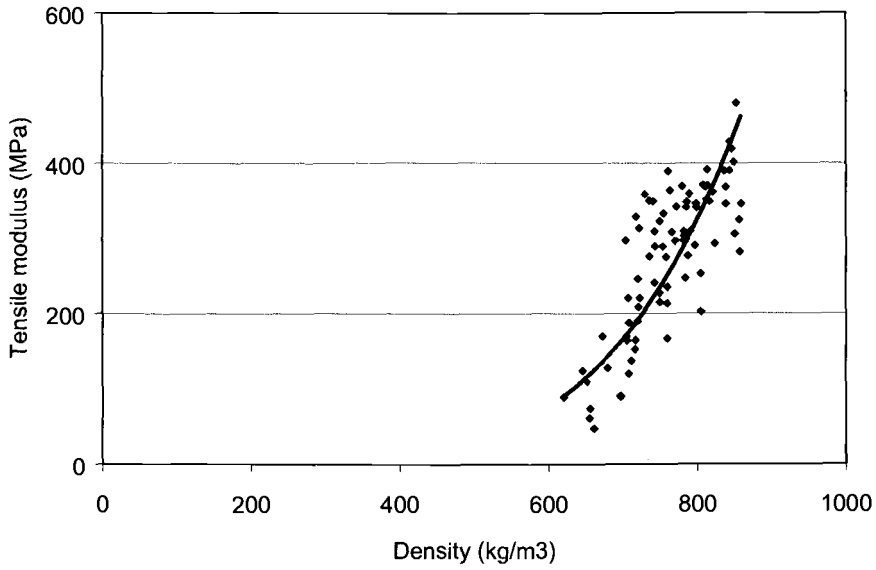

Figure 5.34. Relationship between density and tensile modulus for an ammonia-injected beam made from PF resinated MDF furnish.

The relationship between density and elastic modulus is as follows.

$$E_1 = 5\times10^{-12}\,\rho^{4.7513} \qquad (5.2)$$

Where E_1 is tensile elastic modulus (MPa) and ρ is density (kg/m^3).

These two equations were used to derive maximum tensile yield strength and modulus of elasticity from any given density of the material.

5.6.2. Stress analysis of a hypothetical density-graded beam

Internal stress distributions within a hypothetical beam during flexure are here analyzed to demonstrate the potential benefits of creating beams with property gradients. Density and corresponding mechanical property gradients of actual beams made by sequential gas injection pressing were measured, and mathematical relationships between density and mechanical material properties were derived (section 5.6.1). Based on the asymmetric density gradient of actual test beams, a hypothetical beam, consisting of two elongated test beams bonded together to create a beam of symmetric cross-sectional density distribution was employed. Mechanical behavior of the hypothetical beam during loading is explored using a transformed-section method. The analysis was conducted with a view to explaining and demonstrating the potential increase in specific (density corrected) performance that may be accrued by the use of pressing-induced property control.

5.6.2.1. The transformed-section method

The transformed-section method is a well-established procedure for analyzing stresses within beams of non-uniform properties especially layered ones loaded in bending (Bodig and Jayne, 1984). According to this method, the true cross-sectional shape of a beam is transformed into an equivalent shape of an imaginary beam which is composed of only one material. Then the imaginary beam with this new transformed cross-section is analyzed for a beam of that material. Finally, the stresses derived for the transformed cross-section may be converted to those in the original cross-section. In a layered composite beam, modulus of elasticity of each lamina in the direction of span (E_l) is sufficient for simple analysis of the beam (excluding shear deformation and poison's ratio effects and assuming linear elasticity in both tensile and compression loading). For this

purpose, the beam is sub-divided into lamellae lying in the x-z plane; orthotropicity in the x-z plane is assumed (Figure 5.35).

If we select the face layer as a reference, then the relationship between width of each layer and modulus of elasticity can be written as

$$W_i = W_n(E_i^1 / E_n^1) \tag{5.3}$$

where W_i is the width of, and E_i^1 is the modulus of elasticity of ith laminae, whereas W_n is the width, and E_n^1 is the modulus of elasticity of the reference laminae. The moment of inertia of the transformed cross-section is given by

$$I_2^{'} = 2\sum_{i=1}^{n}[I_0^i + A_1^i(d^i)^2] \tag{5.4}$$

where

$$I_0^i = w_i(t_i)^3 / 12$$
$$A_0^i = w_i t_i$$
$$d^i = \sum_{1}^{i-1} t^{i-1} + (t_i / 2)$$

and where

I_0^i = moment of inertia of ith laminae

w_i = width of ith laminae

t_i = thickness of ith laminae

d_i = distance from the neutral axis of transformed beam to the center of ith laminae

The equation for the area moment is given by

$$Q_2^{'} = \sum_{i=1}^{n} A_1^i d^i$$

It follows that mid-span deflection is given by

$$u = CPL^3 / E_1^n I_2^{'} \qquad (5.5)$$

where

C = a constant depending on the loading condition (in this case 3-point bending, C=1/48)
P = concentrated load at mid-span
L = span of the beam

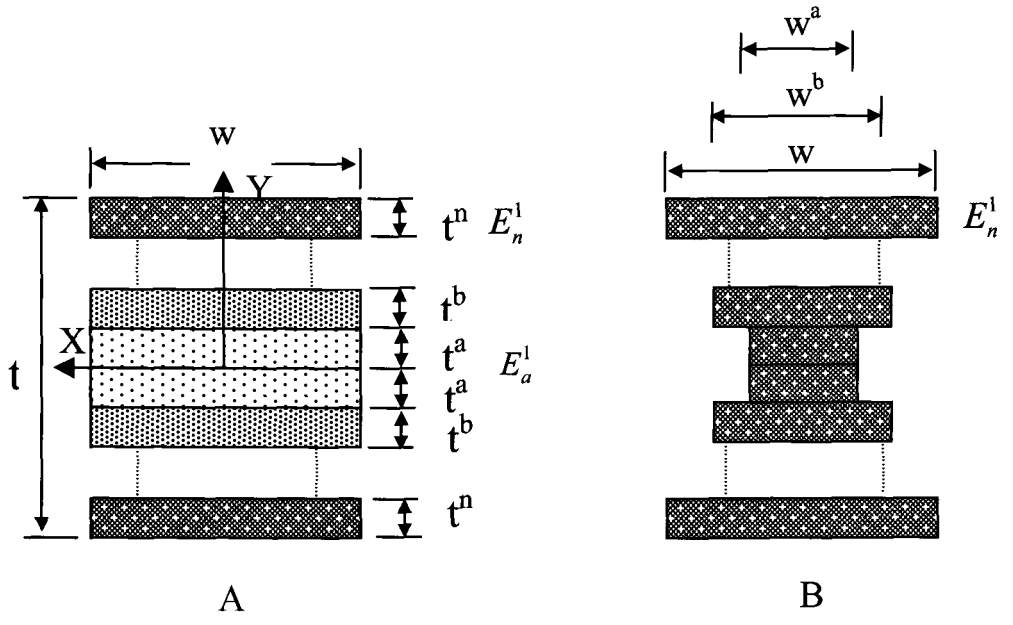

Figure 5.35. Cross-section of a multilayer symmetrical laminate before (A) and after (B) transformation (t: thickness; w: width; E^1_a:modulus of elasticity of *a*th laminae E^1_n:modulus of elasticity of *n*th laminae)

These equations were used in a spreadsheet to calculate tensile stress distribution as well asmid-span deflection values in the modeled beam for given loads at mid-span.

5.6.2.2. Stress analysis of the hypothetical beam in bending

Maximum allowable tensile strength and tensile modulus values were calculated for given density values. The manufactured test beams had an asymmetrical density profile and a large ratio of thickness-to-length (13:1=length:thickness). If such a beam were tested in bending, damaging compression stresses would occur above the neutral axis. Also, if the ratio of length-to-thickness of the beam is not sufficiently large (typically, greater than 21:1), shear deformation may be significant during bending. Thus, a beam was proposed such that the lower density sides of two beams were adequately bonded to form a single beam (Figure 5.37).

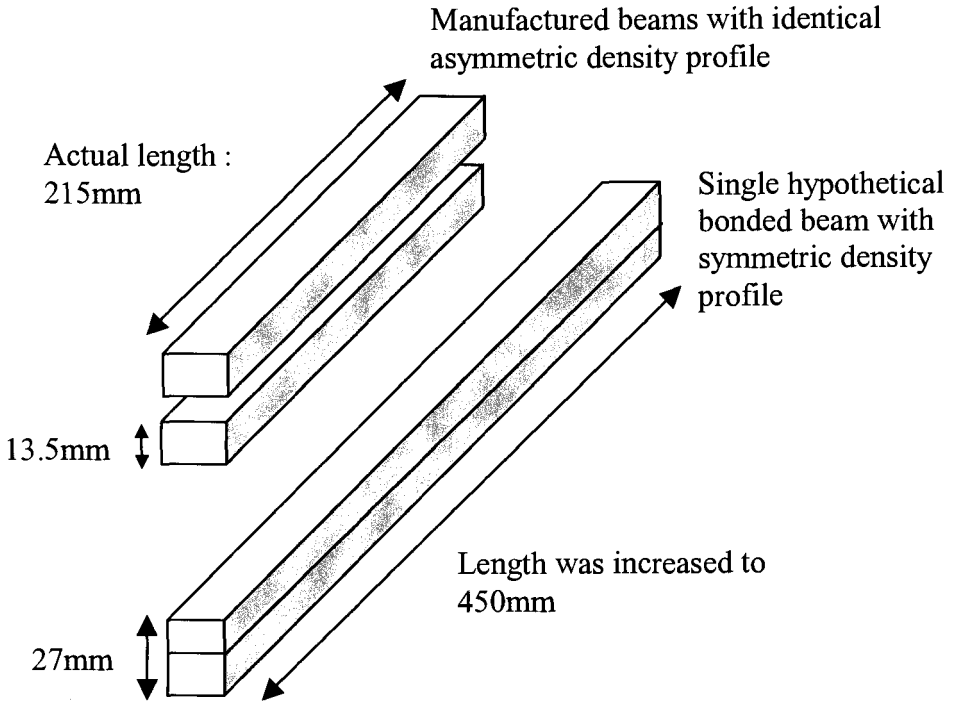

Figure 5.36. Dimensions of manufactured beams and that of a single hypothetical beam.

Based on the density profile of the hypothetical beam, maximum tensile strength and tensile modulus values were calculated for each lamina. Since the resolution of the density profile data was limited by that of the x-ray densitometer to 0.1mm, it was assumed that a lamina of 0.1mm thickness had uniform density and thus had uniform tensile strength and tensile modulus through its thickness. The spatial resolution of the analysis was therefore 0.1mm. The half-thickness of the hypothetical beam was 13.5mm and the width was 20mm. The span of the beam was defined as 450mm in order to minimize the effect of shear deflection. The hypothetical beam was loaded in 3-point bending and load was incrementally applied until any one lamina in the hypothetical beam reached its maximum allowable tensile stress. The critical load that resulted in failure of a lamina is here termed 'load at local failure'.

Only the lower half of the beam was analyzed because of the assumption of cross-sectional symmetry about the neutral axis. For this hypothetical beam, internal stress distribution at various cross-sectional positions at mid-span was calculated. At the onset of the numerical simulation, initial load was assumed to be 0N and the stress due to the weight of the beam itself was neglected.

5.6.2.3. Behavior of modeled beam during bending

Starting with a load of 0N, load was increased until the first lamina failed. This, (as expected, but not to be assumed) was located at the lower surface. After the first lamina failed at the calculated critical load, the effective thickness of the beam was reduced. The new internal stress distribution was then calculated when the next lamina (internal lamina) failed. This process was continued until the thickness of the beam was reduced to 110mm and calculated failure loads had pasted their peak value.

Figure 5.37 shows the density profile of the hypothetical beam and density-dependent maximum tensile yield strength. Internal stress distributions calculated by the transformed-section method for a selection of applied loads are also shown. The density and consequent maximum allowable stress of the first and second lamina of the hypothetical beam was very low and thus they failed at a very low applied mid-span load. The density of the lamina at point A in Figure 5.37 is 350kg/m^3 and the derived maximum allowable material strength was 1.1MPa. The stress distribution within the hypothetical beam shows that the calculated stress values at the lamina (point A) coincide with density driven maximum allowable strength of that lamina. In turn, the lamina at point A (the third lamina from bottom surface) would support up to 61N of load and would fail above that load. The next stress distribution within the hypothetical beam was based on the reduced thickness due to the failure of that lamina. At point B, in Figure 5.37 the density is 760kg/m^3 and the maximum allowable strength is 6.1 MPa. The maximum load that the lamina at point B can support increases to 140N. At point E, the load was increased to the maximum of 151N. Above that load, the internal stress will surpass the maximum allowable yield strength of several lamina (point F), which results in a decrease of the thickness of the beam and thus an increase in the internal stress level again until the internal stress overwhelms the maximum allowable yield strength of all the lamina (point G).

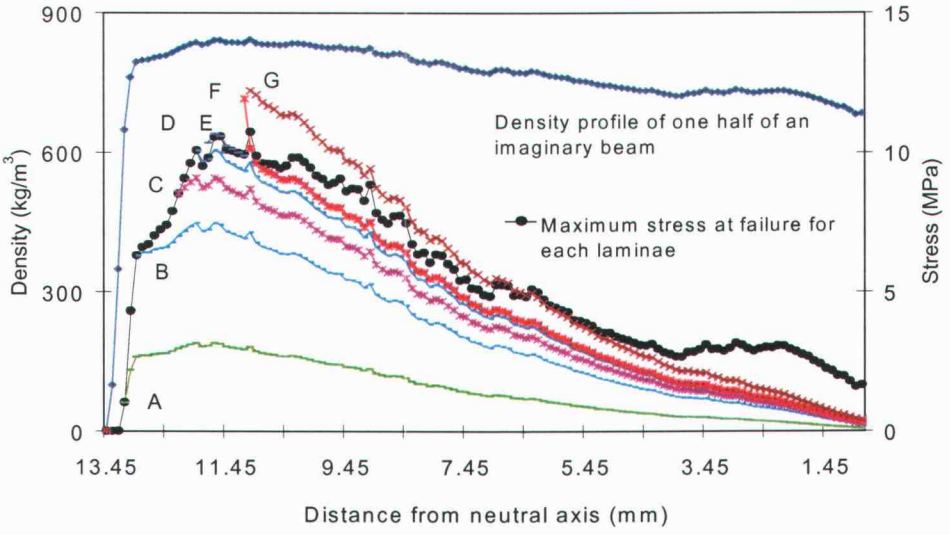

Figure 5.37. Internal stress distribution of the hypothetical beam. Density profile and density derived maximum allowable yield strength data are also shown.

The position at failure versus the load at failure is shown in Figure 5.38.

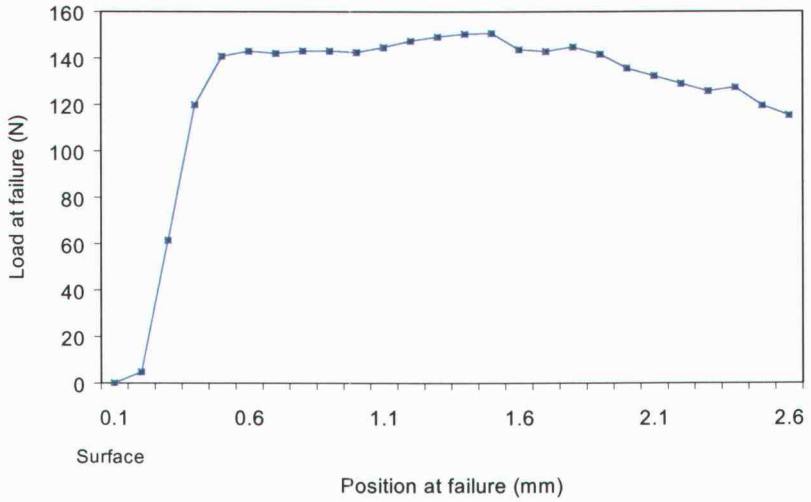

Figure 5.38. Load at local failure versus position of that failure for the analyzed hypothetical beam.

It was found that the load to local failure rapidly increased from its minimum for the lowest lamina. This is because the density of each lamina increased over a distance of 0.6mm from the lower face toward the neutral axis. The load at local failure then stabilized at around 140N and later increased up to 150N. It was found that the maximum load supported by the beam was limited by the strength of a lamina which had slightly less density than the peak value of 841kg/m^3, about 1.9mm above the lower face; the limiting failure located 1.5mm from the surface.

Clearly, such a progressive failure sequence, where loads may increase after initial failure of the lower surface, would not occur if the beam were isotropic in the vertical direction. It is the gradient of properties that leads to the observed behavior in load bearing ability with decreasing vertical section.

For the purposes of comparison, another hypothetical beam, which had the same average density of 735kg/m^3 and overall dimensions as the one modeled previously, but with uniform density profile was analyzed. Application of simple beam theory suggested that the beam could support only 70N. This is less than 100% of the load bearing capacity of the density-graded beam. This result confirms that by distributing properties of materials inside the beam, we can increase its load bearing capacity.

6. CONCLUSIONS AND POSSIBLE FUTURE RESEARCH

6.1 SOME CONCLUSIONS OF THE CURRENT RESEARCH

An underlying objective of this research was to develop techniques to aid in the formation of small natural fiber structural composite beams using novel sealed pressing approaches. A gas injection system for consolidating pre-formed natural fiber networks under highly controlled mechanical, chemical, and thermal conditions was developed and used. This system has provisions for vapor phase chemical injection and removal during pressing.

The principal conclusions of this research are as follows:

1. Studies of anatomical and mechanical features of hemp revealed the mean size of individual hemp slivers to be 305mm in length, 249μm in width and 35μm in thickness. Electron microscopy revealed that the hemp fiber has thick cell walls with very small slit-like lumens. The mean tensile strength of cell wall material was measured at 819MPa but of high variability.
2. Miniature PF bonds between individual hemp strands that include an outer (waxy epidermal) surface never exceed shear strength values of 1.5MPa. The strengths of such pairs were very low regardless of bond curing time, while non-epidermal (inner) surfaces together formed bonds with strengths in excess of 5 MPa. Further, the isothermal strength development rate of miniature PF-bonded hemp fiber networks was found to increase by 22% with the controlled application of methyl formate. Final, fully cured strengths were enhanced by 24%. The shear strength of the oriented hemp fiber networks (with 10mm overlap) had values quite consistent with measured strengths of individual strand pairs (compensating for surface interactions).

3. Strengths of partially cured PF-to-wood bonds tested at low temperature were significantly greater than those tested at forming (elevated) temperatures. This instantaneous increase in bond strength upon cooling may be closely related to polymeric change of the resin. Such transitions may be due to cooling below glass transition temperature of partially cured PF resin. The technique may enable means of reducing hot pressing times for fiber-based composite to be found; pressing times depend on the ability of the resin to transfer stress upon press opening.
4. The effect of ammonia treatment on densification of natural fiber networks has been explored and found to be significant and rapid. Substantial temperature increases have been detected inside mats during ammonia injection, and this effect has been attributed to sorption.
5. Formation trials have been conducted to create cross-sectional density gradients in miniature structural beams by sequentially injecting ammonia and methyl formate in concert with the application of pressing force. Density graded samples were successfully created by simultaneously injecting ammonia from one pressing surface and air from the other surface. The difference of density between two opposing surfaces was about 10%.
6. Tensile strength and stiffness of material within the consolidated samples were measured and statistical correlations with density established. Stress analysis for 3-point bending of a density-graded beam was performed. The study indicated that density-graded samples support flexural loads more efficiently than do corresponding homogeneous beams.

6.2 FUTURE RESEARCH

1. The refinement and improvement of the experimental technique may provide opportunities to produce objects with optimal density gradients for specific

applications. However, such use of gas injection process may need substantial further development.

2. The gas injection pressing system may be improved to provide a fully sealed environment. This will enable us to study a range of important furnish material properties including thermal conductivity, chemical reactivity, and gas permeability as functions of consolidation. This study may aid in the development of sealed gas injection and removal systems with zoned control to affect both in-plane and cross-sectional gradients of structure and resultant properties. Composite objects with elaborate three-dimensional shape may thereby be synthesized by creating contoured permeable plates in the system.
3. Studies on anatomical, physical and mechanical properties of non-wood natural fiber are needed to understand thermal, chemical, and rheological behavior of the pre-form network. In the future, it may be necessary to include non-wood fibers for synthesizing advanced natural fiber composites.

BIBLIOGRAPHY

Bariska, M., C. Skaar, and R.W. Davidson. 1969. Studies of the wood-anhydrous ammonia system. Wood Science 2(2): 65-72.

Bariska, M., and R. Popper. 1975. Ammonia sorption isotherms of wood and cotton cellulose. Wood Science and Technology 9: 153-163.

Bloomer, J.J. 2000. Practical fluid mechanics for engineering applications. Marcel Dekker Inc. New York, NY. U.S.A.

Bodig, J., and B.A. Jayne. 1982. Mechanics of wood and wood composites. van Nostrand Reinhold Company Inc. New York, NY. U.S.A.

Bolton, A.J., 2000. Making the most of plant resources. Forestry Starker Lecture Series. Oregon State University, Corvallis, OR. U.S.A.

Bolton, A.J., and P.E. Humphrey. 1994. The permeability of wood-based composite materials. Part I. A review of the literature and some unpublished work. Holzforschung 48(supplement): 95-100.

Bolton, A.J., P.E. Humphrey., and P.K. Kavvouras. 1989. The hot pressing of dry-formed wood-based composites. Part III. Predicted vapour pressure and temperature variation with tie compared with experimental data for laboratory boards. Holzforschung 43(4): 265-274.

Bowen, M.E. 1970. Heat transfer in particleboard during pressing. MS thesis. Colorado State University. Boulder, CO. U.S.A.

Budinski, K.G. 1996. Engineering materials: Properties and selection. Princeton-Hall, Inc. Upper Saddle River, NJ. U.S.A.

Bunsell, A.R., 1988. Fiber development for composite materials. In: A.R. Bunsell (Editor), Fiber reinforcemet for composite materials. Elsevier. New York, NY. U.S.A. pp. 1-17.

Bunsell, A.R., G. Simon., Y. Abe., M. Akiyama. 1988. Ceramic fibres. In: A.R. Bunsell (Editor). Fiber reinforcements for composite materials. Elsevier. New York, NY. U.S.A. pp. 427-478.

Calundann, G., M. Jaffe., R.S. Jones., H. Yoon. 1988. High performance organic fibres for composite reinforcements. In: A.R. Bunsell (Editor). Fiber reinforcements for composite materials. Elsevier. New York, NY. U.S.A. pp. 211-248.

Carlsson, L.A. 1991. Thermoplastic composite materials. Composite materials series. Elsevier Science Publishers. Amsterdam, Netherlands.

Catling D. and J. Grayson. 1982. Identification of vegetable fibres. Chapman and Hall Ltd. NewYork, NY. U.S.A.

Chase, M.W., Jr. 1998 NIST-JANAF Thermochemical tables. 4th Edition. Journal of physical chemistry reference data. Monograph 9.

Chou, T.W. 1992. Microstrucural design of fiber composites. Cambridge University Press. Cambridge, U.K.

Chow, S. 1972. Thermal analysis of liquid phenol-formaldehyde resin curing. Holzforschung 26: 229-232.

Chow, S., and P.R. Steiner. 1979. Comparisons of the cure of phenol-formaldehyde novolac and resole systems by Differential Scanning Calorimetry. Journal of Applied Polymer Science 23: 1973-1985.

Chow, S., P.R. Steiner, and G.E. Troughton. 1975. Thermal reaction of phenol-formaldehyde resins in relation to molar ratio and bond quality. Wood Science 8(1): 343-349.

Chow, S.Z. 1969. A kinetic study of the polymerization of phenol-formaldehyde resin in the presence of cellulosic materials. Wood Science 1(4): 215-221.

Chowdhury, M.J.A., 1999. Sealed consolidation of natural fiber composites with chemical reactant injection and removal. Ph.D. Thesis, Oregon State University. Corvallis, OR. U.S.A.

Christiansen, A.W. and L. Gollob. 1985. Differential Scanning Calorimery of phenol-formaldehyde resoles. Journal of Applied Polymer Science 30: 2279-2289.

Christiansen, A.W., R.L. Geimer, R.A. Follensbee, J.A. Koutsky, and G.E. Myers. 1993. Phenol-formaldehyde resin curing and bonding in steam-injection pressing. Part II. Differences between rate of chemical and mechanical reasons to resin cure. Holzforschung 47: 76-82.

Christiansen, R.L., W.H. Anderson., and S.D. Stewart. 1987. The influence of particleboard structure on formaldehyde emissions, 21st International particleboard symposium, Washington State University. Pullman, WA. U.S.A.

Clegg, D.W., and A.A. Collyear. 1993. The structure and properties of polymeric materials. The Institute of Materials, London. U.K

Dalen, H., and T.D. Shorma. 1996. The manufacture of particleboard from wheat straw, 30th International particleboard/composites material symposium, Washington State University. Pullman, WA. U.S.A., pp. 191-196.

Davidson, R.W. 1968. Plasticizing wood with anhydrous ammonia, Brochure prepared by State University of New York. Syracuse, NY. U.S.A.

Davidson, R.W., and W.G. Baumgardt. 1970. Plasticizing wood with ammonia. A progress report. Forest Products Journal 20(3): 19-25.

Enns, J.B., J.K. Gilham. 1983. Effect of the extent of cure on the modulus, glass transition, water absorption and density f an amine-cured epoxy. Journal of Applied Polymer Science 28: 2831-2846.

Fitzer, E., M. Heine, 1988. Carbon fibre manufacture and surface treatment. In: A.R. Bunsell (Editor), Fiber reinforcements for composite materials. Elsevier. New York, NY. U.S.A. pp. 73-148.

Follensbee, R.A., J.A. Koutsky, A.W. Christiansen, G.E. Myers, and R.L. Geimer. 1993. Development of dynamic mechanical methods to characterize the cure state of phenolic resole resins. Journal of Applied Polymer Science 47: 1481-1496.

Geimer, R.L., and H.M. Montrey, and W.F. Lehmann. 1975. Effects of layer characteristics on the propertis of three-layer particleboards. Forest Products Journal 25(3): 19-29.

Geimer, R.L., R.A. Follensbee, A.W. Christiansen, J.A. Koutsky, and G. Myers. 1990. Resin characterization. In: T.M. Maloney (Editor), 24th International particleboard/composite materials symposium. Washington State University, Pullman, WA., pp. 65-83.

Gupta, P.K. 1988. Glass fibers for composite materials. In: A.R. Bunsell (Editor). Fiber reinforcements for composite materials. Composite materials series. Elsevier Science Publisher. Amsterdam, Netherland. pp. 20-71.

Haselein, C.R. 1998. Numerical simulation of pressing wood-fiber composites. Ph.D. Thesis, Oregon State University. Corvallis, OR. U.S.A.

Hata, T., B. Subiyanto., S. Kawai., and H. Sasaki. 1989. Production of particleboard with steam-injection. Part III: Effects of injection time and timing on board properties. Mokusai Gakkaishi 35(12): 1080-1086.

Haygreen, J.G., and J.L. Bowyer. 1982. Forest products and wood science. Iowa State Universty Press, Ames, IA. U.S.A.

Heebink, B.G., W.F. Lehmann, and F.V. Hefty. 1971. Reducing particleboard pressing time: Explatory study, General Research Paper 180, USDA Forest Product Lab.

Hon, D.N.S. 1996. Chemical modification of lignocelluosic materials. Marcel Dekker Inc., New York, NY, U.S.A.

Humphrey, P.E. 1982. Physical aspect of wood particleboard manufacture, University of Wales, Bangor, U.K.

Humphrey, P.E. 1993. A device to test adhesive bonds., U.S. Patent Office. Washington DC, U.SA.

Humphrey, P.E. 1994. Engineering composites from oriented natural fibres: a strategy, Proceedings in Second Pacific Rim BioBased Composites Conference. Vancouver, BC. Canada. pp4-11

Humphrey, P.E., A.J. Bolton. 1979. Urea formaldehyde resin bond strength development with reference to wood particleboard manufacture. Holzforschung 33(4): 129-133.

Humphrey, P.E., and A.J. Bolton. 1989a. The hot pressing of dry-formed wood-based composites. Part II. A simulation model for heat and moisture transfer. Holzforschung 43(3): 199-206.

Humphrey, P.E., and A.J. Bolton. 1989b. The hot pressing of dry-formed wood-based composits. Part V. The effect of board size: comparavility of laboratory and industrial pressing. Holzforschung 43(6): 401-405.

Humphrey, P.E., D. Zavala. 1989. A technique to evaluate the bonding reactivity of thermosetting adhesives. Journal of Testing and Evaluation 17(6): 323-328.

Humphrey, P.E., S. Ren. 1989. Bonding kinetics of thermosetting adhesive systems used in wood-based composites: the combined effect of temperature and moisture content. Journal of Adhesion Science and Technology 3(5): 397-413.

Humphrey, P.E., M.J.A. Chowdhury, and H. Thömen. 2001. Consolidation-induced structure of high performance wood-based composite materials, Proceedings of the 4th international ESAFORM conference on material forming, vol 1:7-16

Ilvessalo-Pfäffli, M.S. 1994. Fiber atlas, I. Springer-Verlag, Berlin, Germany.

Jang, B.Z. 1994. Advanced polymer composites. ASM International. Materials Park, OH. U.S.A.

Jayne, B.A. 1960. Some mechanical properties of wood fibers in tension. Forest Products Journal 10(6): 316-322.

Kamke and L.J. Casey. 1988a. Gas pressure and temperature in the mat during flakeboard manufacture. Forest Products Journal 38(3): 41-43

Kamke, F.A., and L.J. Casey. 1988b. Fundamentals of flakeboard manufacture: Internal-mat conditions. Forest Products Journal 38(6): 38-44.

Kamke, F.A., and M.P. Wolcott. 1991. Fundamenals of flakeboard manufacture: wood-moisture relationships. Wood Science and Technology, 25: 57-71.

Katovic, Z. 1967. Curing of resole-type phenol-formaldehyde resin. Journal of Applied Polymer Science 11: 85-93.

Kawai, S., and H. Sasaki. 1989. Oriented medium density fiberboard produced with an electrostatic field. I. Mokusai Gakkaishi 35: 218-226.

Kawai, S., and H. Sasaki., and M. Norimoto. 1987. Aligning torque generated on wood particles by an electrostatic field. I. Mokusai Gakkaishi 33: 872-878.

Kawai, W., and H. Sasaki. 1986. Production technology for low-density particleboard Part I: Forming a density gradient and its effect on board properties. Mokusai Gakkaishi 32(5): 324-330.

Kenji, O., Y. Okudaira., M. Zhang., and S. Kawai. 2000. Manufacture and properties of oriented medium density fiberboard from non-wood lignocellulosic fibers. I. Mokusai Gakkaishi 46: 114-123.

Kessler, R.W., R. Kohler. 1996. New strategies for exploiting flax and hemp. Chemtech 26(12): 34-42.

Kim, M.G., W.L.S. Nieh, and R.M. Meacham. 1991. Study on the curing of phenol-formaldehyde resole resins by Dynamic Mechanical Analysis. Industrial and Engineering Chemistry Research 30: 798-803.

von Klauditz, W., H.J. Ulbricht., W. Kratz., and A. Buro. 1960. Herstellung und eigenschaften von holz-panwerkstoffen mit gerichter festigkeit. Holz als Roh- und Werkstoff, 18: 377-385.

Kozlowski, R., B. Mieleniak., and A. Przepiera. 1994. Plant residues as raw materials for particleboard, 28th international particlebaord/composites materials symposium, Washington State University. Pullman, WA. U.S.A. pp. 181-197.

Lehmann, W.F. 1972. Moisture-stability relationships in wood-based composition boards. Forest Products Journal 22(7): 53-59.

Lindner, T. 2000. Curing characteristics of PF-to-wood bond using ABES. M.S. Thesis. University of Hamburg. Hamburg, Germany.

Lu, X., and A. Pizzi. 1998. Curing conditions effects on the characteristics of thermosetting adhsives-bonded wood joints. Holz als Roh- und Werkstoff 56: 393-401.

Maciel, G.E., I.S. Chuang, and L. Gollob. 1984. Solid state ^{13}C NMR study of resole-type phenol-formaldehyde resins. Marcromolecules 1984(17).

Mallick, P.K. 1993. Fiber reinforced composites. Marcel-Dekker Inc., New York, NY. U.S.A.

Marra, A.A. 1992. Technology of wood bonding. von Nostrand Reinhold, New York, NY. U.S.A.

Matthews, F.L., and R.D. Rawlings. 1994. Composite materials. Chapman & Hall. London, U.K.

McKeever, D.B., J.A. Youngquist., and B.W. English. 1995. Sources and availability of recovered wood and fiber for composites products, 29th international particleboard/composites materials symposium, Washington State University, Pullman, WA. U.S.A., pp. 197-214.

Meyers, G.E., A.W. Chistiansen, R.L. Geimer, R.A. Pollensbee, and J.A. Koutsky. 1991. Phenol-formaldehyde resin curing and bonding in steam-injection pressing. I. Resin synthesis, characterization, and cure behavior. Journal of Applied Polymer Science.(237-250).

Nebel, K.M. 1995. New processing strategies for hemp. Journal of the International Hemp Association 2(1): 1-9.

Neville, A.C. 1993. Biology of fibrous composites. Cambridge University Press. Cambridge, U.K.

Pilato, L.A., and M.J. Michno. 1994. Advanced composite materials. Springer-Verlag. New York, NY. U.S.A

Pizzi, A. 1983. Wood adhesives. Marcel-Dekker Inc. New York, NY. U.S.A.

Pizzi, A., and A. Stephanou. 1994a. Phenol-formaldehyde wood adhesives under very alkaline conditions. Part 1: Behavior and proposed mechanism. Holzforschung 48: 35-40.

Pizzi, A., and A. Stephanou., 1994b. Phenol-formaldehyde wood adhesives under very alkaline conditions. Part 2: Esters curing acceleration, its mechanism and applied results. Holzforschung 48: 150-156.

Pizzi, A., X. Lu, and R. Garcia. 1999. Lignocellulosic substrates influence on TTT and CHT curing diagrams of polycondensation resins. Journal of Applied Polymer Science 71: 915-925.

Plath, E., and E. Schnitzler. 1974. Das rohdichteprofil als beurteilungsmerkmal von spanplatten. Holz als Roh- und Werkstoff 32: 443-449.

Polany, M. 1932. Theories of the adsorption of gases. A general survey and some additional remarks. Trans Faraday Society 28:316-333

Prime, R.B. 1997. Thermosets. In: E. Turi. (Editor). Thermal characterization of polymeric materials. Academic Press. Brooklyn, NY. U.S.A. pp. 1380-1766.

Pulido, O.R., S. Kawai. Y. Yoshida., H. Sasaki., 1990. Oriented medium density fiberboard produced with an electrostatic field II. Mokusai Gakkaishi 36: 29-35.

Pulido, O.R., H. Sasaki., S. Kawai., and Y. Yoshida. 1991a. Oriented mat-former with high voltage electrode system. Mokusai Gakkaishi 37: 1167-1176.

Pulido, O.R., Y. Yoshida., S. Kawai., and H. Sasaki. 1991b. Aligning torque generated in wood particles by an electostatic field. IV. Mokusai Gakkaishi 37: 135-141.

Pulido, O.R., Y. Yoshida., Q. Wang., S. Kawai., and H. Sasaki. 1991c. Aligning torque generated in wood particles by an electrostatic field. V. Mokusai Gakkaishi 37: 711-718.

Ren, S. 1991. Thermo-hygro rheological behavior of materials used in the manufacture of wood-based composites. Ph.D. Thesis, Oregon State University. Corvallis, OR. U.S.A.

Rials, T.G., and M.P. Wolcott. 1996. Physical and mechanical properties of agro-based fibers. In: Rowell, Roger; Young, Raymond A.; and Rowell, Judith K., eds. In: Paper and Composites from Agro-Based Resources. Chapter 4.: pp. 64-79.

Riber, B.H. 1981. A method for measuring adhesive shear properties. Adhesive age 24(12): 30-33.

Robson, D., and J. Hague. 1998. A comparison of wood and plant fiber properties, Forth international conference on wood fiber-plastic composites. Forest Products Society. Madison, WI. U.S.A.

Rowell, R.M. 1983. Chemical modification of wood. Forest Products Abstract, 6: 363-382.

Rowell, R.M., R.A. Young, and J.K. Rowell., eds. 1996. Paper and composites from agro-based resource. Lewis Publishers. New York, NY. U.S.A.

Russell, C.W. 1996. The straw resource: A new fiber basket? 30th International particleboard/composites materials symposium, Washington State University. Pullman, WA. U.S.A. pp. 183-190.

Sauter, S.L. 1996. Developing composites from wheat straw, 30th International particleboard/composites material symposium, Washington State University. Pullman, WA. U.S.A., pp. 197-214.

Schuerch, C. 1963. Plasticizing wood with liquid ammonia. Industrial and Engineering Chemistry Research 55: 39.

Schulte, M., and A.Früwald. 1996a. Shear modulus, internal bond and density profile of medium density fibre board. Holz als Roh- und Werkstoff 54: 49-55.

Schulte, M., and A.Früwald. 1996b. Some investigations concerning density profile, internal bond and relating failure position of particleboard. Holz als Roh- und Werkstoff 54: 289-294.

Schwartz, M.M., 1996. Composite materials. Princeton-Hall Inc., Upper Saddle River, NJ.

Seber, D.H., and Lloyd, E.H. 1996. Bast fiber applications for composites, 30th International particleboard/composites materials symposium, Washington State University. Pullman, WA. U.S.A., pp. 215-235.

Shaler, S.M. 1993. Mechanics of the interface in discontinuous wood fiber composites. In: M.P. Wolcott (Editor), Wood fiber/Polymer composites: Fundamental concepts, process, and material options. Forest Products Society. Madison, WI. U.S.A.

Shao, M. 1989. Thermal properties of wood fiber network. M.S. Thesis, Oregon State University. Corvallis, OR. U.S.A.

Simon, S.L., J.K. Gilham. 1994. Conversion-temperature-property diagram for a liquid dicyanate ester/high-T_g polycyanurate thermosetting system. Journal of Applied Polymer Science 51: 1741-1752.

Skeist, I. 1990. Handbook of Adhesives. Van Nostrand Reinhold. New York, NY. U.S.A.

Skinner, C. 1999. Status of release technology of oriented strand board bonded with MDI based binders, Wood Adhesives 2000. Lake Tahoe, NV. U.S.A.

Smith, D.C. 1982. Waferboard press closing strategies. Forest Products Journal 32(3): 40-45.

Snell, R., J. Hague., and L. Groom. 1998. Characterizing agrofibers for use in composite materials, Fourth international conference on wood fiber-plastic composites. Forest Products Society. Madison, WI. U.S.A.

Song, D., and S. Ellis. 1997. Localized properties in flakeboard: A simulation using stacked flakes. Wood and Fiber Science, 29(4): 353-363.

Sperling, L.H. 1986. Introduction to physical polymer science. John Wiley & Sons. New York, NY. U.S.A.

Stamm, A.J. 1955. Swelling of wood and fiberboard in liquid ammonia. Forest Products Journal 5(6): 413-416.

Steffen, G., A. von Haas., P.E. Humphrey., H. Thömen. 1999. Temperature and gas pressure in MDF-mats during industrial continuous hot pressing. Holz als Roh- und Werkstoff 57: 154-155

Steiner, P.R., and S.R. Warren. 1981. Rheology of woo-adhesive cure by Torsional Braid Analysis. Holzforschung 35: 273-278.

Strickler, M.D. 1959. Efects of press cycle and moisture content on properties of douglas-fir flakeboard. Forest Products Journal 28(9): 203-215.

Suchsland, O. 1959. An analysis of the particleboard process. Quaterly bulletin. Michigan State University. Agricultural Experiment Station 42: 350-372.

Suchsland, O. 1967. Behavior of a particleboard mat during the press cycle. Forest Products Journal 17(2): 51-57.

Suchsland, O., and G.E. Woodson. 1987. Fiberboard manufacturing practices in United States, USDA Forest Service Agricultural Handbook No. 640, Washington D.C. U.S.A.

Suo, S., and J. Bowyer. 1995. Modeling of strength properties of structural particleboards. Wood and Fiber Science 27(1): 84-94.

Talbott, J.W. 1974. Electrically aligned particleboard and fiberboard. In: T.M. Maloney (Editor). 8th Particleboard symposium. Washington State University. Pullman, WA. U.S.A. pp. 153-182.

Talbott, J.W., and E.K. Stefanakos. 1972. Aligning forces on wood particles in an electric field. Wood and Fiber Science 4: 193-203.

Thömen, H., 2000. Modeling of physical process in natural fiber composites during batch and continuous pressing. Ph.D. Thesis. Oregon State University, Corvallis, OR. U.S.A.

Thömen, H., and P.E. Humphrey. 2002. Hot pressing of wood-based composites: Selected aspects of the physics investigated by means of simulation. Wood and Fiber Science (in review).

Thömen, H., and P.E. Humphrey. 1998. Modeling physical mechanisms of composite hot pressing process, Presented at the Technical Forum of 55th Forest Products Society Annual meeting, Lake Tahoe, NV. U.S.A.

Tsuomis, G. 1991. Science and technology of wood. Chapman & Hall. New York, NY. U.S.A.

Wang, S., P.M. Winistorfer., T.M. Young., and C. Helton. 2001a. Step-closing pressing of medium density fiberboard; Part I. Influence on vertical density profile. Holz als Roh- und Werkstoff 59: 19-26.

Wang, S., P.M. Winistorfer., T.M. Young., and C. Helton. 2001b. Step-closing pressing of medium density fiberboard; Part II. Influence on panel performance and layer characteristics. Holz als Roh- und Werkstoff 59: 311-318.

Wang, S., and P.M. Winistorfer. 2000. Consolidation of flakeboard mats under theoretical laboratory pressing and simulated industrial pressing. Wood and Fiber 32(4): 527-538.

Wang, X.M., B. Riedl, A.W. Christiansen, and R.L. Geimer. 1994. Differential scanning calorimetry of the effects of temperature and humidity on phenol-formaldehyde resin cure. Polymer 26: 2485-2492.

Wawner Jr., F.E. 1988. Boron and silicon carbide/carbon fibers. In: A.R. Bunsell (Editor), Fiber reinforcements for composite materials. Elsevier, New York, NY. U.S.A. pp. 371-425.

White, R.H., and T.F. Rust. 1965. Cure rate of phenolic resins by Differential Thermal Analysis. Journal of Applied Polymer Science 9: 777-784.

Winistorfer, P.M., T.M. Young, and E. Walker. 1996. Modeling and comparing vertical density profiles. Wood and Fiber Science 28(1): 133-141.

Wisanrakkit, G., J.K. Gilham, and J.B. Enns. 1990. The glass transition temperature as a parameter for monitoring the cure of an amine/epoxy systemat constant heating rate. Journal of Applied Polymer Science 41: 1895-1912.

Wong, E.D., M. Zhang, Q. Wang, and S. Kawai. 1998. Effects of mat moisture content and press closing speed on the formation of density profile and properties of particleboard. Journal of Wood Science 44: 287-295.

Wong, E.D., M. Zhang, Q. Wang, and S. Kawai. 1999. Formation f the density profile and its effects on the properties of particleboard. Wood Science and Technology 33: 327-340.

Wong, E.D., M. Zhang, Q. Wang, G. Han, and S. Kawai. 2000. Formation of the density profile and its effects on the properties of fiberboard. Journal of Wood Science 46: 202-209.

Woodson, G.E. 1976. Density profile and fiber alignment in fiberboard from three southern hardwoods. Forest Products Journal 27(8): 29-34.

Xu, W. 1999. Influence of vertical density distribution on bending modulus of elasticity of wood composite panels: A theoretical consideration. Wood and Fiber Science 31(3): 277-282.

Xu, W., and O. Suchsland. 1998. Modulus of elasticity of wood composite panels with a uniform vertical density profile: A model. Wood and Fiber Science 30(3): 293-300.

Xu, W., and P.M. Winistorfer. 1996. Fitting an equation to vertical densty profile data using Fourier analysis. Holz als Roh- und Werkstoff 54: 57-59.

Yang, H.H., 1988. Aramid fibers. In: A.R. Bunsell (Editor). Fiber reinforcements for composite materials. Elsevier, New York, NY. U.S.A. pp. 249-329.

Yoshida, Y., O.R. Pulido., S. Kawai., and H. Sasaki. 1988. Aligning torque generated in wood particles by an electrostatic field II. Mokusai Gakkaishi 34: 401-408.

Yoshida, Y., O.R. Pulido., S. Kawai., and H. Sasaki. 1990. Aligning torque generated on wood particles by an electrostatic field III. Mokusai Gakkaishi 36: 523-530.

Yoshida, Y., S. Kawai., O.R. Pulido., and H. Sasaki. 1989. Production of oriented particleboard. I. Mokusai Gakkaishi 35: 227-233.

Young, R.H., P.W. Kopf, and O. Salgado. 1981. Curing mechanism of phenolic resins. TAPPI 64(4): 127-130.

Zauscher, S., and P.E. Humphrey. 1997. Orienting lignocellulosic fibers and particles by means of a magnetic field. Wood and Fiber Science 29(1): 35-46.

Zavala, D., Humphrey, P. E. 1996. Hot pressing veneer-based products: The interaction of physical process. Forest Products Journal, 46(1): 69-77.

APPENDICES

APPENDIX A

A. FIBERS AND ADHESIVES THAT COULD BE USED IN FIBER COMPOSITE MATERIALS

A.1. SYNTHETIC FIBERS

A.1.1. Glass Fibers

Glass fibers are the most common of all reinforcing fibers for polymerically matricised composites. The principal advantages of glass fibers are their high tensile and impact strength, high chemical resistance, excellent insulating properties and rather low cost. The disadvantages are their rather low tensile modulus (72-85Gpa; Jang, 1994), relatively high density (approximately 2500Kg/m^3; Jang, 1994), low fatigue resistance, and poor adhesion to matrix resins (Mallick, 1993). Unlike other types of synthetic fibers, such as polymeric or carbon fiber which are anisotoropic, glass fiber is isotropic. Two important types of glass fibers used in the fiber composite industries are termed E-glass and S-glass. E-glass is cheap and widely used in composite manufacturing whereas S-glass is more expensive but has higher structural organization and consequent tensile strength and elastic modulae (72Gpa for E-glass and 85Gpa for S-glass; Bunsell *et al.*, 1988; Jang, 1994). Glass fibers can be manufactured in various forms such as strands (bundles of filaments), woven roving, and chopped strand. The average tensile strength of freshly drawn glass fibers may exceed 3.5GPa. However, surface damage during processing tends to reduce the strength to 1.7-2.0GPa (Budinski, 1996).

A.1.2. Carbon fibers

Carbon fibers are commercially available with a variety of tensile moduli, typically ranging from 200GPa to 1,030GPa. In general, the low-modulus carbon fibers have lower relative density, lower cost, and higher tensile strain-to-failure than do the high-modulus fiber types. The main advantages of carbon fibers are their high specific tensile strength and modulus, low coefficient of linear thermal expansion and high fatigue strength. The disadvantages are their low impact resistance, high electrical conductivity, and high cost (Mallick, 1993; Bunsell *et al.*, 1988). High strength, high modulus carbon fibers are manufactured by treating precursors such as pitch and polyacrylonitril with heat and tension, leading to a highly ordered carbon structure (Jang, 1994). Structurally, carbon fibers contain a blend of amorphous carbon and graphitic carbon. The high tensile modulus results from the graphitic form in which carbon atoms are arranged in crystalographically parallel planes of regular hexagons. The planes are held together by a Van der Waals-type forces, and strong covalent bonds exist between the carbon atoms within planes (Figure 2.9).

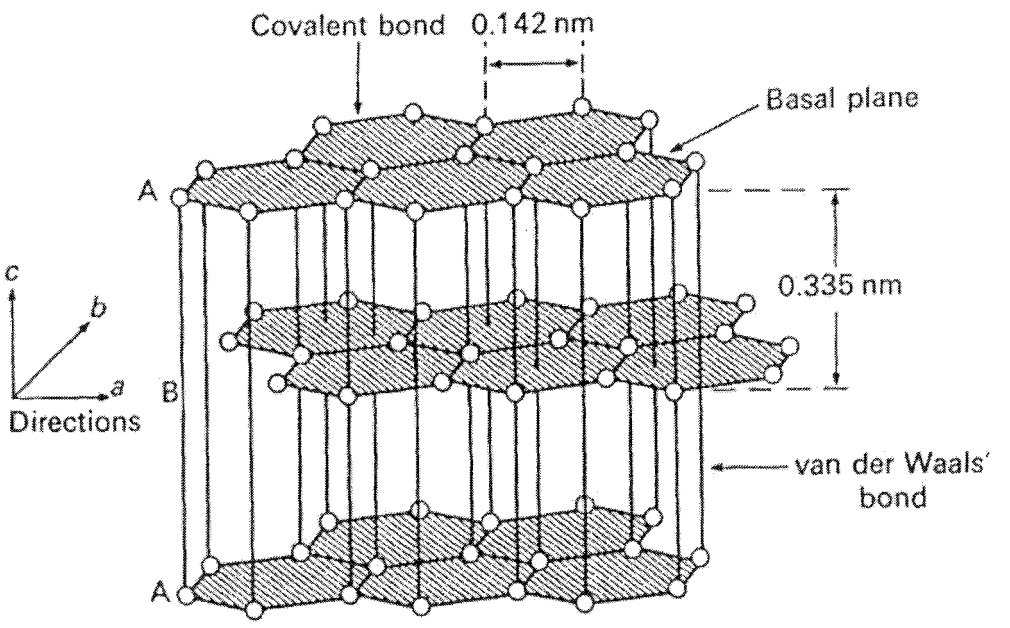

Figure A.1. Crystal structure of carbon fibers (Matthews *et al.*, 1994)

This results in high strength and modulae values (Matthews *et al.*, 1994); they are commercially available in three basic forms which are usually broadly termed "long and continuous tow", "chopped", and "milled". The long, continuous tow form can be woven into two- or three-dimensional fabrics of various styles. Carbon fibers are often combined with carbon matrix to produce composites with high heat resistance. Attention is given here to carbon fibers since they may well prove useful as a reinforcing element in the types of natural fiber composites to be synthesized in the present study.

A.1.3. Polymeric fibers

One of the great advantages of polymeric fibers is their relatively high specific strength. Their low density makes them very attractive for applications where weight saving is a primary objective. Negative attributes of the polymeric fibers include their relatively low temperature tolerance and rather poor compressive properties (Bunsell, 1988). Important examples of high specific strength polymeric fibers are aromatic polyamides known as aramide (Kevlar®) and extended chain polyethylene fibers known as Spectra®. Aramid fibers are composed of poly(p-phenylene terephthalamide). The fiber can be spun by extrusion from a polymer solution which is followed by a stretching and drawing process. The strong covalent bonds in the fiber axis direction provide high longitudinal tensile strength, whereas the weak hydrogen bonds in the transverse direction result in low transverse tensile properties (Budinski, 1996).

In contrast to the above, polypropylene is sometimes used for low modulus fiber reinforcement in composite manufacturing. The main advantages of these fibers are their alkali resistance, relatively high melting point (165°C), and low price, while disadvantages are their low modulus and sensitivity to sunlight and oxygen. Extended chain polyethylene fibers, (Spectra®) are produced from high molecular weight polyethylene and have high specific strength and high abrasion resistance. Although the melting point of Spectra® fibers is 147°C, they exhibit a high level of creep above 100°C, and thus their application temperature is typically limited to 80-90°C. Acrylic, nylon, and polyvinyl acetate are also being used for reinforcement in fiber composites (Bunsell, 1988; Mallick, 1993).

A.1.4. Boron fibers

The most prominent feature of boron fibers is their extremely high tensile modulus which typically ranges from 379 up to 414GPa. These fibers also have excellent resistance to buckling. The principal disadvantage of boron fiber is its high cost. For this reason, its use has been largely restricted to aerospace applications (Schwartz, 1996).

A.1.5. Ceramic fibers

Fibers from silicon carbide (SiC) and aluminum oxide (Al_2O_3) are examples of ceramic fibers which are used in high temperature applications in metal and ceramic matrix composites. Silicon carbide retains its strength above 650°C, and aluminum oxide has excellent strength up to 1370°C. Both types of fiber are suitable for reinforcing metal matrices for which carbon and boron fibers are not suitable (Bunsell *et al.*, 1988).

A.2. MATRICES AND ADHESIVES USED FOR FIBER COMPOSITE MATERIALS

A.2.1. Polyvinyl acetate

Polyvinyl acetate (PVA) is a thermoplastic adhesive used for various applications. PVA exhibits versatility for bonding of wide variety of substrates. In particular, PVA is capable of producing strong and durable wood-to-wood bonds. Properties of PVA cannot be generalized because of the chemical modification and addition of emulsifiers, plasticizers, stabilizers and so on. PVA is derived from vinyl acetate monomer and after polymerization under emulsion condition, it

becomes a so-called "white glue" or "cold glue" which is often used in the wood industry and craft shops (Pizzi, 1983; Marra, 1992).

Emulsified PVA can form bonds in very short times but full bond strength is typically achieved in about 24 hour. The formed bonds are strong and durable but, being thermoplastic, PVA deforms under elevated temperatures. It is also susceptible to creep failure and water ingress (Marra, 1992).

A.2.2. Epoxy resins

Thermosetting matrices such as epoxy are widely used for manufacturing synthetic fiber composites. The PF resins and isocyanate resins mentioned in section 2.4.4 are also used as matrices for synthetic fiber composites.

One of the most outstanding properties of epoxy resins is that they are liquids with 100 percent solid content. Therefore, they do not contain any solvents to be dissipated and consequently experience very low shrinkage upon curing. Chemically, the resin is based on the reactions of the epoxide ring which is three-membered with one oxygen and two carbon atoms. A typical starting material is diglycidyl ether of bisphenol A. Properties of a cured epoxy resin depend primarily on the cross-link density. In general, the tensile modulus, glass transition temperature, thermal stability, and chemical resistance are improved with increasing cross-link density, but strain-to-failure and fracture toughness are inversely correlated with cross-linking beyond some transitional level. Factors that effect the cross-link density are the chemical structure of the starting liquid resin, functionality of the curing agent, and reaction conditions such as time and temperature (Marra, 1992; Pizzi, 1983). Reaction of epoxy resin is shown in Figure A.2.

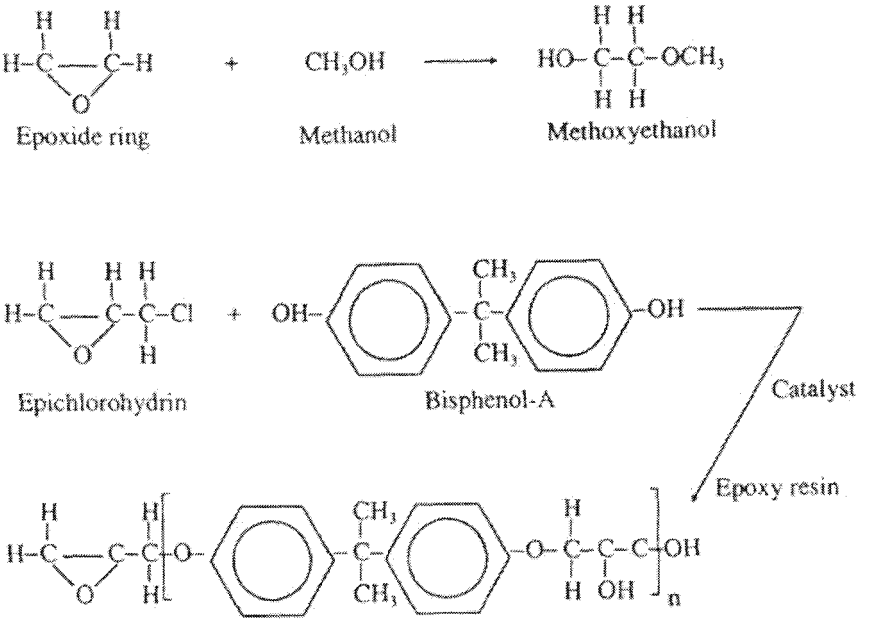

Figure A.2. Reaction of epoxy resin (Marra, 1992)

A.2.3. Polyesters

The starting material for a thermosetting polyester matrix is an unsaturated polyester resin that contains a number of C=C double bonds. Polyester is prepared from maleic anhydride with ethylene or propylene glycol. The curing reaction of polyester resins is initiated by adding small quantities of a catalyst. The curing time depends on the catalyst employed, along with temperature. The elastic modulus, glass transition temperature and thermal stability of cured polyester resins are generally increased by increasing cross-linking density, but the strain-to-failure and impact energy are reduced. Polyester resins can be formulated with a variety of properties ranging from hard and brittle to soft and flexible. The main advantages of the polyester are low viscosity, fast curing time, and low cost. However, their

properties are generally lower than those of epoxies. The principal disadvantage of polyesters over epoxies is their high volumetric shrinkage (Mallick, 1993; Schwartz, 1996).

A.2.4. Vinyl ester

The starting material for a vinyl ester is an unsaturated vinyl ester resin, which may be produced by the reaction of an unsaturated carboxylic acid and an epoxy resin. Vinyl polyester resins possess good characteristics of epoxy resins, such as excellent chemical resistance and high tensile strength, and of unsaturated polyester such as low viscosity and fast curing. However, the volumetric shrinkage of vinyl ester resin is about 5-10%, which is higher than that of epoxy resins (Mallick, 1993; Schwartz, 1996).

A.2.5. Polyimides

Thermosetting polyimides are obtained by addition polymerization of liquid monomeric or oligomeric imides to form a cross-linked structure. The fully cured thermosetting polyimides offer high temperature resistance and high chemical and solvent resistant. Bismaleimides are the most widely used thermosetting polyimides in the advanced composite industry (Mallick, 1993).

A.2.6. Polyethylene

In thermoplastic polymers, individual molecules are almost always linear in structure with no chemical links between them. These molecules are normally held

in place by a week secondary bonds (Van der Waals) and hydrogen bonds. With the application of heat and pressure, these intermolecular bonds can be temporarily broken, and the molecules can be moved relative to each other to flow into new positions. Upon cooling, the molecules "freeze" in their new positions, thus restoring the secondary bonds between them. Thermoplastic polymers can therefore be heat softened, melted and reshaped repeatedly (Budinski, 1996; Carlsson, 1991).

Thermoplastic polymers can be divided into commodity thermoplastics such as polystyrene and polypropylene, and engineering plastics such as acrilonitrile butadiene styrene (ABS). Most of thermoplastics have the potential to be used as a matrix material in composites. A series of polymers with greatly different characteristics can be obtained by altering the monomer structurally; substituting at least on hydrogen atom to another functional atom or group in ethylene (Budinski, 1996).

The basic monomer of polyethylene is ethylene. The polymers made from the ethylene monomer vary with molecular weight (chain length), crystallinity, and branching characteristics (Budinski, 1996). Polyethylene may be further categorized according to its relative density ;low density polyethylene ranges from 0.91 to 0.95 of specific density whereas high density polyethylene ranges from 0.94 to 0.96). The low-density grades have a significant degree of branching, which means a lower melting point, lower strength, and lower elasticity. The low-density grades have good clarity in film form and they are most often used for packaging films, paper coatings, wire coatings, and similar nonstructural applications. The high-density grades of polyethylene are predominantly used for injection molded consumer items. There is also linear low-density polyethylene (LLDPE) in which the polymer chain has no branches at all, and ultra high density molecular weight polyethylene (UHMWPE) which is linear and of very high molecular weight (Schwartz, 1996). Polyethylenes generally exhibit good chemical resistance and flexibility but are of low strength and heat resistance.

A.2.7. Polypropylene

The monomer of polypropylene has a substitute of methyl group (CH_3). Polypropylene is similar to polyethylene, but its mechanical properties make it more suitable for molded products. Polypropylene is stiffer, harder and often of higher strength than polyethylene. It has good fatigue resistance and is resistant to higher temperatures. A unique property of polypropylene is its low relative density (0.90 to 0.915). The two largest uses of polypropylene are for injection molding parts and for fibers or filaments (Budinski, 1996).

A.2.8. Polyvinyl chloride

Polyvinyl chloride, known as PVC, is one of the most widely used plastics in terms of volume produced. The monomer has one chlorine atom substituted for a hydrogen atom. Plasticized PVC has low strength, and is used for imitation leather, decorative laminates, and many other consumer products. PVC is also widely used as an insulating coating on wires and is often used over other plastics because of its nonflammable properties. Rigid PVC has sufficient strength and stiffness to qualify as an engineering plastic. It has good moldability and fabricability. Rigid PVC is widely used for piping, guards, ducting, and fume hoods. It is very resistant to many acids, but has poor resistance to some organic solvents. The other major limitation of rigid PVC is its poor toughness and notch sensitivity. PVC can be co-polymerized with other polymers for increased toughness and other properties (Budinski, 1996).

A.2.9. Polyvinyl acetate

The monomer of polyvinyl acetate (PVA) has an acetate substitute replacing a hydrogen atom on an ethylene molecule. PVA is a relatively soft thermoplastic mainly used for coatings and adhesives rather than for molded parts. As an adhesive, it is white glue for most wood workings. Other uses include textile fibers and textile finish coatings (Budinski, 1996).

A.2.10. Polystyrene

Because of their low cost, polystyrenes are widely used for throw-away items such as plastic food container and toys. Polystyrene is made from ethylbenzene. A large bezene ring replaces a hydrogen atom on an ethylene molecule. The presence of a large molecule as the substitute on a carbon atom chain causes chain stiffening. Deformation by relative chain movement is inhibited by the interaction of benzene rings on adjacent chains. This structural effect is responsible for the inherent brittleness, poor impact strength and hardness of polystyrene. Polystyrene has excellent moldability. Its melting point is only 115°C and it can be made into a rigid foam. The foams are widely used in insulation and floatation devices (Pilato, 1994).

A.2.11. Polymethyl methacrylate

Polymethyl methacrylate (PMMA) is the polymer used to make the unbreakable windows or low cost camera lenses. Another name of PMMA is acrylic, which are esters obtained by reacting an acid such as methyl acrylic with an alcohol. The acrylics are rigid and clear, making them useful on machines for

guards, sight glasses, and covers. They are also used as coating and painting materials and are readily injection molded (Pilato, 1994).

A.2.12. Acrylonitrile Butadiene Styrene

Acrylonitrile butadiene styrene (ABS) is a combination of three different polymers of contrasting properties. ABS is an important thermoplastic for the manufacture of consumer goods. As an example of general properties of this plastic, most telephones are injection molded from ABS which has excellent toughness and moderately high strength and stiffness (Budinski, 1996).

A.2.13. Polyamides

The polyamides are polymers formed as a condensation product of an acid and an amine. They all contain the characteristic amid group. There are a number of common polyamides; the various types are usually called nylon 6, nylon 6/6, nylon 6/10, nylon 6/12, and nylon 12. The suffixes refer to the number of carbon atoms in each of the reacting substances involved in the condensation polymerization. Polyamides have sufficient mechanical properties to be used for structural parts and have good melt processability. The biggest disadvantage of polyamides is their tendency to absorb moisture which decreases the tensile strength, stiffness and dimensional stability but increases toughness. Some of the high tensile strength polyamides containing aromatic functional groups can be used as reinforcing fibers (Clegg, 1993).

A.2.14. Polyimides

Polyimides have very complex structures with chain stiffening due to the presence of ring structures. The main characteristic of this polymer is its high resistance to heat. They maintain stability and mechanical properties at temperatures up to 315°C. The stable structure of the aromatic ring does, however, create processing problems. It also has good mechanical properties with high tensile and compression strength. Polyimides are available in molding pellets, in directly formed shapes for machining, and as resins and matrices for for composites (Clegg, 1993).

A.2.15. Polyamide-imides

Polyamide-imide polymers have a chemical structure that is a combination of the typical nitrogen bond of a polyamide and the ring structure of a polyimide. The repeating unit consists of alternating amide and imide. Polyamide-imide is the only polymer that is strengthened by post-molding heat treatment. Post heating for 1 to 6 days at about 250°C can increase the tensile strength and percent elongation. The main characteristics of this polymer is its high strength and high maximum operating temperature (Budinski, 1996; Mallick, 1993).

A.2.16. Polysulfone

Polysulfone is an amorphous rigid thermoplastic material which has high useable temperature. The basic repeating unit of polysulfone contains stable linkages of benzene rings. The mechanical properties of polysulfones are similar to those of polyamides at room temperature, but useful strength and rigidity are maintained at temperatures as high as 180°C. Polysulfones have good optical

clarity and lower moisture sorption than polyamides. The property combination of good strength at elevated temperature and clarity make this polymer popular for such applications as cook-ware (Clegg, 1993; Pilato, 1994).

A.2.17. Polyphenylenesulfide

Polyphenylenesulfide (PPS) is a rigid, crystalline thermoplastic with a stable structure and rigidity provided by the chain stiffening of benzene rings. Most PPS is available in the form of composites with fillers such as glass, mineral, and other polymeric materials. PPS also has good mechanical properties at elevated temperatures. The mechanical properties of PPS at room temperature are similar to those of polyamides but at elevated temperature it has much better strength retention and creep resistance than polyamides. The most suitable applications of PPS are those that take advantage of their high strength and at elevated temperature capabilities (Mallick, 1993; Pilato, 1994).

A.2.18. Polyetheretherketone

The repeating unit of polyetherether ketone (PEEK) has benzene rings that are linked with an oxygen bond, forming a typical R-O-R type of ether structure. They are partially crystalline and can be injection or compression molded. PEEK has low flammability and smoke emmision ratings, excellent resistance to attack by hot water and low pressure steam, and is very resistant to organic solvents. This polymer is usually used as a composite with glass or carbon fiber. When PEEKs are used as the matrix resin for carbon fiber composites, the resulting composites can have a tensile modulus of elasticity of about 125GPa, which makes this composite much stiffer than aluminum. This makes the PEEK a suitable matrix material for

aerospace and aircraft applications and may have potential to be incorporated within future forms of the oriented natural fiber composites created in the present investigation (Budinski, 1996; Clegg, 1993).

A.3. OTHER TYPES OF ADHESIVES/MATRICES

Additional types of resins such as tannin- or lignin-based ones which can be applicable as an adhesive for natural fiber-based composites. Also there is increasing interest in adhesives from renewable resources such as starch and soy. Although phenolic and amino resins are the most prevalent form of adhesives for conventional natural fiber composites, some new types of adhesive have properties that are comparable to, or exceed, the properties of conventional ones.

Metal and ceramic matrices have advantages over polymeric ones in applications requiring long-term resistance to severe environments such as high temperature. The yield strength and elastic modulus of most metals and ceramics are higher than those of polymers, which is an important consideration for applications requiring high strength and modulus. Another advantage of using metal is that they can be plastically deformed and strengthened by a variety of thermal and mechanical treatment methods. However, metals have some disadvantages such as high specific gravity, high melting points, and a tendency to corrode at the fiber/matrix interface.

Ceramics are also considered for applications such as combustion engines, gas turbines, and electronics. They are high modulus materials with high temperature tolerance. However, they may have low failure strain and very low fracture toughness (Mallick, 1993; Schwartz, 1996) (Mallick, 1993; Schwartz, 1997). Ceramics may also prove appropriate for use as contoured pressing surfaces in the new composite manufacturing techniques to be investigated in the present thesis. They can offer significant performance and cost advantages over cast and

forged steel dyes for stamping and forging operations. Ceramics may be fabricated with porous microstructure that may enable pressing surfaces to be used for vapor-phase reactant injection and removal.

APPENDIX B

B ENGINEERING DRAWING

B.1 ENGINEERING DRAWING OF EACH PART OF THE GAS INJECTION PRESSING DEVICE

The upper and lower platens of the press are designed such that the 'T' shape upper platen plunges into the 'U' shape lower platen. The gas injection plate consists of two pieces; back piece and perforated piece. The perforated piece has three long slots and series of small diameter holes are located along the slot. The two end pieces which are attached on upper platen was designed to hold gas injection plate on upper platen.

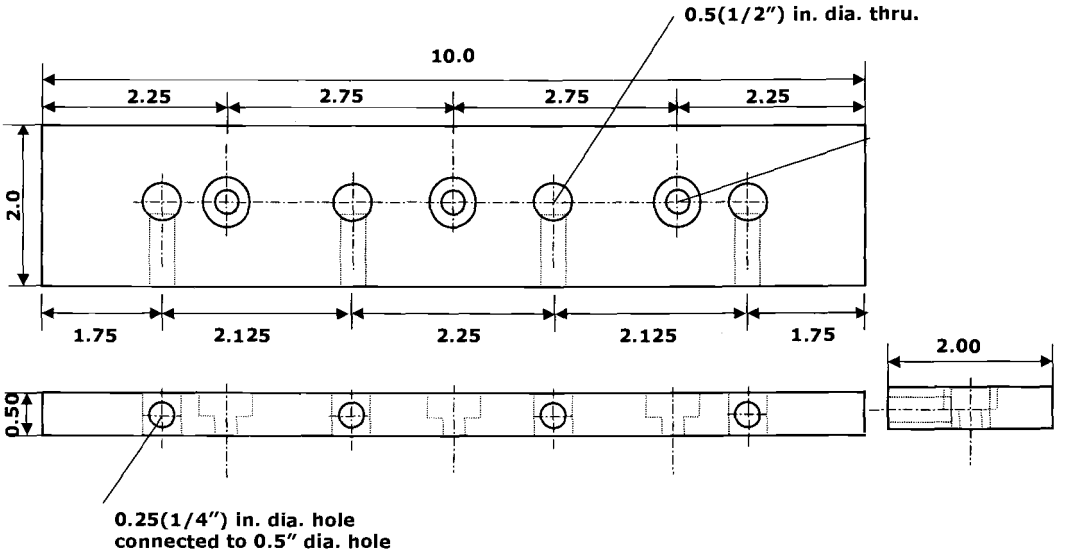

Figure B.1. Top piece of upper platen

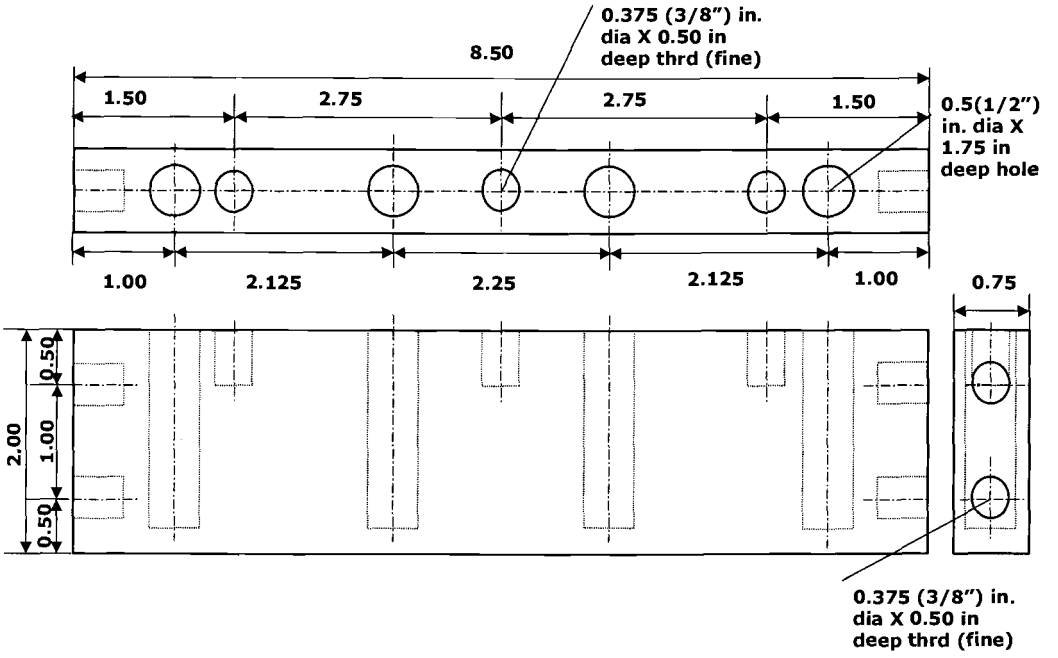

Figure B.2. Slide-in piece of upper platen

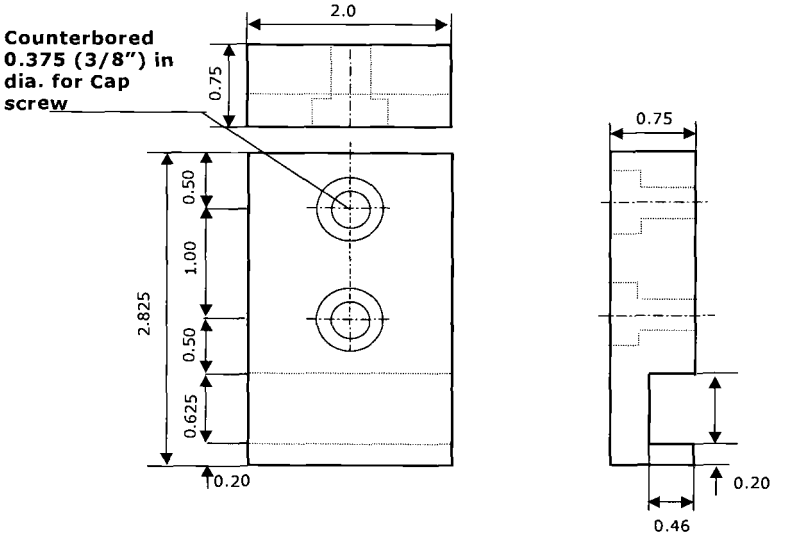

Figure B.3. End piece of upper platen

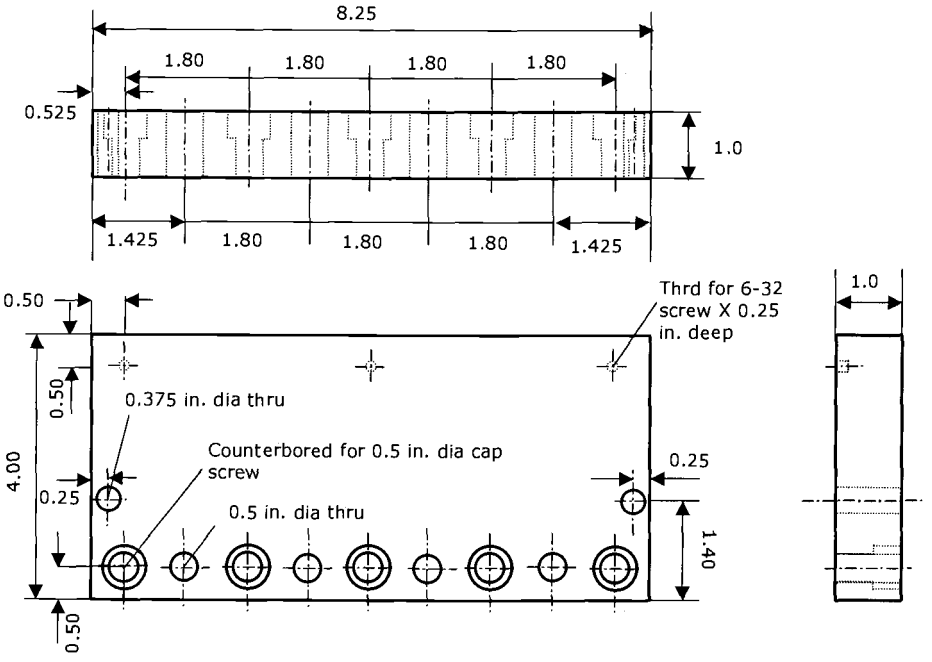

Figure B.4. Side piece (A) of lower platen

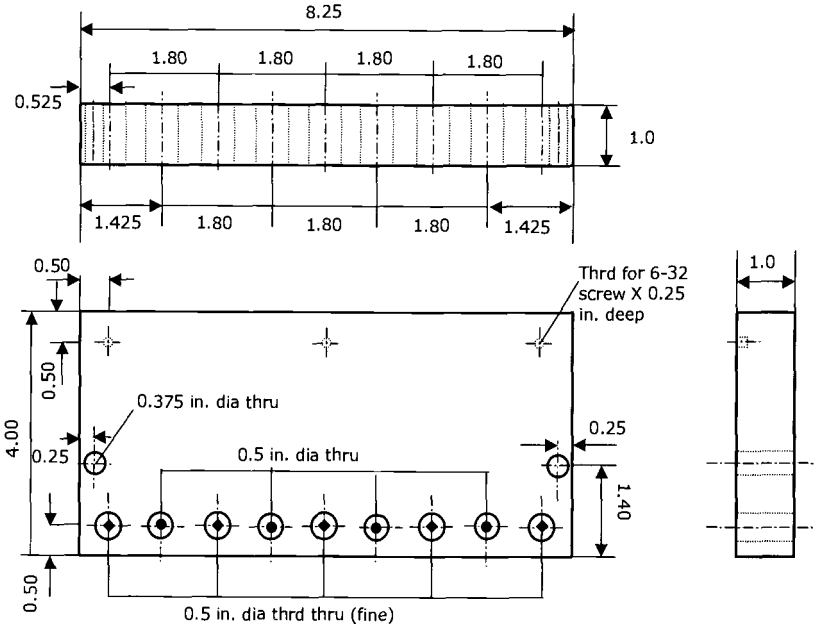

Figure B.5. Side piece (B) of lower platen

B.2 DIAGRAM OF COOLING HEAD

The cooling head consists of two PTFE cooling head block, base plate and two stopping block. The PTFE blocks have "L" shape hole for air path (one end of the hole is sealed) and series of small pin holes are evenly distributed along the vertical part of the hole. These two plates sit on the base plate and connected through pring-loaded rod which guide the movement of the plate when necessary. Base plates are connected pneumatic cylinder whose motion was controlled by a computer controlled air supply.

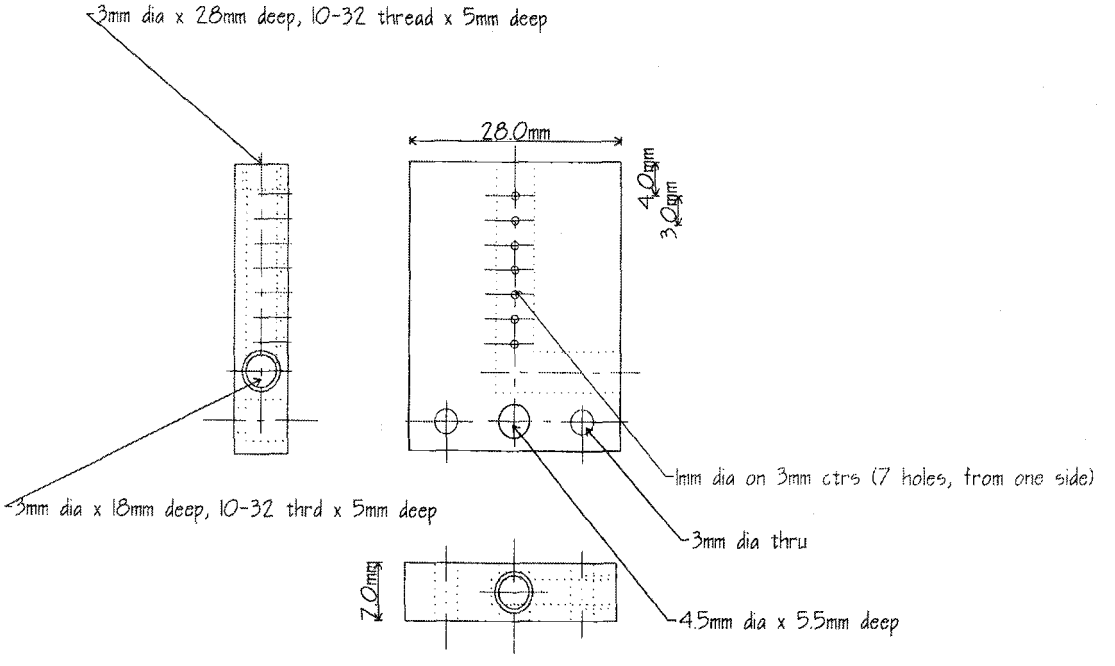

Figure B.6. Diagram of PTFE cooling head block

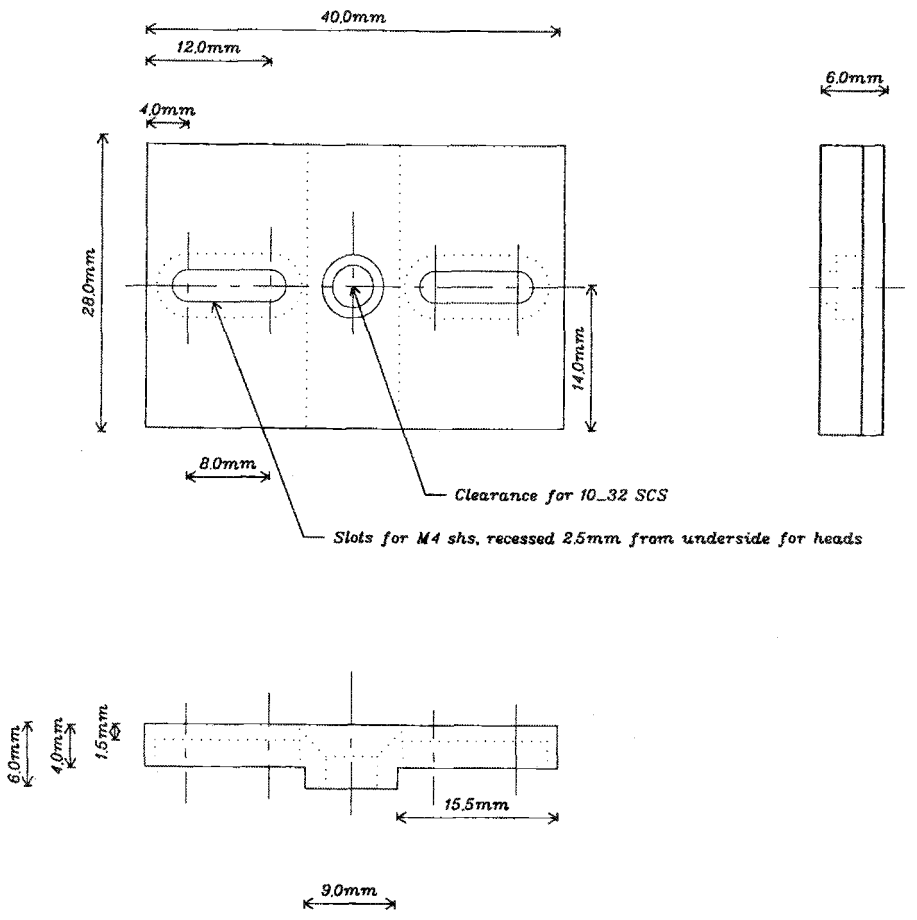

Figure B.7. Diagram of base plate

APPENDIX C

C 7 SELECTED CYCLES

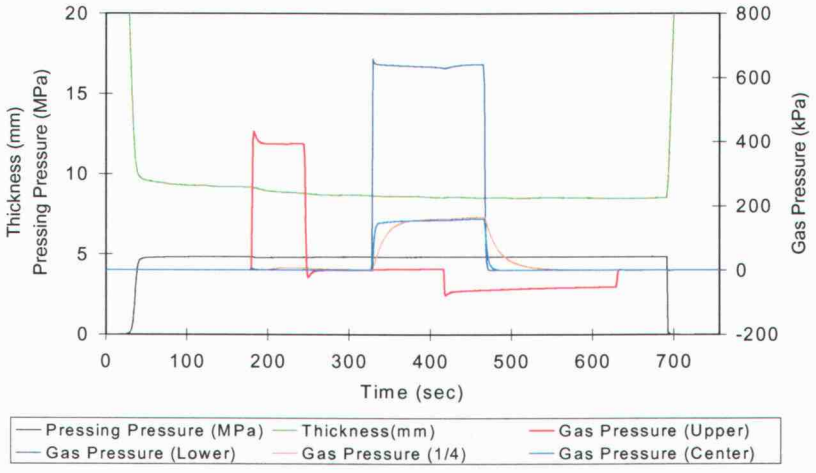

Figure C.1. HL60-70 (1.5mm/sec; liquid PF 10%; 4.84MPa; 392kPa 70seconds; no)

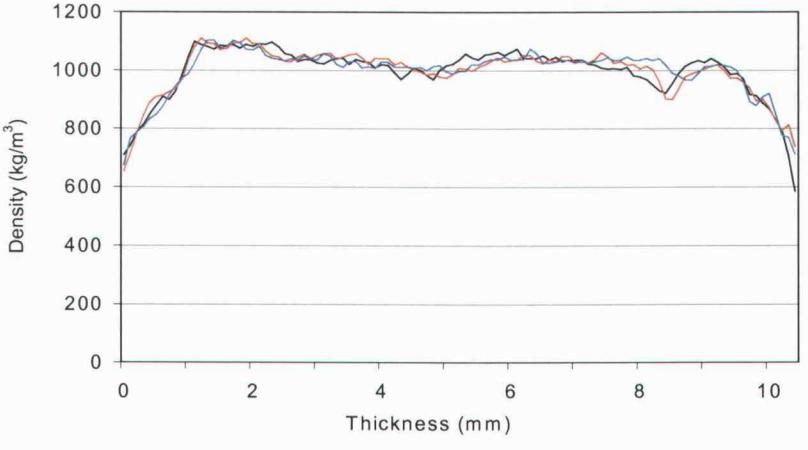

Figure C.2. Density gradient of HL60-70

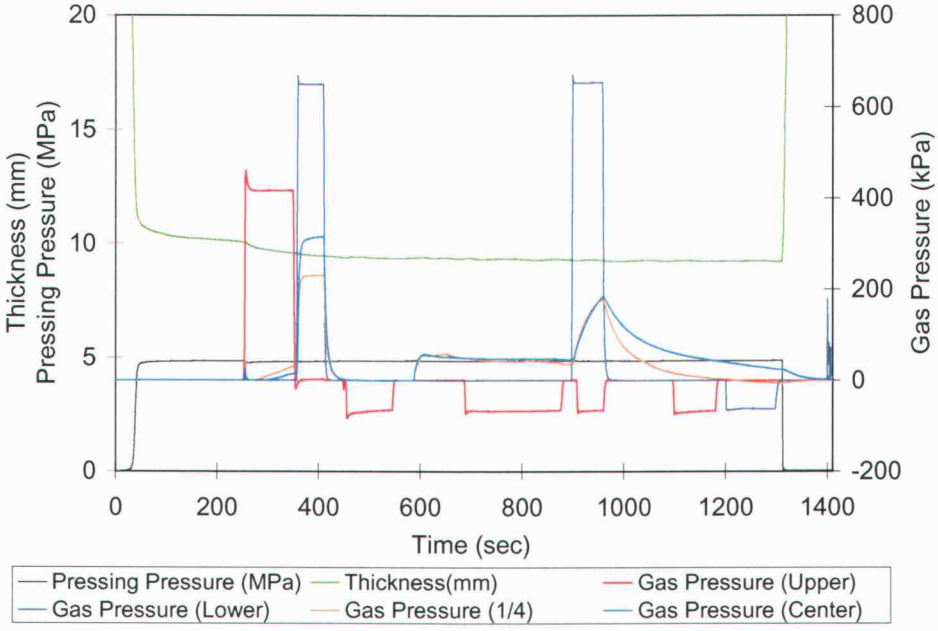

Figure C.3. HL60-100 (1.5mm/sec; liquid PF 10%; 4.85MPa; 416kPa 100 seconds; 25cc)

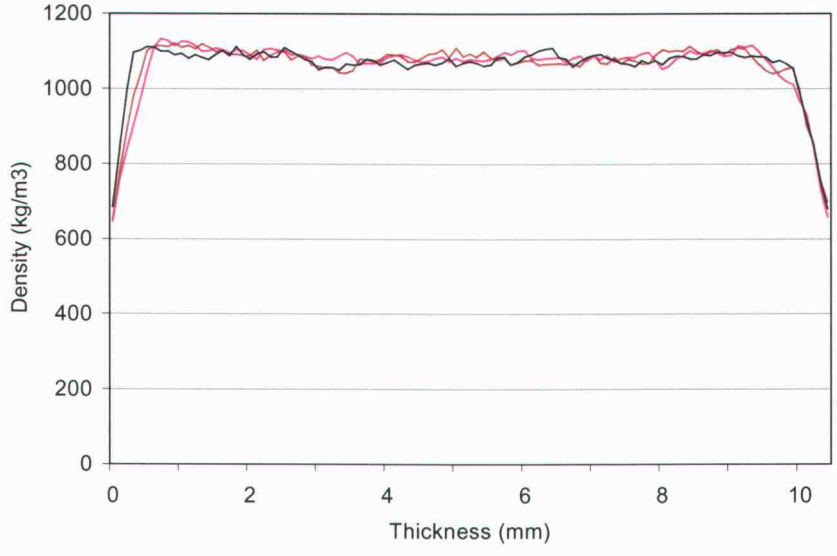

Figure C.4 Density gradient of HL60-100

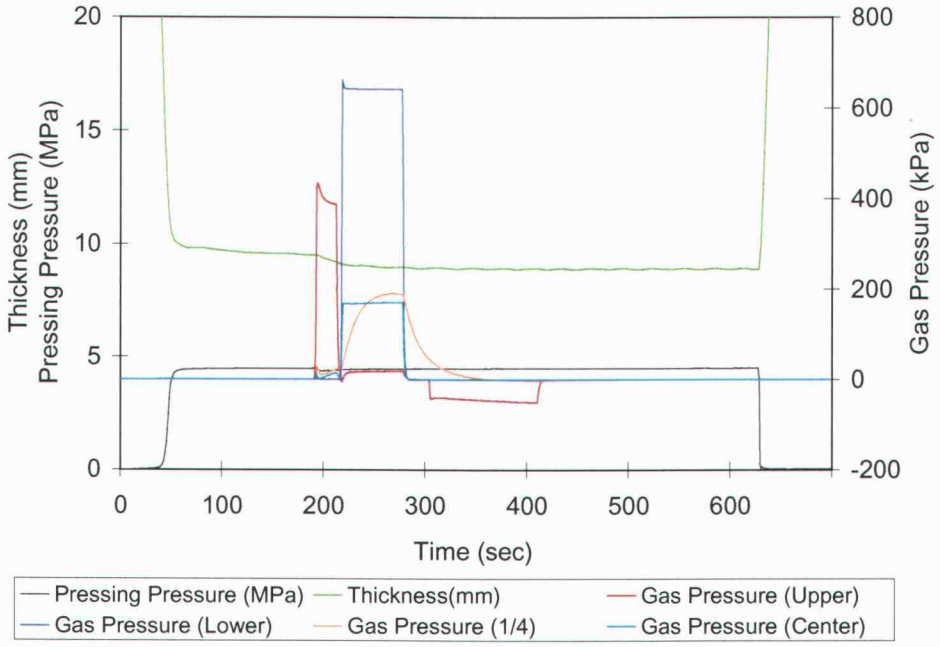

Figure C.5. HL60-20 (1.5mm/sec; liquid PF 10%; 4.47MPa; 391kPa 20seconds; no)

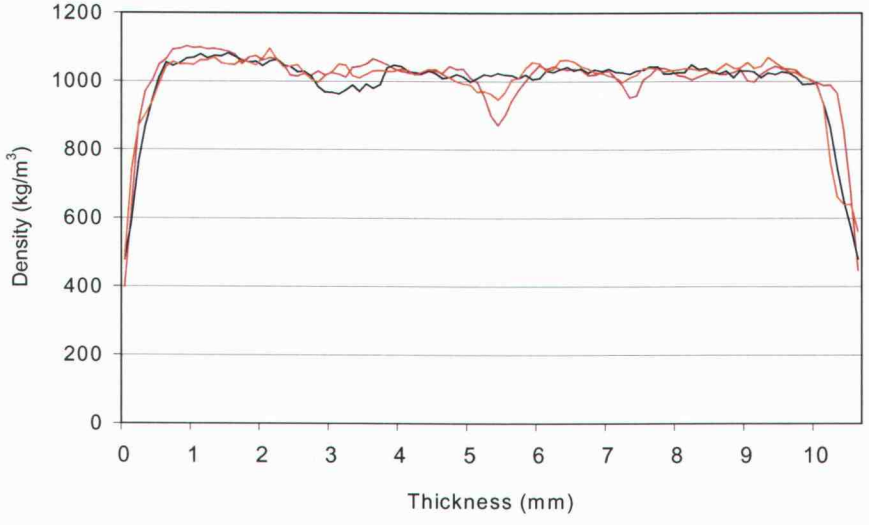

Figure C.6 Density gradient of HL60-20

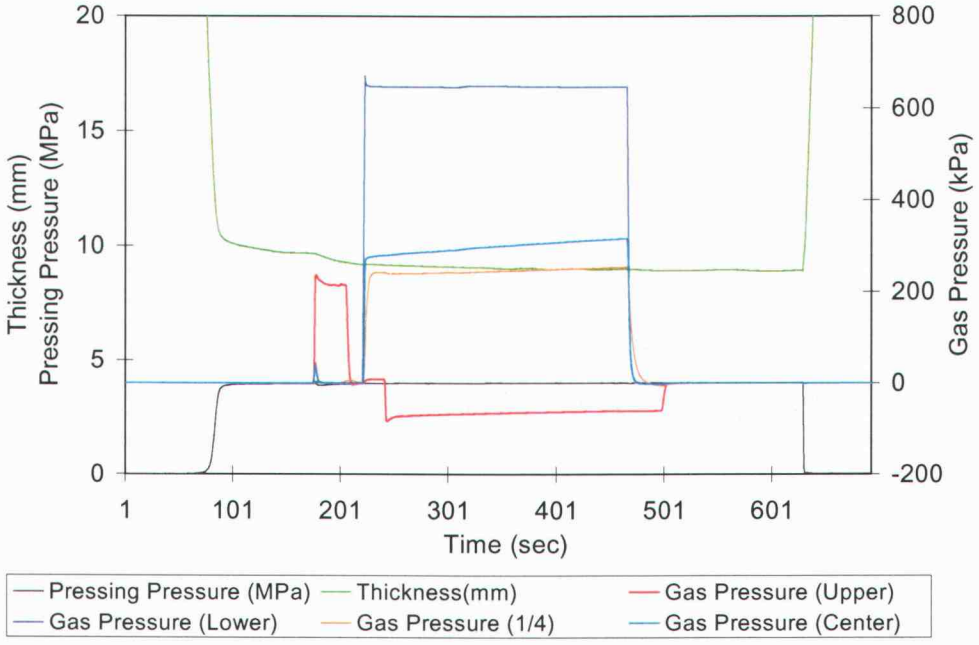

Figure C.7 HL30-20n (1.5mm/sec; liquid PF 10%; 4.02MPa; 214kPa 20seconds; no)

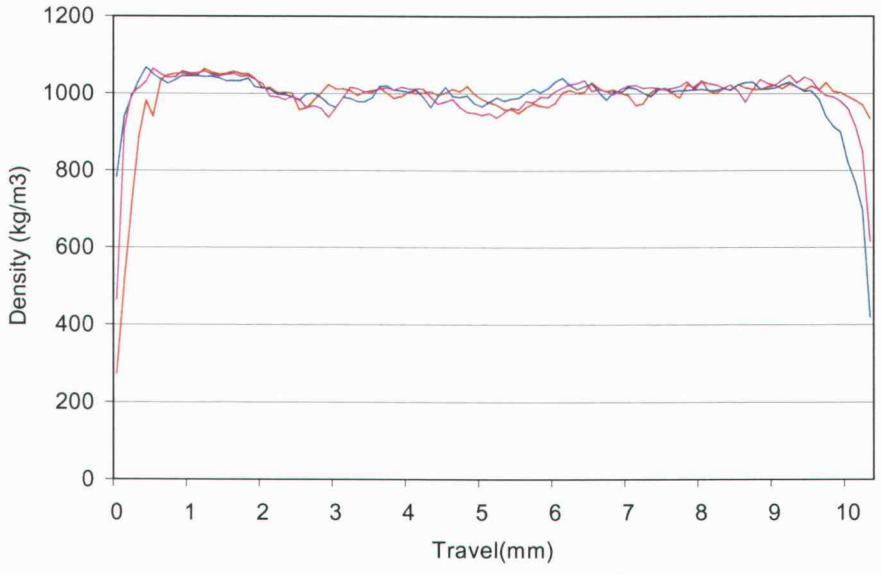

Figure C.8. Density gradient of HL30-20n

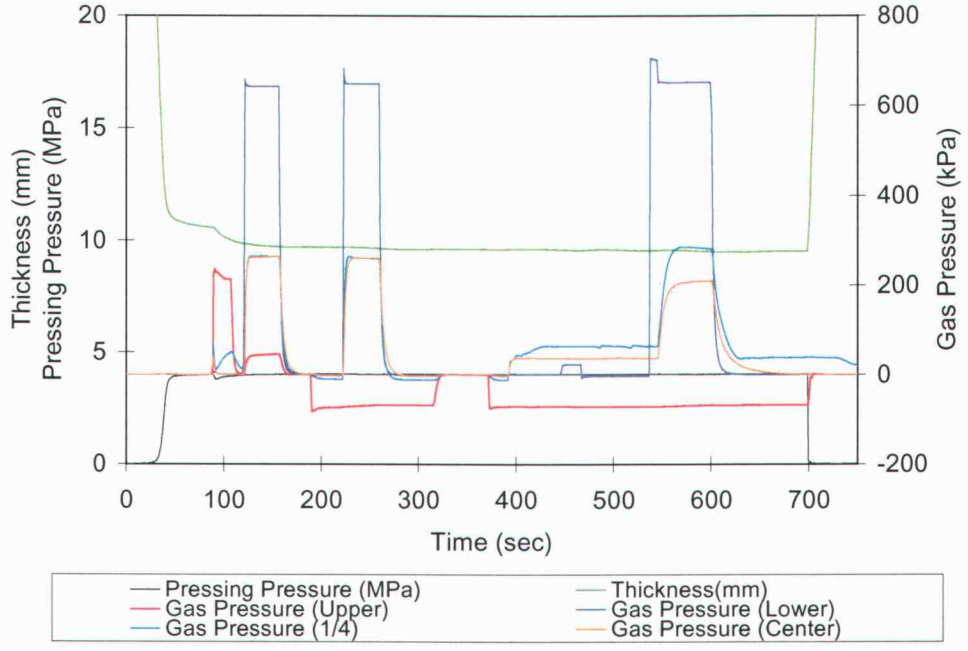

Figure C.9. HL30-20m (1.5mm/sec; liquid PF 10%; 4.04MPa; 214kPa 20seconds; 25cc)

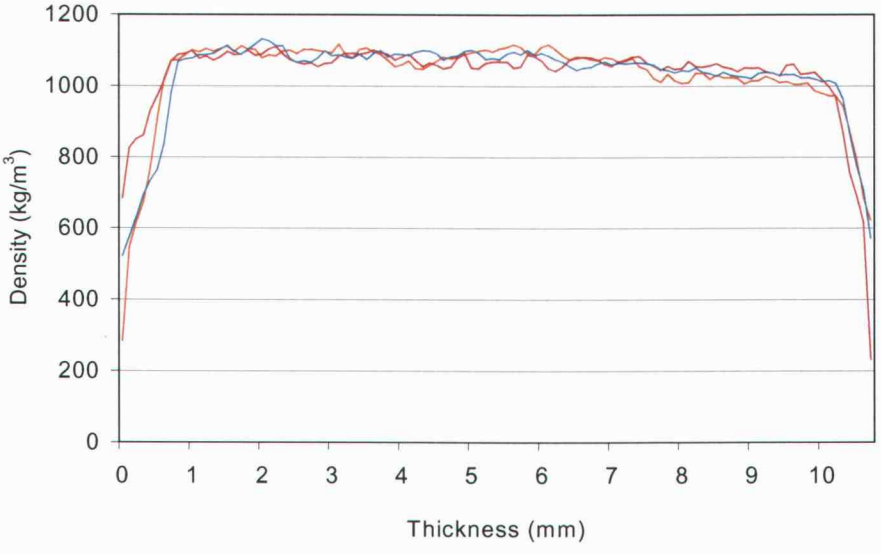

Figure C.10. Density gradient of HL30-20m

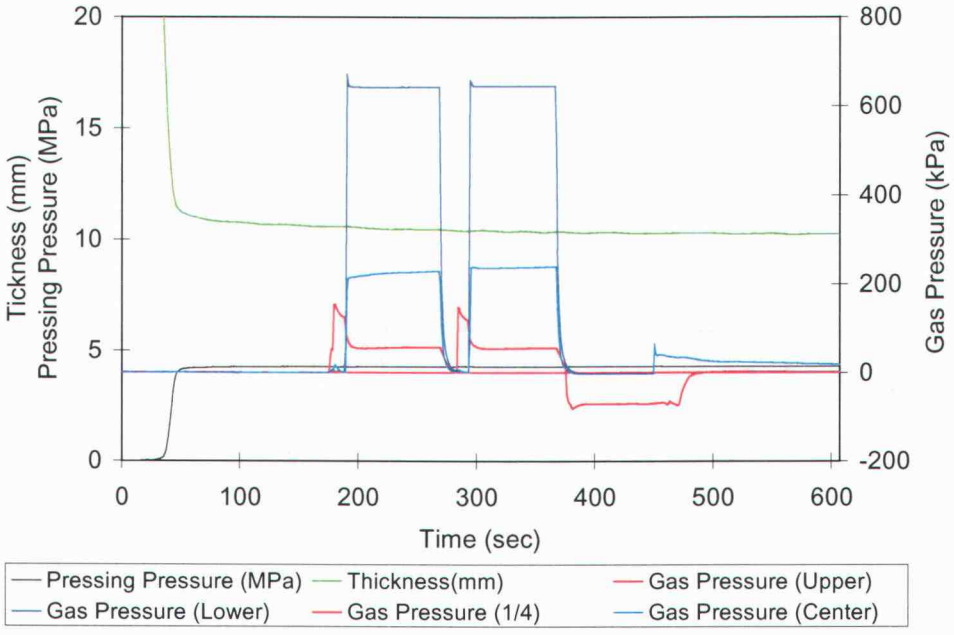

Figure C.11. HL20-100X2 (1.5mm/sec; liquid PF 10%; 4.25MPa; 141kPa 100seconds treated 2 times; 25cc)

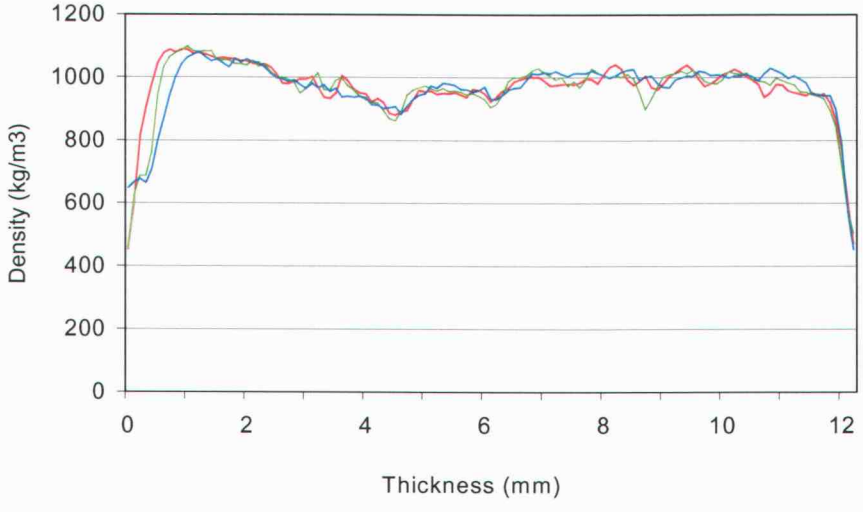

Figure C.12. Density gradient of HL20-100X2

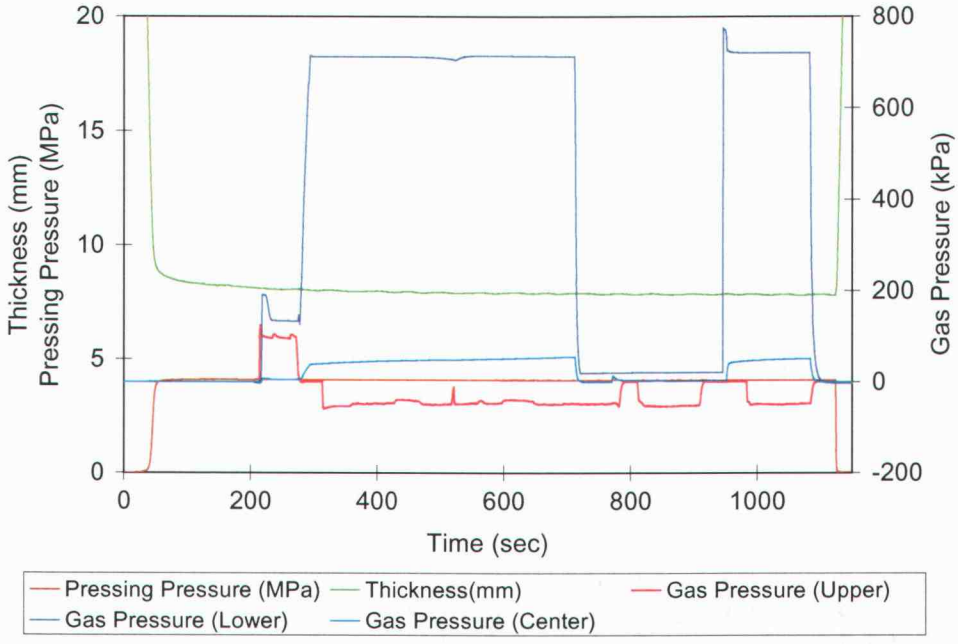

Figure C.13. HL20-40S (1.5mm/sec; liquid PF 10%; 4.11MPa; $NH_3$133kPa , air103 kPa for 60seconds; 25cc)

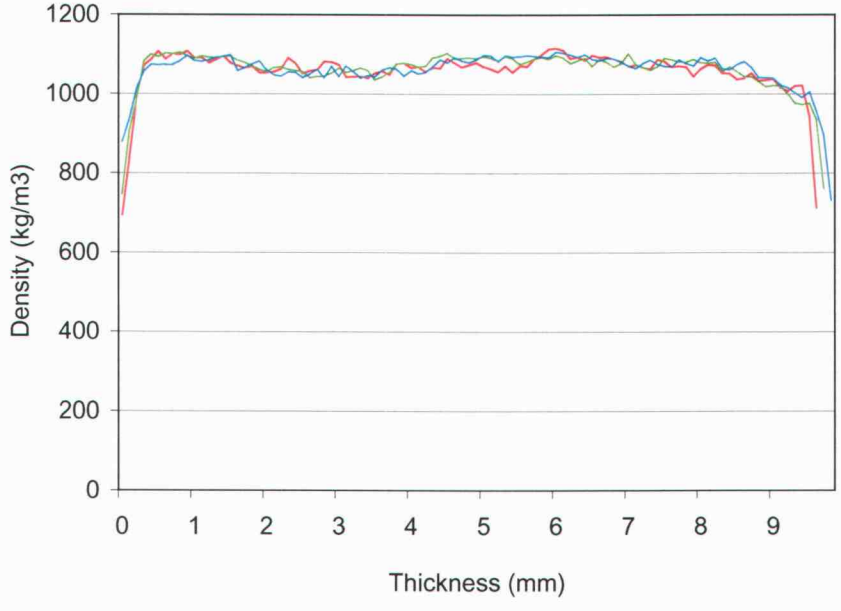

Figure C.14. Density gradient of HL20-40S